QUANTITATIVE TANDEM MASS SPECTROMETRIC IMAGING WITH MATRIX-ASSISTED LASER DESORPTION/IONIZATION

By

DAVID ANDREW PIRMAN, JR.

A DISSERTATION PRESENTED TO THE GRADUATE SCHOOL
OF THE UNIVERSITY OF FLORIDA IN PARTIAL FULFILLMENT
OF THE REQUIREMENTS FOR THE DEGREE OF
DOCTOR OF PHILOSOPHY

UNIVERSITY OF FLORIDA

2011

To my late Mother, may she rest in peace

ACKNOWLEDGMENTS

I would first like to acknowledge my advisor Dr. Richard A. Yost, who has been instrumental in my development as a scientist. Rick has established a research group where independent scientific creativity and thought is encouraged. His teaching and guidance has not only bettered my scientific understanding of chemistry, but has nurtured a foundation for a lifetime of scientific exploration. His excitement and genuine interest in science has inspired me to attain the same attributes, hopefully leading to a successful career in the field, and for that, I thank you. A special thanks to the past-and-present Yosties, for creating and establishing an excellent group dynamic allowing for a research environment where help and advice from fellow students is commonplace

I would also like to thank my family including my parents, specifically my Dad, brother, sister, and my late Mom for their support throughout my life. Our parents always instilled hard work and perseverance and through their support have encourage us to be successful and happy in whatever path we may choose in life. I must thank my Grandparents, Fred and Claudia Pirman, for their love and support throughout my life as well. Without them, the last few years would have been nearly impossible.

A final thank you to my wife, Natasha. You have been an amazing part of my life the past few years. Without your support through some tough times, I may not be at this point. I look forward to the next chapter in our lives together.

TABLE OF CONTENTS

page

LIST OF TABLES

LIST OF FIGURES

Abstract of Dissertation Presented to the Graduate School
of the University of Florida in Partial Fulfillment of the
Requirements for the Degree of Doctor of Philosophy

QUANTITATIVE TANDEM MASS SPECTROMETRIC IMAGING WITH MATRIX-ASSISTED LASER DESORPTION/IONIZATION

By

David Andrew Pirman, Jr.

May 2011

Chair: Richard A. Yost
Major: Chemistry

Mass spectrometric imaging (MSI) allows for direct analysis of tissues by matrix-assisted laser desorption/ionization (MALDI) tandem mass spectrometry (MS^n or MS/MS) provides spatial distribution of an analyte's distribution within the tissue. However, MSI is considered primarily a qualitative technique as a result of the poor quantitative ability of MALDI combined with the challenge of direct analysis from complex tissue samples, without cleanup or chromatography. Variations in the makeup of tissues results in extraction and ionization variations, making tissue-to-tissue comparisons difficult. The use of an internal standard to MSI applications has been suggested to control for MALDI signal variation, and may be used to identify tissue-specific ion signal variation. Applying the internal standard in a uniform manner not only leads to improvements in ion signal reproducibility, but can also help overcome variable ion signal as a result of tissue-specific extraction/ionization differences.

A wide-isolation MS/MS MSI approach was used to increase specificity and sensitivity of the target analytes. Wide-isolation MS/MS allows for tandem MS analysis on both the analyte and a deuterated internal standard within the same MS scan. By

monitoring the ratio of the analyte to internal standard ion signals, successful quantitative MSI experiments were performed for the analysis of cocaine in a human brain sample. These quantitative results compared well to results from high-performance liquid chromatography-MS/MS experiments performed after tissue extraction and homogenization. Furthermore, applying an internal standard coupled with wide-isolation MS/MS was successfully used to identify tissue-specific ion signal variation. By analyzing five different tissues, variations in the analyte signal applied at a constant concentration were observed between the tissues. However, analyzing the analyte-to-internal-standard ratio resulted in comparable ion signal ratios between the five tissues. Since MSI is a direct analysis technique, differences in the physical or chemical makeup of tissues directly affects the resulting ion signal; without the use of an internal standard, these are difficult to identify and account for.

After development of a quantitative method, MSI was employed for quantitative determination of endogenous acetyl-l-carnitine (AC) concentration in a piglet brain sample. Piglets were fed either a normal or ketogenic diet and any resulting changes in acetyl-l-carnitine were monitored by MSI. The results indicate a non-significant change between the two samples, but were limited by error in the quantitative estimations. However, the MSI methods developed were used to make quantitative comparisons between two different samples quantitatively which is a significant advancement of the MSI technique.

CHAPTER 1
INTRODUCTION

Mass Spectrometric Tissue Imaging

Historical Perspective

In most scientific research, the ability to generate visual images of the experiments can result in new interpretations, leading to more conclusive results. From the development of X-Ray technology[1] to magnetic resonance imaging (MRI),[2] improvements in instrument technology have generated new insights resulting in more accurate determinations about a subject. The technology is continuously improving imaging data from generating higher resolution MRI scans for tissue differentiation[3, 4] to molecular differentiation with techniques such as optical fluorescent-labeling imaging[5] and atomic-level imaging with tunneling electron microscopy (TEM).[6] As imaging techniques improve, so does the scientific community's understanding of the research area they are employed to investigate. Through advancements in biochemistry, chemistry, and medicine, the molecular understanding of biological systems is becoming increasingly important in areas such as disease research. For example, identifying new protein targets or metabolic pathways between normal and diseased state tissues may lead to new therapeutic techniques. Most current imaging techniques; however, interrogate samples with little chemical specificity unless targeted through a label (e.g., fluorescent labeling). This lack of chemical specificity is a significant limitation of these imaging methods, specifically for tissue differentiation at the molecular level.

New developments in analyte-specific imaging techniques for biological samples include monitoring compound-specific resonances with nuclear magnetic resonance

(NMR), Fourier-transform infrared spectroscopy (FTIR) and anti-stokes Raman scattering[7]. These techniques are still being developed, but one major limitation in them is the extremely complex spectra generated from direct tissue analysis. Recently, the development of a new imaging technique based on mass spectrometry (MS) has potential to become an important analytical tool to answering biological questions. Mass spectrometric imaging (MSI) differs from classical imaging techniques cited above in the fact that it is actually a micro-sampling technique performed in a two-dimensional array and provides analyte distribution maps in a given sample. MSI offers an untargeted imaging method with improved analyte specificity, particularly, when employing either high-resolution MS (MS) or tandem MS (MS/MS or MS^n). The coupling of MSI with matrix-assisted laser desorption/ionization (MALDI), a surface desorption technique, has resulted in its significant growth as an analytical method for direct-tissue analysis.[8]

Current Technology

Current MSI technology was developed from the idea of using ion microscopy[9] to determine the elemental spatial distribution on a surface. The original ion microscope idea was further developed with the advancement of the ion microscope to secondary ion mass spectrometry (SIMS) and its use for imaging of biological samples. These ionization techniques; however, caused significant fragmentation of the target compounds limiting their application to elemental analysis. They were also considered surface analysis techniques (nm sampling depths) resulting in poor sensitivity due to the small sample size of analysis. The imaging idea was applied with a new instrument, the laser microprobe mass analyzer (LAMMA), which used laser/desorption ionization (LDI) with an ultra-violet (UV) laser to generate ions from backside illumination, which

resulted in complete ablation of the tissue sample.[10, 11] However, LDI still induced significant fragmentation of the molecular species present in the tissue sample, resulting in mostly elemental analysis, with improved sensitivity. An improvement from these techniques was the coupling of the UV ionization source to an ion trap mass spectrometer that was used to generate quantitative MS/MS information directly from liver and brain samples.[12] The MS/MS capabilities allowed for absolute analyte identification during the surface analysis.[12] Eventually, the use of softer ionization techniques such as MALDI, was employed for MSI allowing for analysis of larger biomolecules.[8, 13, 14] In addition, advancements ion gun sources and the development of matrix-assisted SIMS has allowed for analysis of small intact biomolecules including lipids and peptides.[15, 16] A more recent ionization technique developed by Graham Cooks at Purdue University, desorption electrospray ionization (DESI), has been utilized for MSI. DESI allows for direct analysis of tissue sample with no matrix and at atmospheric pressure, thus simplifying the MSI process.[17, 18] A brief comparison of common ionization techniques for MSI is shown in Table 1-1.

Each type of ionization method can be coupled with many types of mass analyzers. Currently, MALDI remains the most common method of ionization for imaging and is the technique used throughout this dissertation. Overall, MSI offers the best ability to perform untargeted, molecular-specific imaging directly from a biological sample. This unique capability, coupled with the numerous types of available instrumentation, has recently generated significant interest amongst the scientific community.

MALDI MSI Background

Obtaining an MS image of an analyte's distribution can be performed on nearly any surface, so long as ions can be generated and detected via MS. The most common application of the technique is for the analysis of biological samples, and is the primary focus of this research. A workflow illustrating the steps in generating MS images via MALDI MS^n is described in Figure 1-1. For quantitative MSI, the addition of calibration standards and internal standards is necessary. A brief summary is described here, and further details will be discussed as they are used in each chapter. After the addition of the standard, excised tissue is first prepared by thin layer sectioning (10–20 μm thick) performed on a cryo-microtome instrument at temperatures between negative −15 and −25° C. The use of a tissue-mounting medium to assist in sectioning is avoided, as these cutting mediums may contaminate the tissue surface, interfering with MS analysis. In this research, tissue samples were mounted to the cryostat stage using de-ionized water, which froze upon the addition of frozen tissue. The thin-layer tissue section is then placed on the MALDI target surface, which may be a standard glass or stainless-steel microscope slide or a MALDI target plate.

For MALDI MSI, a matrix must be applied to the surface of the sample. This is a significant step in order to produce quality MS images, as the matrix serves numerous purposes. First, the MALDI matrix serves as a primary intermediary between the laser source and the target analyte (ionization theory is further discussed in the MALDI subsection). Second, the matrix must be applied uniformly to the tissue section to ensure variations in ion signal are not a result of matrix crystallization differences. The matrix may be applied in numerous ways, including manual pneumatic spray-coating

with an artistic airbrush or nebulizer,[19, 20] microspotted in a confined area with automated instrumentation such as the LabCyte[21, 22] or Shimadzu CHiP, [23, 24] or by automated nebulization with instruments such as a Bruker ImagePrep, which creates fine droplets off the surface of a piezo-electric material or even a modified inkjet printer.[76] Other methods which require no solvent, such as sublimation[25] and sifting fine matrix crystals[26–28] onto the tissue have been shown as alternatives to spray coating methods. The absence of solvent reduces lateral diffusion of analytes within the tissue; however, it also reduces the extraction of analytes from the tissue. Regardless of the technique chosen, the matrix must be applied uniformly producing crystal sizes smaller than the spot diameter of the MALDI laser.

Once the tissue is coated with matrix, it is loaded into the vacuum chamber and moved step-wise with respect to the ionization source. This patterned movement is referred to as rastering. At each raster step, which has specific x- and y-axis values, a mass spectrum is recorded via MS or MS^n. The spatial resolution of the resulting MS images is dependent on the focusing of the MALDI laser as well as the raster step size between collected mass spectra. For MALDI and DESI MSI, typically resolution can be between 20–200 μm. Imaging software is then used to generate specific ion intensity images versus position, as exemplified in Figure 1-2. The figure shows two examples of MS images generated by plotting the intensity of the $[M+Na]^+$ ions of two lipids versus (x,y) position. From the resulting MS images, it is concluded that the sphingomyelin (*m/z* 751) is more abundant in the white matter of the brain, whereas the distribution of a phosphatidyl choline (*m/z* 734) is more abundant in the grey matter of the brain. These types of images can be generated for any ion in the MS or MS^n spectra.

Instrument parameters may also be varied, such as the applied laser energy (LE) and the number of laser shots (LS) performed at each raster step is determined on random areas of the tissue. Varying the LE and LS to achieve adequate ion signal is important for MS analysis. Depending on the type of mass analyzer, these numbers may vary greatly. For instance, analysis with a time-of-flight (TOF) instrument may require a large number of laser shots (~200 LS). In comparison, the linear ion trap (LIT) typically requires only 4 LS to achieve adequate ion signal. However, with the LIT, space-charging is a concern when analyzing a large number of ions (discussed further in the ion trap section). The LE can also be varied to improve ion signal; however, too high a LE may result in increased fragmentation.

MALDI Fundamentals

The coupling of MALDI with MSI offered a significant improvement over previous ionization methods.[8] MALDI produces mainly singly-charged ions e.g., $[M+H]^+$, across a broad mass range (50–200,000 Daltons). MALDI is also considered a sensitive technique with detection limits in the lower attomole levels.[29] The MALDI technique was invented and named by Frans Hillenkamp and Michael Karas[30, 31]. The technique developed by Hillenkamp and Karas used small organic acids as the MALDI matrix, which have proven to be the matrices of choice for most current MALDI applications. The technique was later shown to ionize large biomolecules including proteins by Koichi Tanaka.[32] Tanaka's technique employed cobalt resin suspended in glycerol and was the first to show ionization of large intact biomolecules for which he shared one-quarter of the Nobel Prize in Chemistry in 2002.

Practical Aspects

First, the MALDI matrix is applied to the sample, which can be small molecules, lipids, peptides, proteins, or intact tissue, and the matrix/analyte mixture is allowed to dry producing a matrix crystal layer with analyte incorporated within the crystal lattice. An illustration of the MALDI process is shown in Figure 1-3. This incorporation of the analyte may not actually be inside a crystal, but may be surrounding the matrix crystals. The important step is desorption of both the matrix and analyte during laser irradiation. If working with standards, the matrix to analyte ratio (M/A) is important in producing adequate ion signal. A high M/A results in mostly matrix ions in the mass spectrum. Conversely, a low M/A also results in inadequate signal as the concentration of matrix is too low to produce analyte ions. There exists a range of M/As in which the ion signal observed is mainly from the analyte; however, this M/A range varies with matrix type and analyte.[34] For imaging applications, the M/A ratio is difficult to determine, as the matrix is generally applied atop the tissue samples until a thin layer of crystals is observed, and the amount of matrix is difficult to quantify. Equally difficult to quantify is the amount of analytes possible from a given area of tissue. The tissue and matrix layer may vary in thickness at each raster step, which resulted in variations in the amount of sample analyzed. Also the incorporation of matrix crystals into the tissue may vary based on the chemical and physical composition of the tissue.

Desorption Process

The first step in ion production is the desorption process resulting from irradiation from the laser.[35] As the laser irradiates the sample and a certain amount of energy applied per area is reached, desorption occurs. This energy level for desorption is matrix-dependant, and can vary greatly with matrices and samples. Desorption results

in sublimation of the matrix along with the analyte, which can be considered the first role of the MALDI matrix in generating ions.[35] The MALDI matrix is usually chosen to have a very large molar absorptivity at the irradiation wavelength which allows it to absorb most of the energy imparted by the laser. This results in a lower initial kinetic energy of the target analytes during the ablation process, thus limiting analyte fragmentation from the ion source and producing mainly $[M+H]^+$ analyte ions. The plume is considered to form on the nanosecond time-scale and may last milliseconds above the sample surface. This lasting plume has a high molecular density, resulting in a high molecular collision rate, and leading to the formation of ions through subsequent ion-molecule reactions or declustering of preformed ions.[36, 37]

Ion Formation Theory

The generation of ions from the MALDI process is still not completely understood; however, two models of ion generation currently exist. One theory of ion formation suggests that, as, in the resulting plume after desorption primary and secondary ions are formed. The primary ions are generally matrix ions resulting from photo-ionization effects from the laser irradiation.[35] Secondary ions are formed in the MALDI plume through gas-phase ion-molecule collisions in which the primary ion transfers a charge, in most cases a proton to the target analyte, creating an $[M+H]^+$ ion. These secondary reactions occur between either a matrix ion and matrix neutral, a matrix ion and analyte neutral, or a hydrogen ion and analyte neutral.[35] Aside from ions created from the addition of a proton, the addition of cations is also observed, and can lead to more stable analyte ions and more informative fragmentation pathways in some MS/MS applications.[20]

Another theory of MALDI ionization is termed the “lucky survivor model”.[38] This model retains the idea of the initial desorption and photo-ionization event, but states that analytes retain their charge state from the solution phase and are incorporated into the matrix partially solvated. In the desorption step, the crystal lattice is broken up with varying sizes of molecule clusters, and statistically some of these fragments will be a single analyte ion. The analyte clusters (with many charges) continue to lose neutral solvent or matrix ions and counterions as the plume expands, resulting in neutralization of the clusters charges During the neutralization process as the cluster is reduced in size, only one charged analyte remains, termed “the lucky lurvivor.[37, 38]

Quantitative MALDI

The use of MALDI for quantitative purposes has been limited by the relatively poor ion signal reproducibility. The quantitative possibilities of the technique have been explored previously; however, quantitative data has proven difficult to generate using these techniques.[39–43] Significant ion signal variation and non-linear increases in analyte signal, independent of M/A ratio, have contributed to the poor quantitative ability of MALDI MS. Ion signal variation results from laser shot-to-shot energy variability; however, in most MSI instruments, this effect is minimal because multiple laser shots were used. Inhomogenous MALDI matrix crystallization is the largest contributor to varying MALDI ion signal, thus the importance of producing homogenous matrix layers consisting of uniform small crystals atop the imaging sample. Figure 1-4 shows optical images of different matrix crystals formed for MALDI experiments. On a scale similar to the laser diameter, the ion signal is dependent on the crystal quality at a given location. Other factors limiting the quantitative ability of MALDI for MSI will be discussed in Chapter 3.

Mass Spectrometry

As the ions are produced from the MALDI process, they are then detected via MS or MS^n in terms of the mass-to-charge ratio (*m/z*). Several types of commercial mass analyzers are available for MSI experimentation. Many of these instruments are based on TOF technology, and also include hybrid TOF instruments to provide MS/MS possibilities. There are also instruments equipped with ion trap mass analyzers offering MS^n capabilities, and even newer instrumentation offering high resolution MS^n analysis for MSI. Two instruments were used in the MSI experiments discussed here: a Thermo Scientific MALDI LTQ XL (Thermo Scientific; San Jose, CA, USA) and a Waters Synapt MALDI-Q-Ion Mobility (T-wave cell) TOF (QTOF) (Waters Corp. Milford, MA, USA). The former instrument is a linear ion trap (LIT) mass analyzer, and the latter, a quadrupole coupled with a TOF mass analyzer. The Thermo instrument will be referred to as the LTQ and the Waters instrument will be referred to as the QTOF.

MALDI LTQ

The Thermo Scientific MALDI LTQ XL is a commercially available MSI instrument capable of generating MS and MS^n data with the LIT, as shown in Figure 1-5. The instrument has previously been described in extensive detail.[19] It is equipped with an intermediate-pressure MALDI source (0.07 Torr) and a 337 nm nitrogen laser which fires at a frequency of 60 Hz and variable laser energy (maximum 250 μJ per pulse). The laser is focused to spot size of ~100 μm at an incident angle of 32°. Upon laser irradiation of the sample, ions are transferred through a series of focusing multipoles, lenses, and injected into the LIT for mass analysis.

Linear ion trap

The LIT is a two-dimensional variation of the classical three-dimensional quadrupole ion trap (QIT) developed by Wolfgang Paul and Helmut Steinwedel.[44, 45] The LIT differs from the QIT in that the ions are stored axially in two dimensions opposed to three-dimensional storage capabilities of the QIT. The LIT consists of three sections of hyperbolic quadrupole rods, as shown in Figure 1-6A. Discrete direct-current (DC) voltages are applied to the front and back sections of the LIT, which trap the ions in the center section, and also reduce the possibility of fringe electric field effects during trapping and resonant ejection of the ions. Trapping in the center section is performed by applying an oscillating radio-frequency (RF) voltage to the X and Y rod pairs, as shown in Figure 1-6B. Alternating current (AC) is applied across the X rods for isolation, activation and ejection of ions, also shown in Figure 1-6C. The ions are ejected through 30 mm-long slits along the X rods, strike two conversion dynodes, and are ultimately detected by two electron multipliers, one on each side of the trap. The LIT offers increased storage space within the trap as well as two detectors for ion detection, thus improving sensitivity, and dynamic range compared to the QIT. One limitation in MS analysis with an ion trap is the limited ion storage available, thus limiting the dynamic range of the instrument. As the number of ions increases above a certain limit, an effect known as space-charging is observed. This occurs as the ion density from the trapped ions shields the electric field from the voltages applied to the hyperbolic rods. The results can be mass shifts to high masses, decreased sensitivity, and decreased mass resolution. These effects are dramatically reduced in the LIT compared to the QIT due to the increased storage space.

MS/MS with a LIT

MS/MS analysis on the LIT includes trapping the ions generated from the ion source, mass isolation of the parent ion, activation of the parent ion to induce fragmentation, and finally resonant ejection of the product ions for detection. In a typical MS/MS experiment, after the ions are trapped, isolation of the precursor ion is performed by applying RF and AC voltages to the quadrupole rods for resonant ejection of all other ions from the trap. To isolate a particular ion, a specific *m/z* ratio is chosen by the user along with a specific *m/z* range (isolation window). For instance, the isolation of caffeine which has *m/z* 195 corresponding to the $[M+H]^+$ might be performed by isolation of *m/z* 195 ± 1 *m/z* units. The isolation window for MS/MS analysis would be *m/z* 194–196. Narrow isolation windows increase specificity by isolating only the ion of interest for MS/MS analysis, but also may reduce sensitivity as fragile ions may fragment and be ejected from the trap from the resonant ejection frequencies applied. Wider isolation windows create a more stable environment for isolation, but also leaves a wider mass range of ions in the trap to be fragmented, and possibly complicate the MS/MS spectrum.

After isolation of the precursor ion, a resonant excitation RF voltage is applied to the X rods, corresponding to the secular frequency of the precursor *m/z*. This excitation voltage increases the kinetic energy of the precursor ionsin the trap, and through gas-phase collisions with the He gas, dissociation of the precursor ion occurs. This process is termed collision-induced dissociation (CID) and results in reproducible product ion fragments of the precursor ion. These product ions are subsequently ejected for the trap and detected producing an MS/MS spectrum. The product ions generated can be

used to provide structural information about the precursor ion, or can be used to confirm the precursor *m/z* is free from contamination of other compounds at the same *m/z*. On an ion trap instrument, this process can be repeated by isolating and fragmenting one of the product ions, producing MS^n spectra.[44, 46] Both full-scan MS and MS/MS were used throughout this dissertation.

Wide-isolation MS/MS

The ultimate goal of the presented research is to develop quantitative MALDI MSI methods which will use the ratio of the ion signal of the target analyte to the ion signal of an internal standard (deuterated analog of the target analyte). For MS applications, this is achieved simply by monitoring the $[M+H]^+$ ion signal of both the analyte and internal standard, and calculating the ratio. However, MS analyses of tissue samples typically require sample cleanup steps, such as extraction and chromatography prior to analysis. These steps help reduce the occurrence of interfering peaks in the resulting mass spectra. In MSI analysis, the tissue sample is directly analyzed, thus the ions generated by MALDI represent the entire molecular makeup of the tissue, complicating the spectra and increasing the chances of interfering ions. The use of MS/MS and MS^n can circumvent these issues; provided the target analyte can be ionized sufficiently directly from a biological sample, and the resulting MS^n can be verified to be analyte specific.

Employing MS/MS for simultaneous analysis of an analyte and internal standard can be achieved with high precision by wide-isolation MS/MS.[47] In wide-isolation MS/MS, the center of isolation is moved from the target precursor ion to an *m/*z half way between the target and internal standard. The isolation window is then expanded to include both the target analyte and internal standard. After isolation, fragmentation of isolated ions is induced through CID, and the product ions are monitored, as illustrated

in Figure 1-7. In the product ion spectrum, the analyte and deuterated internal standard can be differentiated, allowing for the simultaneous MS/MS analysis of the analyte and internal standard.[46, 47] Wide-isolation MS/MS has been shown to significantly improve the quantitative capabilities of MALDI for the analysis of cocaine from human brain tissue.[47] This technique will be evaluated and used throughout the presented research to generate quantitative MALDI MSI methods.

MALDI QTOF

The QTOF instrument is a hybrid instrument coupling two mass analyzers, the quadrupole mass filter and a TOF, and the instrument used here, was also equipped with a T-wave ion mobility cell. A schematic of the instrument is shown in Figure 1-8 and has been previously described. [48, 49] The QTOF is equipped with an intermediate pressure MALDI source (0.07 Torr) and a 200 Hz, 335 nm, tripled Nd:YAG laser at a frequency of 200 Hz and spot diameter of 150 μm. Upon irradiation with the laser, the ions are transferred through a series of lenses into the quadrupole for mass selection prior to fragmentation. The ion mobility cell was not used in these experiments, although the last portion of the cell (transfer cell) is used for CID. The quadrupole serves as a mass separating device prior to fragmentation for MS/MS applications.[50, 51] After fragmentation by CID, the product ions are accelerated into the TOF portion of the instrument for mass analysis.

Mass selection with quadrupole

The quadrupole serves as a mass filter prior to fragmentation in the ion mobility cell. A schematic is shown in Figure 1-9, with four parallel rods with each opposing rod pair connected electrically.[51] An RF or DC voltage can be applied to produce an electric field within the four rods. By varying the applied voltages, ions of certain *m/z* have

stable trajectories through the instrument and thus reach the detector. Constant voltages can be applied to allow a small *m/z* range to pass through, or the voltage can be continuously varied to produce a mass spectrum.

Mass analysis with TOF

A TOF mass analyzer measures amount of time it takes for an ion to travel a fixed distance to determine its *m/z,* as shown in Figure 1-10. Ions are accelerated into the TOF region with an electric field of constant strength. Thus, ions of the same charge (usually the +1 state) have the same initial kinetic energy and the velocity of the ion is dependent upon the *m/z*. As the ions travel to the detector, larger ions move more slowly and smaller ions move more quickly, thus a time difference between the ions can be measured. This acceleration voltage may be applied continuously, or a technique known as delayed extraction can be used to improve TOF sensitivity and resolution. On the QTOF, delayed extraction is not used; however, orthogonal injection into the TOF is used. This ensures that ions arriving into the TOF region of the instrument are accelerated from the same initial velocity, irrespective of their velocities from the quadrupole and ion mobility portions of the instrument.

MS/MS and wide-isolation MS/MS with QTOF

MS/MS analysis with the QTOF uses the quadrupole to allow a small *m/z* range to enter into the ion mobility portion of the instrument. Fragmentation of the ions is generated through CID (previously described). The resulting product ions are then accelerated into the TOF for mass analysis. The instrument manufacturer's control software allows the user to control the mass resolution of the quadrupole upon setting a target mass for MS/MS analysis. This was presumably designed for target analytes with a wide isotopic peak envelope such as high molecular weight proteins with multiple

charge states. For quantitative MSI analysis with an internal standard, this feature was used to allow both the target analyte and its deuterated analog to be simultaneously detected in a single MS/MS scan. The simultaneous detection of both the analyte and internal standard is imperative for quantitative MALDI MS^n applications (further discussed in subsequent chapters).

Research Motivation

The overall goal of the presented research was to develop MSI techniques for the comparison of acetyl-l-carnitine (AC) concentration and distribution between piglet brain samples, one fed a ketogenic diet (KD) and one fed a normal diet. The ketogenic diet is used for the treatment of epilepsy cases which fail to respond to the current pharmaceuticals. Its effectiveness is often comparable to the best anti-epileptic drugs available; however, the therapeutic mechanism remains unknown. MSI techniques would provide useful information about any quantitative distribution differences of AC in the brain between piglets fed a ketogenic diet versus a normal diet. However, to use MSI to quantitatively compare endogenous metabolite concentration differences between tissues, new quantitative methods must be developed.

Ketogenic Diet

KDs were designed in the early 1900s to mimic the biochemical changes present during fasting.[52] Fasting has long been known to reduce the amount of seizure activity and has been described in the Hippocratic Corpus dated around 400 BC.[53, 54] The KD is an extremely strict and regulated diet in which the body derives much of its energy from fats rather than carbohydrates. The diet generally consists of 85% fat, 10% protein and 5% carbohydrates at only 75% of the recommended daily caloric intake. Fluids are also reduced to 80% of the normal level. The diet is initiated by fasting for 24–36 hours

to exhaust glucose reserves and force the body to rely on fatty acid β–oxidation as its main source of energy production, resulting in a ketotic state or ketosis, which is a large buildup of ketone bodies resulting from β-oxidation.[53, 54] These ketone bodies consist of β–hydroxybutyric acid and acetoacetic acid, which is spontaneously converted into acetone,[53] and are used as energy sources in the brain. Some of the resulting metabolites of β–oxidation and the breakdown of the ketone bodies for energy are hypothesized to aid in the anticonvulsant mechanism of the KD by controlling potassium channels in the nerve.[52, 54, 55]

Acetyl-l-Carnitine Role in Treatment

Of the metabolic changes resulting from the KD, changes in concentration of acetylcarnitine (AC) has been hypothesized by Dr. Peggy Borum from the Food Science and Human Nutrition Department at the University of Florida to play a key role in the therapeutic effects of the KD. AC belongs to a class of compounds called carnitines, shown in Figure 1-11, that serve as the main transporters of fatty acids and acetyl groups across the mitochondrial membrane for β–oxidation.[56] An increase in carnitines and carnitine translocase proteins is necessary to accommodate for the increased fatty acid oxidation. Aside from the increased need for fatty acid transport, AC also has other metabolic fates such as the production of acetyl-coenzyme A (acetyl-CoA). The normal pathway for acetyl-CoA generation is slowed due to the decreased glucose metabolism during the KD.[57]

AC has also been shown to induce transient seizures in epileptic patients, possibly by interrupting the GABA inhibitory system.[58] Although AC has been shown to increase in tissue during the ketogenic diet and fasting,[59] it may be shunted from other metabolic

pathways, and used primarily for fatty acid transport and conversion to acetyl-CoA which enters the Kreb's cycle.[60, 61]

Methods to detect and quantify acylcarnitines in tissue have been developed using positron emission tomography (PET),[62] liquid chromatography (LC)/MS,[63] and subcutaneous microdialysis (SMD) followed by MS detection.[59] PET provides real-time imaging of the labeled analyte but is limited by its lack of chemical specificity. LC/MS provides excellent quantitative data, but due to tissue homogenization and extraction methods, spatial distribution information is lost. SMD provides minimally invasive sampling directly from tissue; however, it is limited to the area of tissue the probe resides, and no spatial distribution information is acquired. A method to quantify the distribution and concentration of acetylcarnitine and other suspected anticonvulsant metabolites in the brain would provide important information into the mechanism of the therapeutic effects of the KD. Brain tissues from piglet test subjects, were used for the method development and establishing the effects of the KD on concentration and distribution of AC in brain tissue.

Overview of Research

MALDI MSI

Combining MALDI with MS and MS^n has been used for numerous imaging applications.[19, 26, 46, 64-73] Specifically for small molecular applications, MSI has great potential in the area of pharmaceutical development. However, the limitations of using MALDI for quantitative MSI is the main drawback preventing the technique from being used more readily. To highlight both the possibilities and the limitations of MSI, a whole-body MSI experiment is shown in Figure 1-12.[72] The experiment is designed to determine the distribution of a pharmaceutical in a thin-layer whole-body section of a rat

using MALDI MS/MS. From the optical image, Figure 1-12A, different organs are identified and outlined. The resulting MS/MS image of the drug is produced by plotting the main product ion's intensity (color scale) versus (x,y) position, shown in Figure 1-12B. The MS/MS image of the drug shows distribution differences between organs. Comparing signal from the brain to the bladder indicates the drug is present at a higher concentration in the bladder. However, variations in ion signal may not be directly attributed to increases in concentration, as numerous factors other than concentration may affect the detection ion signal.[7, 72-74] These factors include: tissue-dependent matrix crystallization, ionization, and extraction variations.[75] Consider that the drug could be present in both the bladder and brain at equal concentrations. The bladder consists of mainly smooth hollow muscle tissue (which may contain frozen urine or crystallized uric acid) compared to complex, lipid-rich tissue of the brain. As matrix is applied atop the two areas, the formation of crystals can vary significantly. Also, during the matrix application, the matrix solvent plays a role in extracting the target drug from the tissue and subsequent co-crystallization with the matrix. This extraction between the two tissue types may also vary. Finally, MALDI ionization may also vary significantly between the tissue types, thus making any conclusions about the concentration of the drug uncertain. To verify the MS/MS imaging results, the tissues are typically analyzed via another analytical method which typically involves tissue excision and homogenization, analyte extraction, and separation via chromatography. It also typically involves the creation of matrix-matched calibration samples via the quantitative addition of the drug to control tissue. These steps not only increase analysis time and use more resources, they also lose any spatial distribution information within a given a

tissue type (due to homogenization). For MALDI MSI to be used more routinely as an analytical method, the quantitative limitations must be overcome. The overall motivation for this research is to develop quantitative methods for MALDI MSI through the application of an internal standard to account for MALDI MSI ion signal variability.

Quantitative MALDI MSI Method Development

Nucleus accumbens (NA) excised during a post-mortem autopsy was used for quantitative MSI method development. Two samples were used for analysis, a control sample and one which tested positive for cocaine (COC) during the autopsy. COC is an extensively studied drug of abuse with numerous published methods on the extraction and quantitation from blood and tissue.[79] The ability to perform parallel experiments with well-established methods to quantify COC from brain tissue (as well as it being an exogenous compound) made it an ideal candidate for quantitative MSI development. Deuterated analogs of COC are also readily available and were used an internal standard.

The internal standard in any analytical experiment must behave identically to the target analyte, be uniformly applied, and be detected separately. Isotopically labeled analogs provide near identical chemical characteristic and are considered the best option. The challenge in a MSI experiment is applying the internal standard in a uniform manner to the tissue sample, and this can be overcome using a modified inkjet printer.[66, 76] This uniform application is imperative to control for ion signal variations resulting from variations in the matrix application and MALDI process. In an MSI experiment consisting of numerous spectra collected from a tissue sample, each raster spot can be considered a micro-experiment. To better compare the ion signals within these micro-experiments, normalization of the analyte by the internal standard ion signal

may be used to account for ion signal variations.[39, 71, 77, 78] To perform ion signal normalization, the analyte and internal standard should be detected simultaneously in each MS scan at each raster step. Wide-isolation MS/MS allows for the simultaneous detection of both the analyte and internal standard, and provides the increased specificity and sensitivity from tandem MS.[47]

The experiments presented with COC serve primarily as method development experiments in which the quantitative results can be validated by another analytical method, LC-MS/MS. For LC-MS/MS analysis, the tissue samples were homogenized and extracted and the COC determined by comparison to external calibration standards.[46, 79] These results were compared to quantitative MSI results.

Wide-isolation MS/MS was also evaluated for the quantitative evaluation of the tissue extracts in parallel to the LC-MS/MS analysis of the extracts. These experiments highlight the power of using an internal standard and wide-isolation MS/MS for quantitative MALDI applications.

Differences in the chemical and physical makeup of tissues can directly affect the resulting ion signal in a MSI experiment. The use of a deuterated internal standard was evaluated for the identification of tissue-specific ion suppression and is discussed in Chapter 3. AC and acetyl-d_3-carnitine (d_3AC) were used as the target analyte and internal standard, respectively. Both were applied beneath different tissue types and the resulting ion intensity of AC, d_3AC, and the ratio of AC/d_3AC were monitored.

Piglet Brain Tissue Comparison

The research presented in Chapter 4 applies methods developed in Chapters 2 and 3 to quantitatively determine and compare AC distributions between two piglet brain samples. For the analysis of endogenous AC, the standard additions method of

analysis was used for quantitative estimations. One piglet was fed a normal diet after birth consisting of an average ratio of fat, carbohydrate, and protein. These ratios can vary slightly, but typically the formula is rich in carbohydrates >50% by mass compared to protein and fat. The carbohydrate ratio in the ketogenic formula is significantly reduced to keep the piglet in a state of ketosis, thus mimicking the metabolism of KD therapy. After one week of dieting, the brains were excised and AC content was compared with MSI. Establishing quantitative MALDI MSI methods to make these comparisons would be a significant improvement in the MSI methodology.

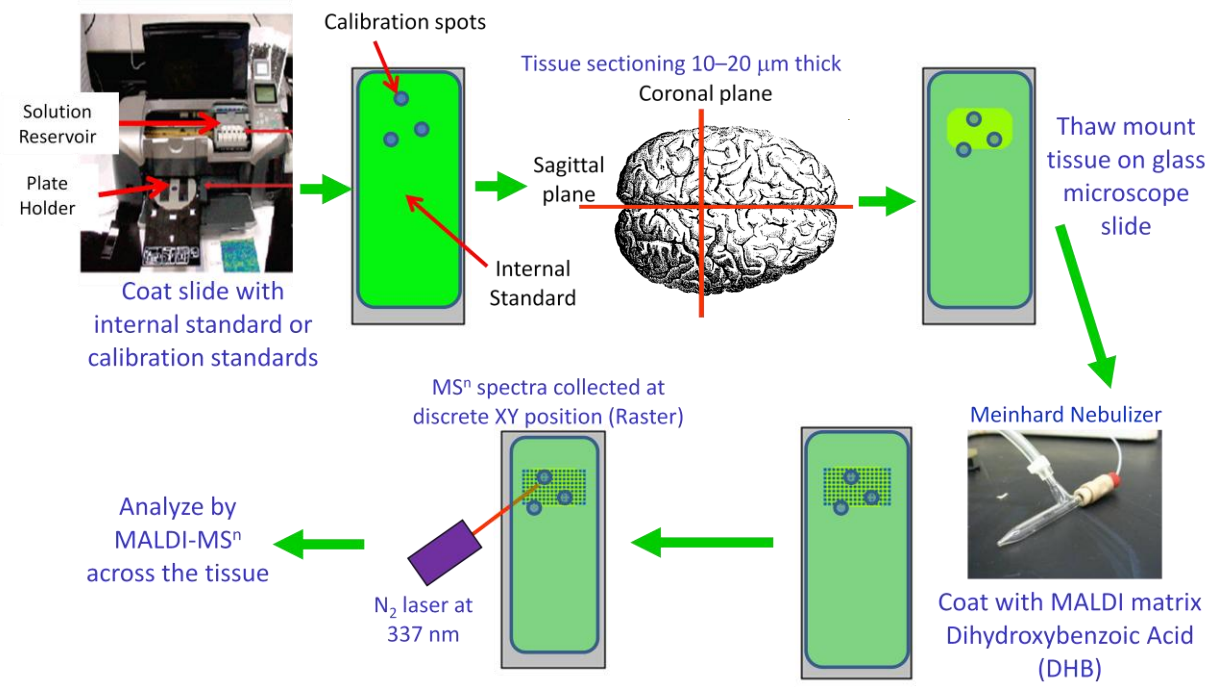

Figure 1-1. Workflow diagram of MSI.

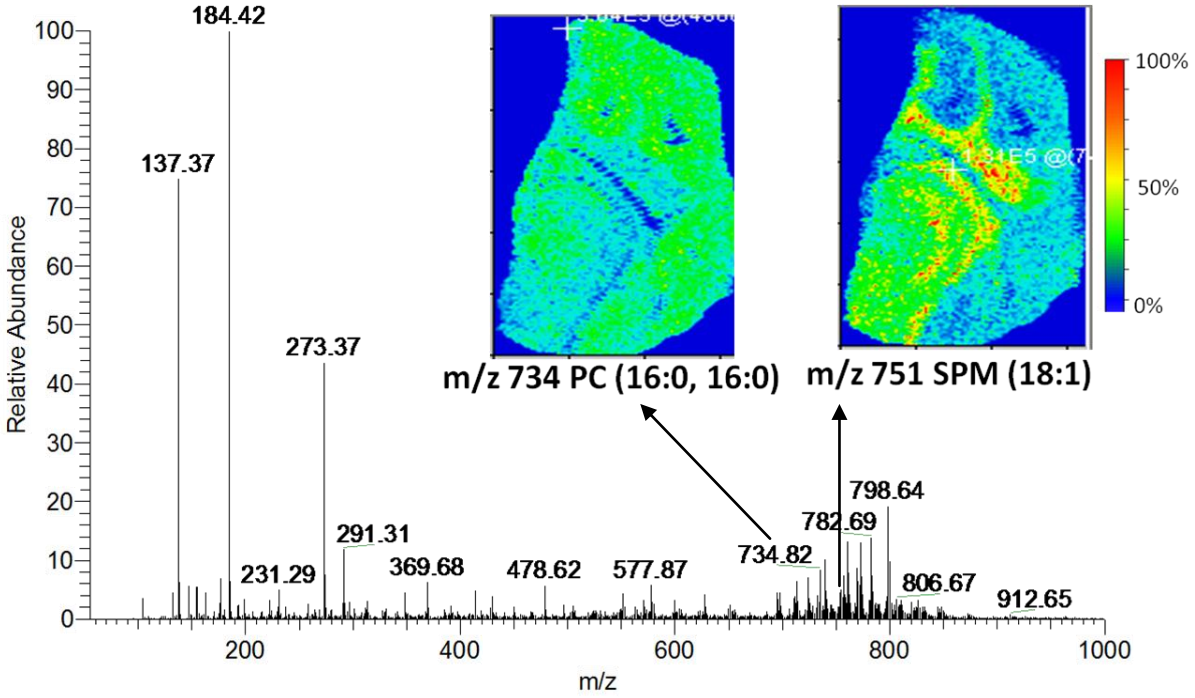

Figure 1-2. Example of MSI from analysis of piglet brain. The intensity of any ion in the mass spectrum can be plotted against (x,y) position to determine its distribution in the tissue sample.

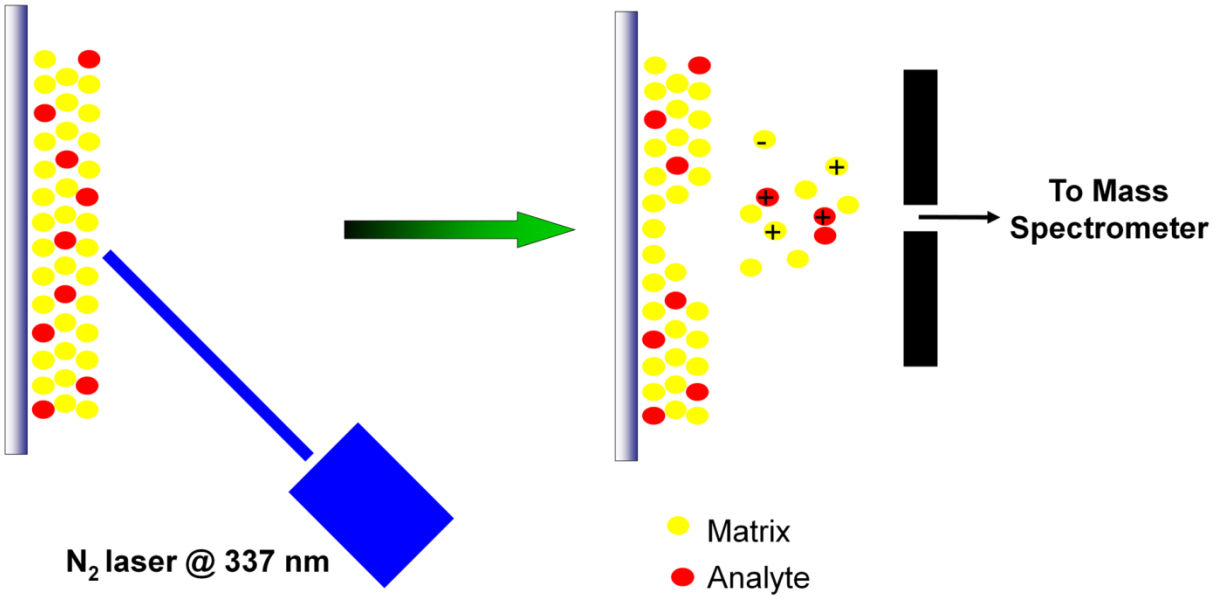

Figure 1-3. Illustration of the MALDI process.

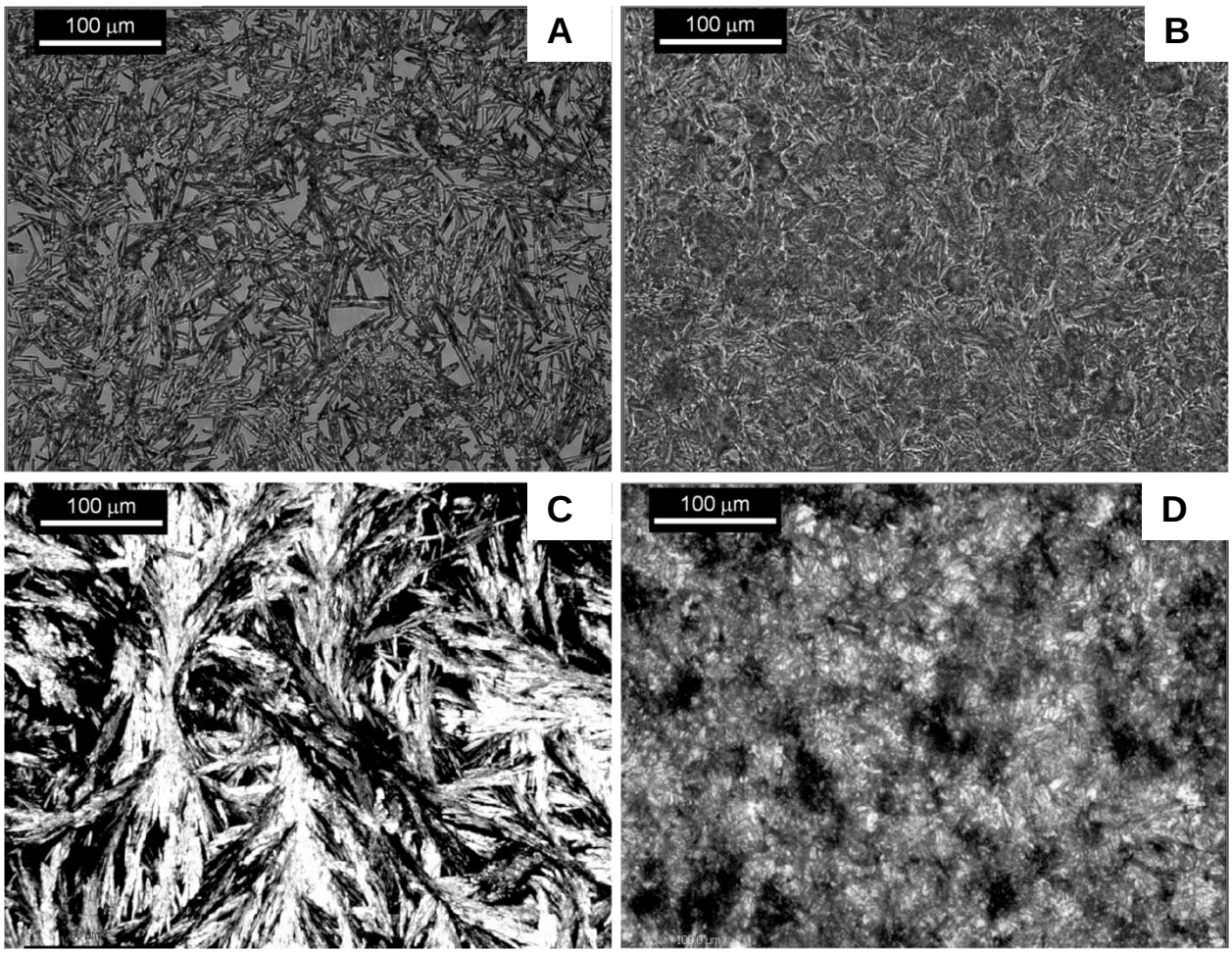

Figure 1-4. Photomicrographs showing differences in DHB crystals. DHB dissolved in different solvents, (a) DHB diluted in 70/30 methanol/water (v/v), (b) DHB diluted in 90/10 chloroform/ethanol (v/v), both applied atop a glass slide. DHB dissolved in different solvents (c) DHB diluted in 70/30 methanol/water (v/v), (d) DHB diluted in 90/10 chloroform/ethanol (v/v), both applied atop piglet brain tissue. Variations in DHB crystals directly affects resulting ion signal. Ideally, DHB would be applied in a uniform manner consisting of small crystals.

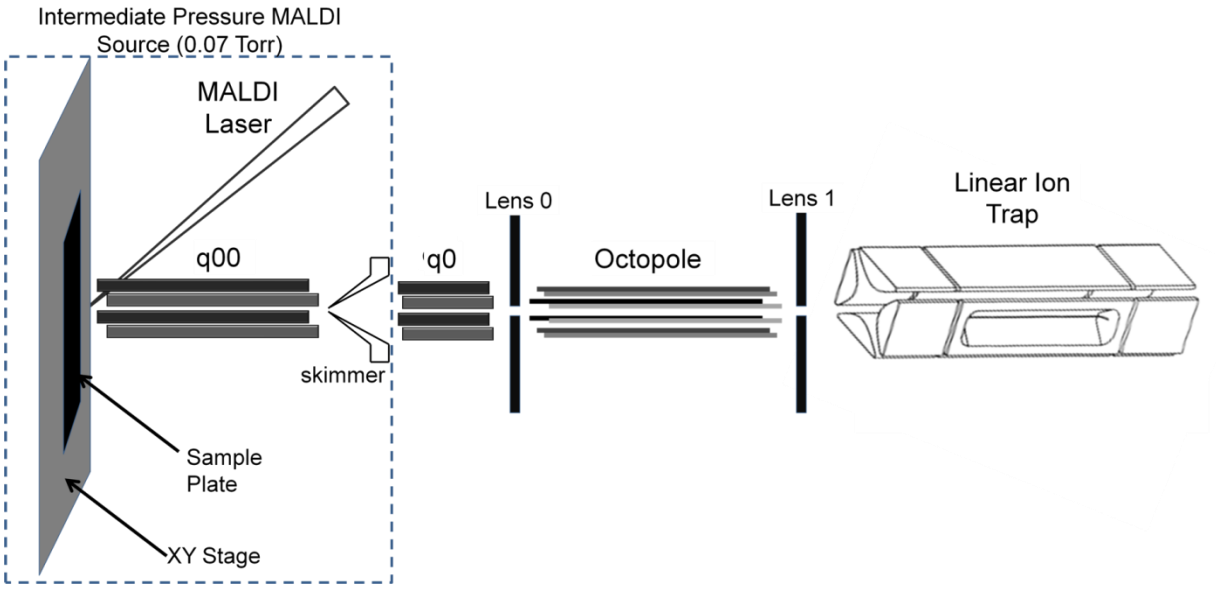

Figure 1-5. Schematic of the Thermo MALDI LTQ XL. Samples are loaded onto an (x,y) stage and rastered beneath the MALDI laser. Position-specific mass spectra are recorded and used to produce an ion-specific distribution image. The LIT offers both MS and MS^n capabilities.[19, 44]

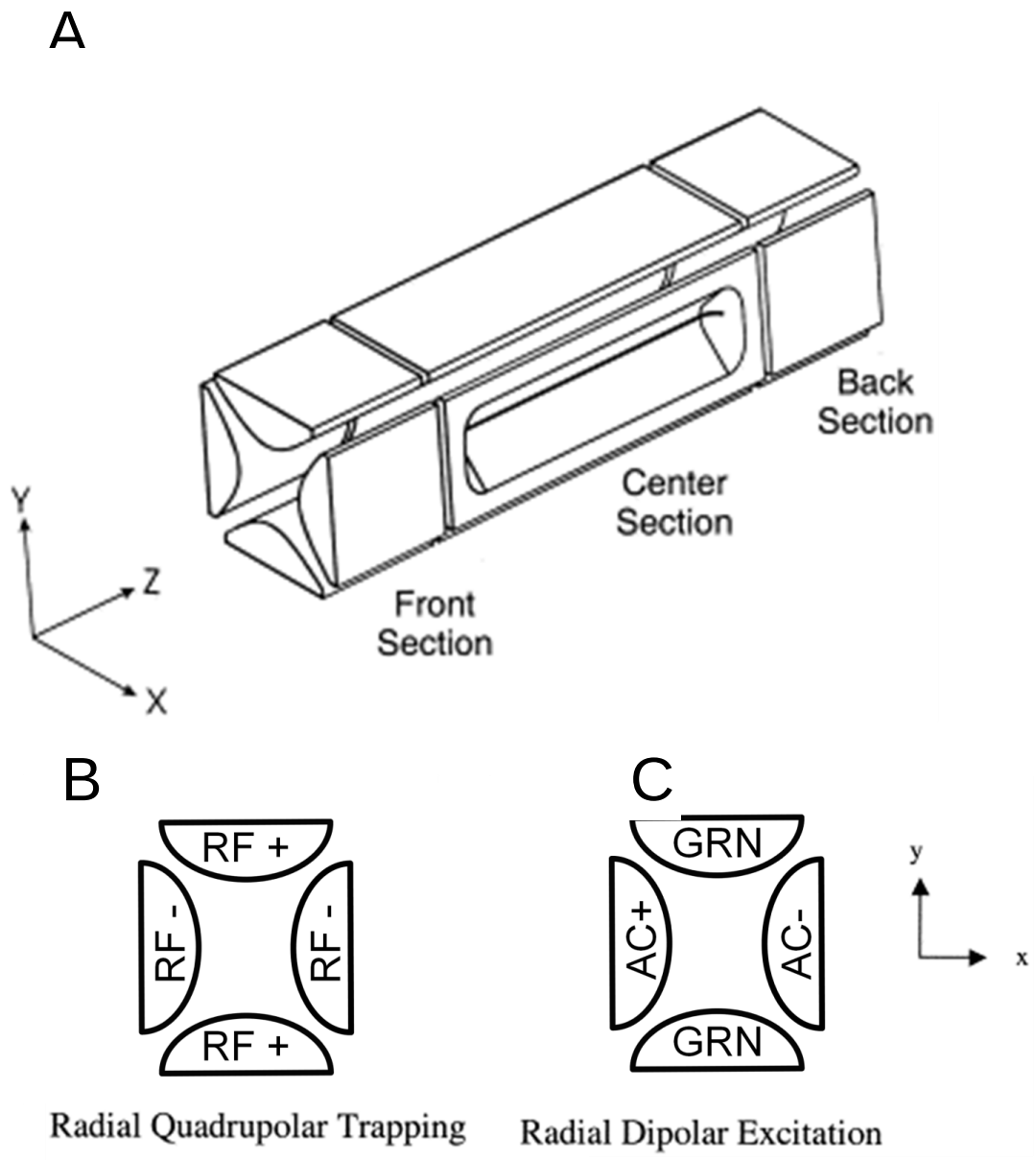

Figure 1-6. Schematic of the LIT. MS or MS^n spectra can be obtained from ions trapped in the center section by applying different RF and AC voltages. (A) LIT (B) Z-axis view and voltages applied for trapping (C) Z-axis view and voltages applied for excitation.

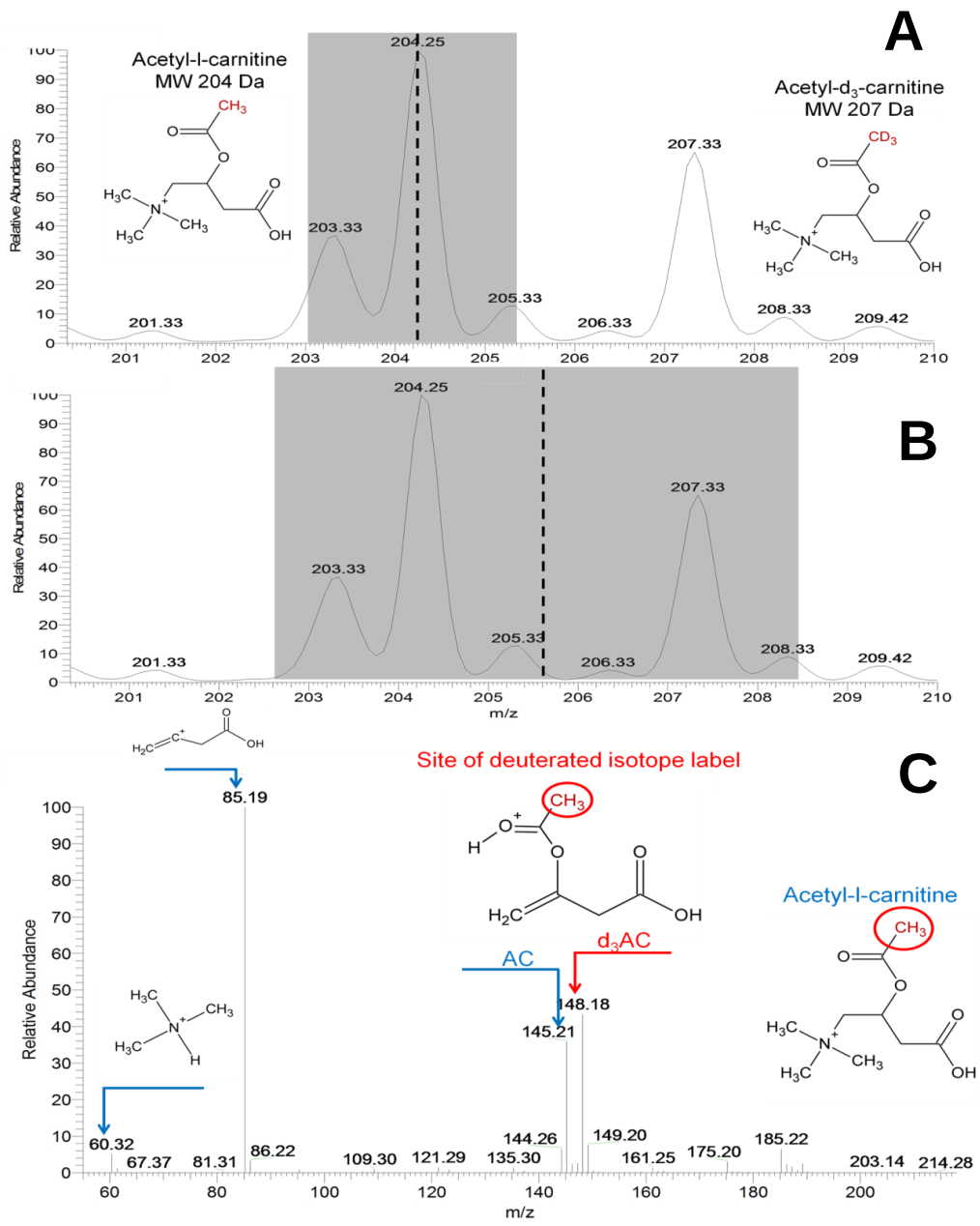

Figure 1-7. Spectra illustrating wide-isolation MS/MS. (A) Narrow isolation window centered at *m/z* 204 ± 1.5 Da employed for MS/MS analysis of AC. (B) Wide-isolation window centered at *m/z* 205.5 ± 3 Da employed for simultaneous detection of AC and d_3AC in a single MS/MS scan, indicated by the shaded window. (C) Product ion spectrum of wide-isolation MS/MS analysis. AC and d_3AC can be differentiated due to the preserved deuterated label in the product ion.

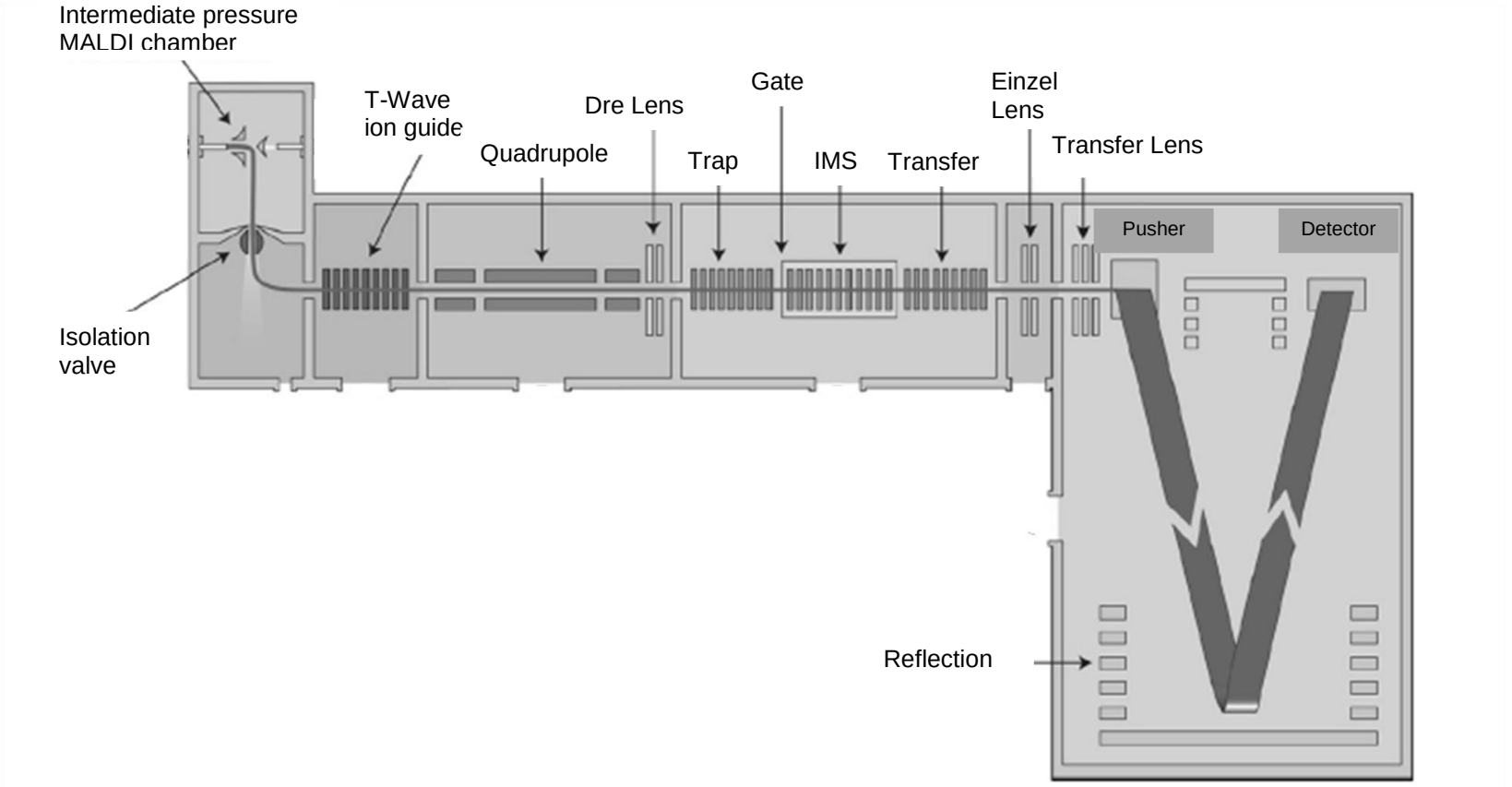

Figure 1-8. Schematic of Waters Synapt QTOF instrument. Modified from Pringle, et al.[49]

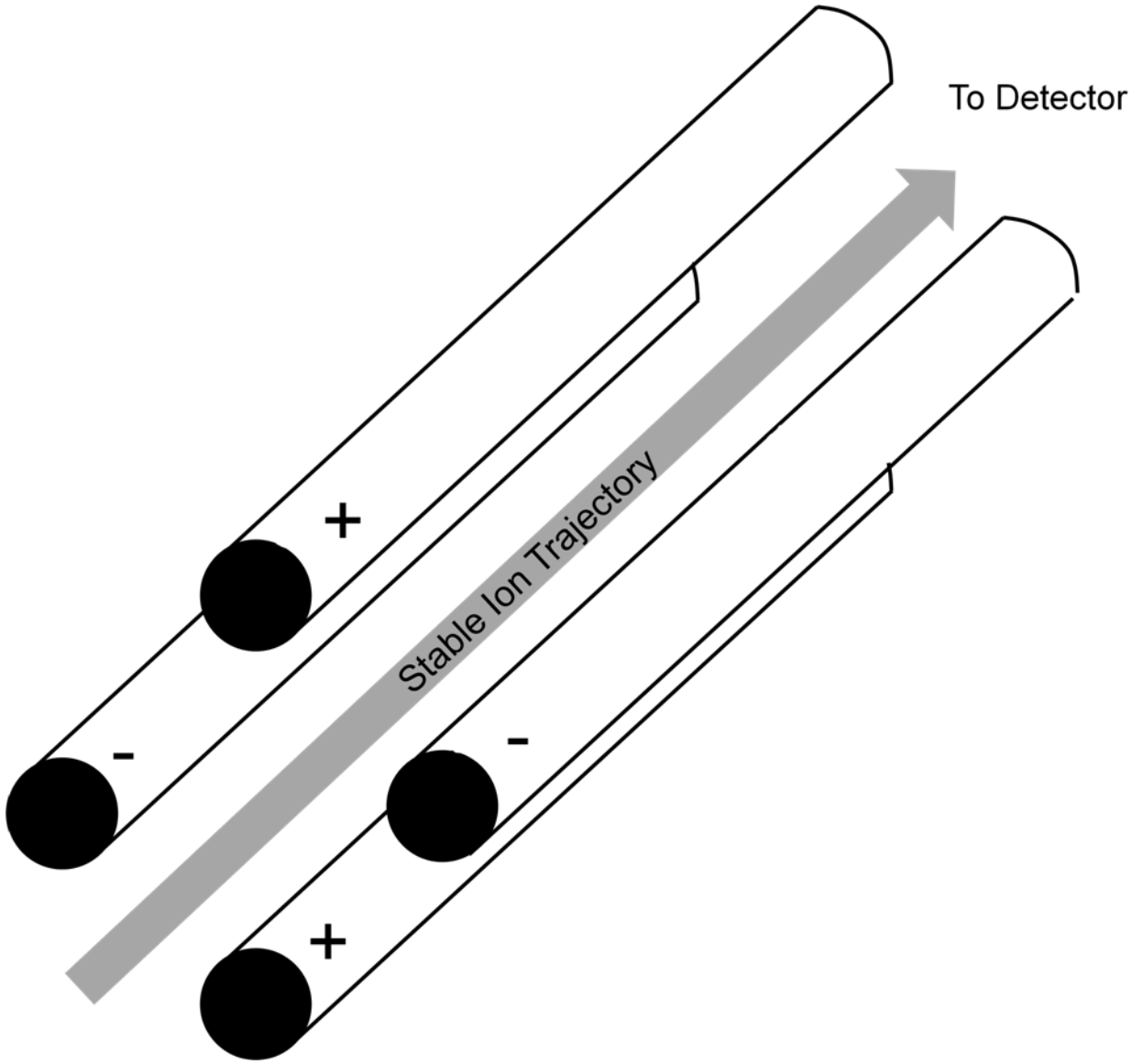

Figure 1-9. Schematic of quadrupole mass analyzer. The quadrupole on the QTOF was used for mass selection prior to CID.

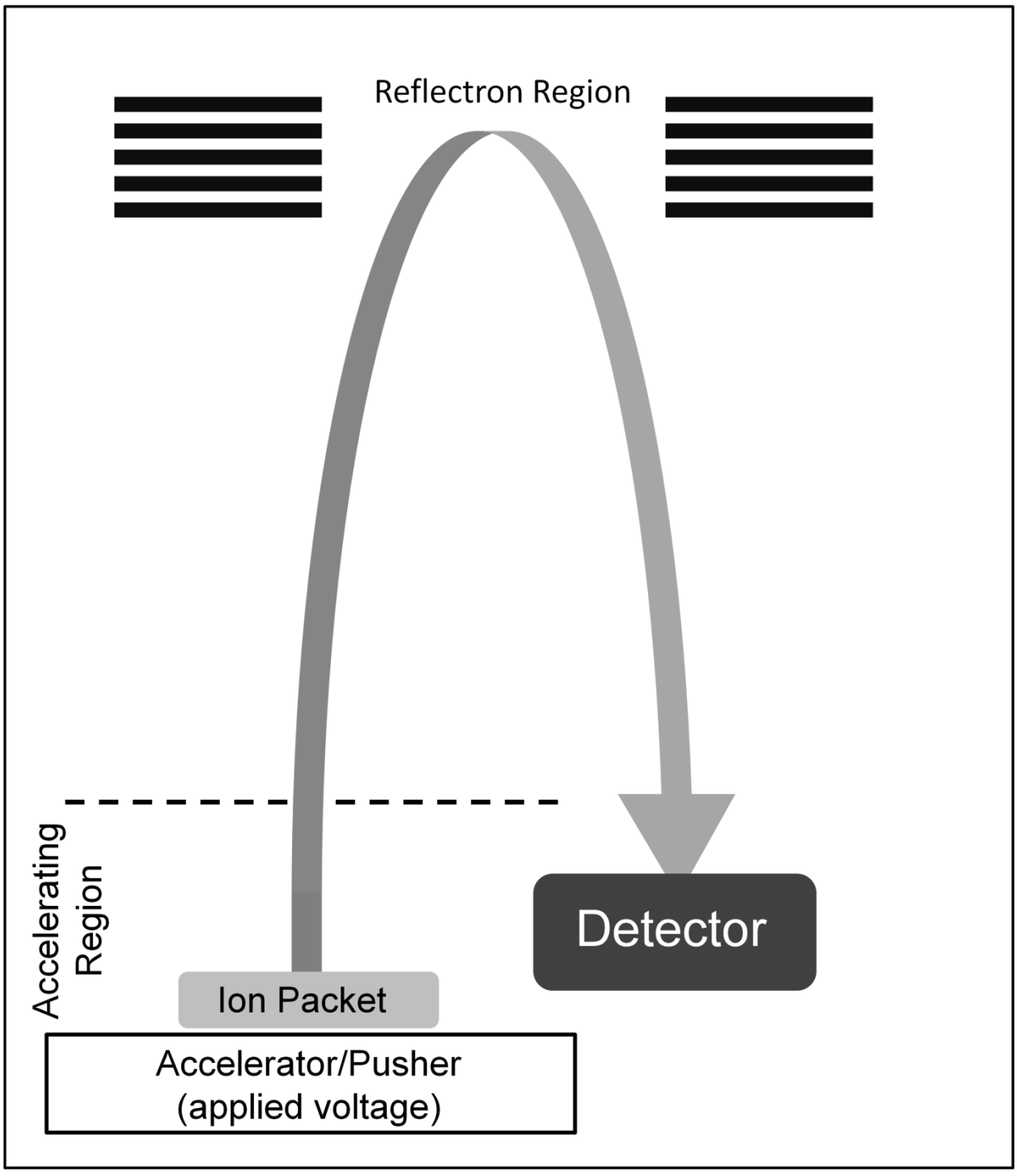

Figure 1-10. Schematic of TOF mass analyzer. Ions are pulsed into the TOF region by an applied voltage on the pusher. All ions have the same kinetic energy, thus smaller ions travel the fixed distance to the detector faster than larger ions.

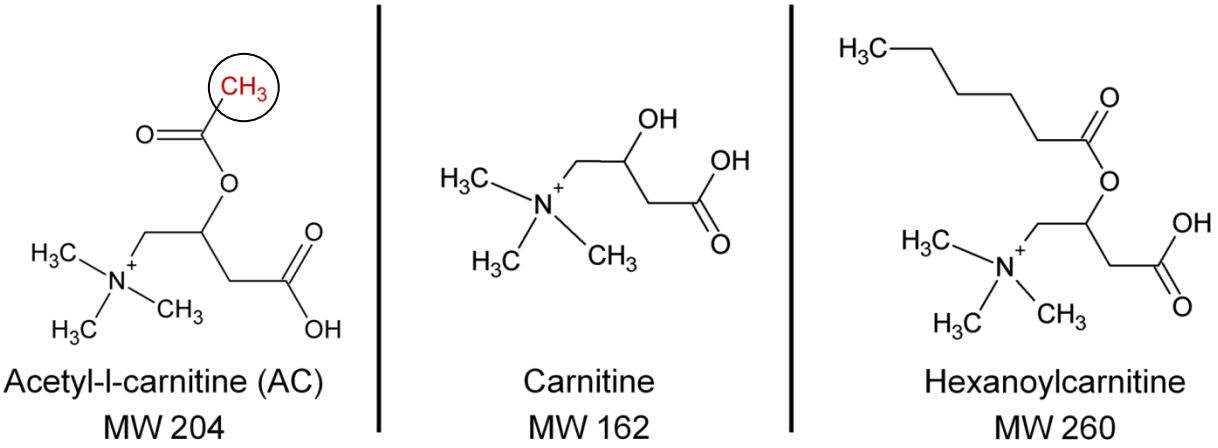

Figure 1-11. Examples of different carnitine compounds. Carnitine's main function is to transport long chain acyl-groups into the mitochondria for β-oxidation. The site of deuteration is circled in the AC structure.

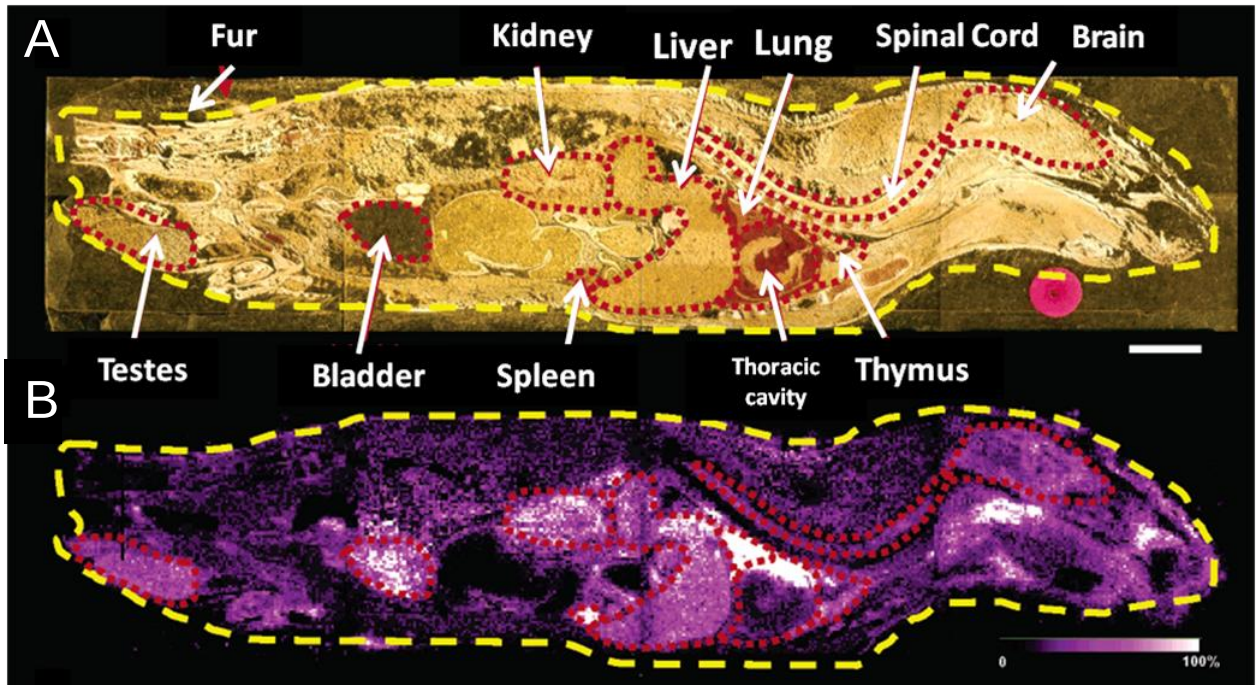

Figure 1-12. Whole-body image of olanzapine distribution in an entire rat. (A) Optical image with identified tissues. (B) MS/MS image of main product ion of olanzapine. Ion intensity is plotted via color gradient, dark areas indicate areas of low ion intensity and white areas indicate areas of higher ion intensity. Modified from Caprioli, et al.[72]

Table 1-1. Summary of common MSI ionization techniques.

Ionization Method	*m/z* Range	Lateral Resolution	Advantages	Disadvantages
SIMS	<1000	<50 nm	Best spatial resolution	Source fragmentation, low sensitivity
LDI	<1000	5–200 μm	Improved sensitivity over SIMS	Source fragmentation
MALDI	50–500,000	10–200 μm	Ionization of large intact biomolecules	Application of MALDI matrix
DESI	<2000	~200 μm	Simpler sample setup, possibly targeted ionization	Poor lateral resolution

CHAPTER 2
QUANTITATIVE IMAGING OF COCAINE FROM BRAIN TISSUE

Introduction To Quantitative MSI

Mass spectrometric imaging (MSI) has rapidly expanded from early applications to protein imaging[8] into numerous compound classes including lipids,[20] pharmaceuticals,[13] and endogenous metabolites.[72] The technique generates two-dimensional (or more recently three-dimensional images) of the distribution and concentration of analytes in a tissue section.[80, 81] The quantitative limitations of MALDI MSI have recently come under scrutiny,[82] as MSI techniques suffer from two major limitations: the inability to control and correct for tissue-specific-ion suppression and the irreproducibility of ion signal from scan to scan. These limitations are caused by numerous factors, including tissue variation, matrix crystal heterogeneity, laser power fluctuations, as well as tissue-specific ion suppression, and preclude in situ quantification.[47, 83] To date, quantitative MSI applications have been limited to relative determinations which require verification from other analytical techniques, such as liquid chromatography tandem-mass spectrometry (LC-MS/MS).[26]

Many quantitative MS analytical techniques rely on internal standards to control for sources of error arising from sample preparation, injection volume irreproducibility, or ion source variability. In most instances, an internal standard is added in a constant amount to the samples being analyzed prior to any additional sample preparation Applying an internal standard to control for the limitations previously listed may improve the quantitative capabilities of MSI. Utilizing an internal standard for traditional MALDI analysis has been shown to improve quantitation;[41, 42, 78, 84] however, these methods simply add the internal standard to the sample droplet, which is not practical in an

imaging experiment. For MSI, the internal standard must be applied uniformly to the tissue. In this work, the internal standard was applied via a modified inkjet printer.[76] Application of an internal standard by inkjet printer has been shown to produce a uniform internal standard layer at a given concentration (Chapter 4). To best mimic the extraction of an analyte from the tissue, the internal standard was applied beneath the tissue (to the glass sample slide before placing the tissue), which then was extracted through the tissue and into the matrix crystals. For the quantitative analysis of cocaine (COC) in brain tissue, deuterated cocaine (d_3COC) was used as an internal standard. Deuterated analogs routinely perform best as an internal standard as they have nearly identical chemical characteristics as their unlabeled counterparts. Applying an internal standard in this manner is shown in Chapter 4 to improve scan-to-scan reproducibility and calibration curve linearity for quantitative imaging applications.

Recently, an MSI experiment reported the quantitative tiotropium bromide distribution in lung tissue.[65] The quantitative estimations were made based on calibration standards pipetted atop a control tissue slice and comparing the signal of the calibration standard to the positive sample. Spotting standards atop a tissue section may not accurately reflect the drug's signal from within the tissue, as the analyte's extraction efficiencies may vary. Also, comparing the signal from two separate tissues sections may be challenging due to differences in thickness, tissue composition, and matrix coating variations. These experiments, however; do show progress in the area of quantitative MSI, as the authors were able to produce a linear calibration curve from the spotted samples, from which they were able to determine a quantitative estimation of the administered drug.

Another recently published study by Murphy[18] examined the relationship between MALDI MSI signal and lipid concentrations in brain tissue and succeeded in making relative quantitative comparisons between MSI and LC-MS results. However, these comparisons were not made before extensive signal normalization and baseline correction, indeed the authors concluded that MSI results are taken with caution due to the complex environment of direct tissue analysis.[74]

To further improve MSI quantitation, normalizing the target analyte ion signal to an internal standard's ion signal was suggested to improve quantitation and help identify tissue-specific ion suppression.[85] Scan-by-scan normalization by a deuterated internal standard for MALDI MSI is shown to improve single reproducibility (Chapter 4), improve image quality and significantly improve the quantitative ability of MALDI MSI.[47] The internal standard must have similar extraction, co-crystallization, and ionization properties as the target analyte for quantitation, thus a deuterated analog is an ideal option. The internal standard may be applied to the tissue in 3 ways: (1) apply a mixture of the internal standard and MALDI matrix to the tissue (2) apply an internal standard atop the tissue prior to applying the matrix[73] and (3) apply the internal standard beneath the tissue sample prior to placing the tissue and applying the matrix. Applying the internal standard along with the matrix does not accurately reflect tissue-specific ion suppression, as the internal standard may not mimic the ionization efficiency of a target analyte being extracted and detected from the tissue, as shown in Chapter 3. Also, if the matrix is applied manually, there may be uneven matrix/internal standard application, resulting in unaccountable analyte to internal standard ratio differences. Applying an internal standard atop the sample may not accurately reflect the analyte

being extracted from within the tissue sample as the internal standard may reside atop the tissue. Applying the internal standard beneath the sample may best reflect the detected ion signal of the target analyte. Both analyte and internal standard must be extracted and co-crystallized from the tissue sample. This approach has been shown to help control for tissue variation as well as extraction differences from different tissue types, shown in Chapter 3. Lastly, due to the significant amount of signal variation in MALDI, the internal standard and analyte should be detected in the same analytical MS^n scan. Detecting the analyte and internal standard in separate MS scan has been shown to offer no quantitative advantage due to the signal variation form the MALDI process.[47] For MS applications, this is easily done by detecting a mass range large enough to incorporate both ions; however, for tandem mass spectrometry (MS/MS) applications a wide-isolation window must be utilized.[47] From the structure of COC shown in Figure 2-1, the location of the deuterated label allows for differentiation between COC and d_3COC when using MS/MS. By combining the advantages of a uniformly applied internal standard beneath a tissue sample with the specificity of wide-isolation MS/MS with scan-by-scan COC to d_3COC normalization,[47] absolute quantitative MSI was performed for the analysis of COC in a brain tissue section. These results were compared to LC-MS/MS and MALDI MS/MS results from tissue extracts of the same brain sample.

Experimental

Chemicals

Standards of COC (MW: 303) and d_3COC (MW: 306) were purchased from Ceriliant (Round Rock, TX, USA). Superfrost glass plus microscope slides and LC-grade methanol (MeOH), acetonitrile (ACN), and water (H_2O) were purchased from

Fisher Scientific (Pittsburgh, PA, USA). Stainless steel microscope slides were purchased from Thermo Scientific (San Jose, CA, USA). For MSI analysis, working standards of COC and d_3COC were diluted to 10 ng/μL in ACN used for LC analysis and 10 ng/μL in 50/50 MeOH/ H_2O (v/v) used for MSI . Calibration standards of COC used for MALDI imaging were made to 0.030, 0.060, 0.13, 0.25, and 0.50 ng/μL in 50/50 ACN/H_2O (v/v) and 1 μL of each calibration standard were pipetted onto a stainless steel microscope slide prior to the d_3COC application. Tissue concentrations were estimated from the area of the detected signal and the thickness of the tissue, assuming the density of wet tissue is ~1.0 g/mL. The MALDI matrix 2,5-dihydroxybenzoic acid (DHB) was purchased from Acros Organics (Geel, Belgium) and prepared to a concentration of 20 mg/mL in 70/30 MeOH/H_2O (v/v).

For LC, working standards of COC were prepared to 0.50 and 5.0 ng/μL and working standards of d_3COC were prepared to 0.50 ng/μL. Calibration standards were spiked into control brain tissue during tissue homogenization at concentrations of 50.0, 100, 200, 400, 1,000, and 2,000 $ng_{COC}/g_{wet\ tissue}$ and the internal standard was spiked at 40 $ng_{d3COC}/g_{wet\ tissue}$.

Tissue Preparation for MSI

For quantitative MSI, calibration standards of COC in MeOH/H_2O were pipette onto a microscope slide and allowed to dry under ambient conditions. An Epson (Long Beach, CA, USA) Stylus R280 was used to apply 3 coats of the d_3COC in MeOH/H_2O to the microscope slides. Positive and negative control samples of the nucleus accumbens excised from the brain were provided by the El Paso County Coroner's Office in Colorado Springs, CO. The nucleus accumbens was extracted during autopsy,

snap frozen in liquid nitrogen and stored at −80 °C. Sectioning of the brain tissue was performed on a Microm HM 505E cryostat (Waldorf, Germany). Tissue was sliced at −25 °C to a thickness of 20 μm and thaw mounted onto the microscope slides previously coated with COC calibration standards and d_3COC. DHB was then applied to the tissue samples using the inkjet printer.[76]

MSI Quantitation

For the MSI experiments, all mass spectrometric images were acquired with either a Synapt MALDI-Q-Ion Mobility (T-wave cell) Time of Flight (QTOF) equipped with a 200 Hz, 335 nm, Nd:YAG laser at a frequency of 200 Hz and spot diameter of 150 μm (Waters Corporation) or a MALDI LTQ XL equipped with a 60 Hz, 337 nm, nitrogen laser with a spot diameter of 100 μm (Thermo Corp. San Jose, CA, USA). The QTOF instrument was operated in MS/MS mode with the resolution of the quadrupole decreased to include the $[M+H]^+$ ions of both COC (*m/z* 304) and d_3COC (*m/z* 307) prior to fragmentation through collisions with He. Sample slides were inserted into the vacuum chamber and rastered beneath the laser at a step size of 250 μm, with a laser spot size of 100 μm. Wide-isolation MS/MS spectra were summed from 200 laser shots at each raster step. For MS/MS imaging experiments on the LTQ, the isolation window centered at *m/z* 305.5 ± 3 to trap the $[M+H]^+$ ions of both COC and d_3COC prior to fragmentation.. Upon insertion of the samples into the vacuum chamber, the sample was rastered beneath the laser at a step size of 250 μm, with a laser spot size of 100 μm. Wide-isolation MS/MS spectra were collect using 8 laser shots at each raster step. The ions of interested were fragmented in both instruments by collision-induced dissociation (CID) and the fragments of each precursor ion were monitored; COC *m/z*

304→182 and d_3COC *m/z* 307→185. Resulting MS/MS data from the QTOF were processed using BioMap (Novartis, Basel, Switzerland) and images from the LTQ were processed with QualBrowser (Thermo Scientific, San Jose, CA, USA) and Surfer 8 (Golden, CO, USA). Normalized images were generated using the divide function in BioMap to generate COC/d_3COC (*m/z* 182/185) images. By plotting the ratio of *m/z* 182/185 versus position, normalized images from the LTQ were generated in Surfer 8 from data extracted from QualBrowser. For quantitative determinations of COC, a standard additions method analysis was performed utilizing the product ion ratio of COC/d_3COC from the spotted COC calibration standards beneath the positive tissue. Quantitation by external calibration was also performed with calibration standards spotted beneath a control tissue section and a quality control (QC) standard of COC (0.25 ng/μL) spotted beneath a positive tissue section to ensure ion signal was comparable between tissues. The resulting signal from the COC was compared to the calibration curve calculated from the control tissue. All quantitative MSI data was then compared to LC-MS/MS and MALDI-MS/MS data from extracts of the brain tissue

Tissue Extraction/Quantitation

Nucleus accumbens samples were extracted using manual tissue homogenization and solid-phase extraction (SPE) according to the procedure published by Lowe et al.[79] Two 100 mg sections of the positive COC tissue samples were dissected and extracted. The extracts were compared to calibration sample extracts from 100 mg sections of the negative control sample. The total sample makeup was two positive samples, six calibration samples, and one negative control sample. Calibration samples were prepared at the concentrations previously stated and following SPE, the samples were

reconstituted in 100 μL of H_2O/ACN 90/10 (v/v). A 5-μL aliquot was taken for wide-isolation MALDI-MS/MS analysis. The remaining 95 μL of each sample was submitted for triplicate LC-MS/MS analysis on a Thermo Finnigan TSQ 7000 triple quadrupole mass spectrometer (QqQ) equipped with an Agilent 1100 LC system (Santa Clara, CA, USA). Mobile phase A was composed of H_2O with 0.1% formic acid and mobile phase B was composed of ACN with 0.1% formic acid. A gradient LC program was utilized starting with 5 minutes of 10% B, then a ramp up to 90% over 8 minutes with a 3 minute hold at 90%, and re-equilibrated for 3 minutes at 10% B. A 5-μL aliquot of each extract were loaded onto the LC column followed by MS/MS analysis by positive-mode electrospray ionization (ESI) and multiple reaction monitoring for COC (*m/z* 304→182) and d_3COC (*m/z* 307→185) for quantitative analysis.

MALDI-MS/MS of the 5-μL aliquots was performed with a Thermo Scientific MALDI LTQ XL utilizing a wide-isolation window centered at *m/z* 305.5 ± 3 Da with scan-by-scan COC to d_3COC. From the 5-μL aliquot, 1 μL of each sample (2 positive samples, 6 calibration samples, and 1 negative control) was spotted in duplicate onto a glass plus microscope slide. 40 mg/mL of DHB dissolved in MeOH/H_2O 70/30 (v/v) was applied uniformly to the slide utilizing a Meinhard nebulizer (Golden, CO, USA) at a flow rate of 2.4 mL/min. Within each spotted sample, two areas of 50 MS scans were analyzed by MALDI-MS/MS with a step size of 200 μm, laser energy of 14 μJ, and 8 laser shots per step. This resulted in quadruplicate analysis of each sample. From each 50-scan MS/MS experiment, the extracted ion current for COC (*m/z* 304→182) and d_3COC (*m/z* 307→185) were plotted using data extracted to Microsoft Excel from QualBrowser.

From each MS/MS experiment, the ratio of *m/z* 182/185 was calculated, averaged, and used for quantitation.

Results and Discussion

For successful quantitation of COC from brain tissue by MSI, results from imaging experiments must be validated with quantitative results using accepted quantitative analytical techniques such as LC-MS/MS. Four requirements have been suggested[86] for successful quantitation of small molecules by MALDI: a high repetition rate laser (for analysis with a QqQ), tandem MS (for increased selectivity), sample cleanup (for proper co-crystallization), and an internal standard (for increased precision). In these MSI experiments, these requirements were addressed by employing wide-isolation MS/MS imaging experiments that allow for scan-by-scan MS/MS ion signal normalization of the COC ion signal by the internal standard ion signal, d_3COC. With wide-isolation MS/MS, the advantages of MS/MS are preserved (improved selectivity and sensitivity) while also improving MALDI quantitation and ion signal reproducibility through the scan-by-scan normalization of the analyte to internal standard.[47] Scan-by-scan ion signal normalization circumvents the need for a high repetition rate laser and has been shown to improve signal reproducibility five-fold (Chapter 2). Co-crystallization of the target analyte (COC) and internal standard (d_3COC) has been enhanced by applying the MALDI matrix in a uniform manner with an inkjet printer.[76] In MSI, co-crystallization of the target analytes can also be enhanced by improved extraction of the analyte from the tissue with the matrix solvent. Improving the extraction and co-crystallization of the target analytes can lead to improved sensitivity. In this study, we show extraction of spiked COC and d_3COC from beneath the tissue; however, this extraction could be

further optimized by evaluating other matrix solvents and the effect of tissue thicknesses.

Quantitative Detection of COC by MS/MS Imaging

Adapting a wide-isolation MS/MS approach from the LTQ to the QTOF, allowed for simultaneous MS/MS detection of COC and d_3COC, as shown in Figure 2-2. For the QTOF, this was accomplished by decreasing the resolution of the resolving quadrupole to include both COC (*m/z* 304) and d_3COC (*m/z* 307) after CID, product ions from both are detected in the MS/MS spectrum (COC, *m/z* 304→182; d_3COC, *m/z* 307→185).

Prior to performing quantitative imaging on a tissue experiment, the instrumental parameters, laser energy (LE) and laser shots (LS) were optimized for wide-isolation MS/MS analysis of a mixture of COC and d_3COC. More important than the optimization of LE and LS, was the identification that the internal standard can account for signal variation arising from laser energy fluctuations. Ion signal can be altered with variations in both the number of LS and the amount of LE at each raster position. Plots of these changes are shown for varying LS and LE are shown in Figure 2-3 and Figure 2-4; respectively. Although the signal may change significantly with these changes in instrumental parameters, the detected A/I is preserved, indicating the d_3COC is similar in ionization behavior to that of COC.

The tissue imaging experimental setup for the quantitative detection of COC is illustrated in Figure 2-5. Calibration standards were spotted onto a MALDI target followed by the uniform application of the internal standard, d_3COC. Tissue is then placed over that standards and coated with MALDI matrix. Images and quantitative analysis were produced from either the intensity of *m/z* 182 or the ratio of *m/z* 182/185 intensity determined from the MS/MS spectrum, illustrated in Figure 2-6. The MS/MS

images of the product ion intensity of *m/z* 182 (Figure 2-6 A), the normalized COC/d_3COC (*m/z* 182/185) image (Figure 2-6 C), and the corresponding standard additions plots (Figures 2-6 B and 2-6 D, respectively) were generated from the wide-isolation MS/MS experiment performed on the positive COC section of NA. Normalizing the COC/d_3COC ion signal ratio for quantitative analysis improved the linear correlation coefficient (R^2) while decreasing the width of the 95% confidence limits by a factor of two and decreasing the uncertainty in the best-fit slope from ±100% to ±40%. These improvements are a reflection of the improved ion signal reproducibility observed when monitoring the ion signal ratio of analyte to internal standard

Analysis of three serial sections with the QTOF by standard additions, exemplified in Figure 2-6, yielded an average COC concentration of 240 ± 100 ng/g_{tissue}. The improvements in calibration curve linearity and signal reproducibility from normalizing by the internal standard is attributed to an improvement in scan-to-scan reproducibility as well as controlling for extraction and ionization variability resulting from tissue makeup differences across the sample. Scan-to-scan signal variation and back extrapolation to the x-axis contribute significantly to the calculated error. Also, error in the calculated concentration of the spotted COC standards can affect the resulting quantitative COC determination. The calculated COC tissue concentration of standards relies on two assumptions: (1) the spotted COC is distributed evenly throughout the 20-μm thick tissue section and (2) the diameter of the COC remains consistent for the calibration spots (minimal lateral diffusion). How evenly the spotted COC standard is distributed through the tissue has proven difficult to determine; however, shown in Figure 2-6 signal was detected in areas of the spotted COC standards indicating extraction. To estimate

this extractions, d_3COC signal detected from the tissue was 1–2% of the detected d_3COC signal from the slide alone. However, this reduction in ion signal may not correlate well to extraction efficiency due to ionization efficiency differences from the slide and tissue. Standards of COC could also be spotted atop the tissue; however, this also may not accurately reflect extraction efficiency of standards spotted beneath tissue as the spotted COC atop tissue may reside atop the tissue and not distribute evenly through the thickness of the tissue sample. Scan-by-scan normalization by a deuterated internal standard that has also been extracted through the tissue is the best method of signal normalization and quantitation, as the internal standard behaves similarly to the target analyte in terms of extraction, co-crystallization, and ionization efficiency.

Concentration of COC was also measured by comparing the COC/d_3COC signal ratio from the positive tissue to the spotted COC standards beneath a control section of tissue (external calibration). The resulting calibration plot with the MS/MS ion ratio of *m/z* 182/185 is shown in Figure 2-7. The spotted concentration of the applied QC from the positive sample was determined to be ~4000 ng_{COC}/g_{tissue}. This concentration was determined from the area of the applied COC standard assuming even extraction into the 20-μm thick tissue. Calculating the concentration of the QC sample from calibration curve generated from the control tissue by using the *m/z* 182/185 ion ratio averaged over the entire area of the QC COC spotted standard resulted in a calculated concentration of 4100 ± 400 ng_{COC}/g_{tissue}, indicating that the MS/MS ion signal ratios from the two tissues are comparable. This is important in quantitative MSI, as different tissue composition, variations in tissue thickness, inconsistent matrix application, and

uneven internal standard concentrations can all affect the detected ion signal. Four areas from the positive sample were integrated and compared to the calibration curve generated from the control tissue. This resulted in an average concentration of ~400 ± 50 ng_{COC}/g_{tissue}. Error in calculation of the spotted COC standard concentrations in tissue may also contribute to error in the determined COC concentration from the positive sample, as stated previously.

The MSI results from the QTOF were compared to similar experiments performed on the LTQ. The same sample preparation protocol was followed and similar instrument settings were utilized, except that the isolation window on the LTQ was centered at *m/z* 305.5 ± 3 AMU which allowed for trapping the $[M+H]^+$ ions of both COC and d_3COC simultaneously. An example of the resulting ratio MS/MS image of COC to d_3COC (*m/z* 182/185) is shown in Figure 2-8A and the resulting standard additions plot in Figure 2-8B which yielded a COC concentration of 550 ± 1000 ng/g_{tissue}. The large error in the 95% confidence interval, compared to Figure 2-8B, is due to the high signal variation as well as the error in back extrapolation to the x-axis. However, we report fairly good linearity (R^2 = 0.9853) from the spiked calibration standards. Analysis of three serial sections by standard addition from the MSI experiments with the LTQ yielded an average concentration of 880 ± 300 ng/g_{tissue}: A summary of the MSI analyses from both the LTQ and QTOF is shown in Table 2-1 and Table 2-2, respectively.

The MS/MS images from the LTQ were similar to those obtained with the QTOF; however, a significantly large amount of error was observed in these measurements. The differences in error between the two instruments may be attributed primarily to the

ion source. MSI analysis with the QTOF was performed with a significantly more powerful solid state 200 Hz, frequency tripled Nd:YAG laser fired 200 times at each raster step. This resulted in nearly complete ablation of the 20-μm thick sample, resulting in all the tissue ablated and analyzed as indicated by the visual ablation of tissue at each raster position. MSI analysis with the LTQ equipped with a 60 Hz, nitrogen laser on the LTQ and was fired only 8 times per raster step and, resulted in no visible damage to the tissue after MSI analysis and indicated a thin layer of sample was interrogated. More laser shots and energy could not be used on the LTQ for numerous reasons. Since the LTQ is an ion trap, space-charging within the trap is always a limitation; however, previous experiments in our lab have shown this effect to be minimal when employing MS/MS and can further be reduced by employing "injection waveforms" which selectively inject ions into the trap based on the mass range of analysis. Another reason is the inability to sum spectra over hundreds of laser shots in a practical manner. Summing spectra with TOF instruments is routinely performed to increase ion signal and reduce background noise; however, the lower repetition rate of the LTQ laser combined with a slower scan speed of the ion trap inhibit this summing ability. The last and arguably the most limiting factor limiting the sample size consumption on the LTQ is the ablation of the MALDI matrix. Previous analysis in our lab, has shown that a limit exists on the number of analyses which can be performed on a given tissue with matrix applied[66]. As the matrix is ablated away, ion signal is decreased significantly over subsequent analyses. More MALDI matrix can be applied and ion signal restored; however, this is not a practical experiment for tissue imaging. This effect was not observed with the QTOF instrument as the spectra were summed

from the 200 laser shots at each raster position and subsequent analysis was impossible due to the complete ablation of the sample

LC and MALDI Quantitation From Tissue Extracts

Sections of the nucleus accumbens (~100 mg) were dissected and extracted according the procedures previously outlined. The extracts were analyzed by both MALDI wide-isolation MS/MS with scan-by-scan COC to d_3COC normalization and LC-MS/MS with a QqQ. MALDI has been previously employed successfully to quantify small molecules[41, 42, 78, 84]; however, these experiments were not performed with scan-by-scan normalization of the analyte and internal standard signal. Employing wide-isolation MS/MS for analysis of the tissue extracts with scan-by-scan COC to d_3COC normalization on the LTQ resulted in a significant improvement in signal reproducibility for each calibration standard. The average relative standard deviation (RSD) of the 50 MS/MS scans for the sample spots analyzed was 45% for COC (*m/z* 182) ion intensity. By normalizing the COC intensity of each MS/MS scan by the d_3COC signal (*m/z* 185), the average RSD was reduced to 17% across the spotted tissue extracts. We have previously shown this signal variation in both the COC and COC/d_3COC ion signal is primarily due to matrix crystal differences across the area of the sample being analyzed, shown in Chapter 4.

Table 2-3 compares the analytical performance of MALDI wide-isolation MS/MS to LC-MS/MS of the same tissue extracts as well as the quantitative values determined via MSI. It is informative to compare MALDI quantitative results (MSI and tissue extracts) to LC-MS/MS experiments with MRM from a QqQ, as this is a well characterized quantitative analytical method. An example of the LC-MS/MS chromatogram emplolying MRM is shown in Figure 2-9. The calibration curves produced form the two

experiments are shown in Figure 2-10. A nearly ideal slope (~1.0) was observed from the LC-MS/MS experiment, indicating a linear instrument response factor to increasing analyte concentration. The deviation of the slope from 1.0 with MALDI may be attributed to background signal from the matrix or interfering compounds from the extracts, since no chromatographic method was used prior to MS analysis of the extracts. Another factor contributing to the non-unity slope with MLADI may be the varying matrix to analyte ratio (M/A) of the analyte within the calibration standard concentrations. Varying the M/A ratio has been previously shown to have non-linear effects on ion signal across a broad range of concentrations.[34] This effect was evaluated by applying different amounts of matrix to the samples, as shown in Figure 2-11. The amount of matrix could not be precisely determined due to spray-coating; however, the time for spray-coating was doubled from 30 seconds to one minute and double again to two minutes to increase the amount of DHB applied. This resulted in a calibration curve differences attributed to varying M/A of the calibration standards of COC. There appears to be an optimal range of the M/A ratio to produce adequate quantitative results. Standardizing the matrix application with automated matrix addition instruments (e.g., and inkjet printer or Bruker ImagePrep) would allow for a more reproducible matrix addition in a uniform manner. More importantly, using the best linear MALDI calibration curve, COC concentration from the tissue extracts with MALDI-MS/MS were similar to concentrations (within error) of COC from the brain samples determined by LC-MS/MS.

Including spotting the samples (two spots of 1 μL) and quadruplicate MALDI-MS/MS analysis of each scan, the total experiment time was less than 1 hr. Comparing

this to LC-MS/MS experiments, the LC gradient for each sample was 18 min with a total triplicate analysis time of ~13 hr including the analysis of solvent blanks to determine carryover. The total sample size for each MALDI analysis was 2 μL of the tissue extract compared to the 15 μL injection volume for LC (triplicate analysis of 5 μL each). There is also a significant reduction in solvent use for MALDI analysis since the LC separation step is avoided. Improvements in MALDI sensitivity for the tissue extract could also be gained by reducing the reconstitution volume of the tissue extracts as well as reducing the area of the spotted extract solution on the MALDI target, both leading to a greater concentration of the analyte per area for analysis by MALDI..

The quantitative results from the MSI experiments are compared to the LC-MS/MS results for the tissue extracts is also shown in Table 2-3. The quantitative MSI results compare favorably to analysis by LC specifically MSI quantitation by a standard addition method. The error in quantitative MSI results were significantly larger, which is to be expected when performing direct tissue analysis with no sample cleanup. However, normalizing the wide-isolation MS/MS to the internal standard signal led to significant improvements in quantitative performance. These results show a significant improvement in quantitative MSI, which may lead to the use of the technique for relative or absolute quantitative determinations, particularly for whole body imaging studies.

Conclusions Of Quantitative MSI

Here we have improved quantitative MSI by incorporating a uniformly applied internal standard combined with scan-by-scan COC and d_3COC ion signal normalization. This approach overcomes the challenges associated with quantitative MALDI by accounting for significant ion signal variability. For MSI, employing an

internal standard applied beneath a tissue sample for MSI not only improved quantitation but may also identify instances of tissue-specific ion suppression resulting from either poor analyte extraction or ionization. This may lead to conclusive MS images providing valuable information about a particular ion's distribution in a specific organ or entire body without the need for further analysis. These techniques are applicable to numerous types of analysis, but may be most useful in the area of pharmaceutical development specifically for determining a new drug and its metabolites' distribution in a whole-body sample with the specificity advantages of MS. Further development of quantitative MSI would allow the technique to be used universally for physiological and pharmaceutical determinations.

Employing an internal standard not only allowed for quantitative MSI, but quantitative MALDI analysis of tissue extracts as well. Analysis with MALDI MS/MS reduced the analysis time from 13 hr to 1 hr, a significant reduction in analysis time per sample. In some instances, MALDI with wide-isolation MS/MS could replace LC-MS/MS analysis with little reduction in analytical performance.

.

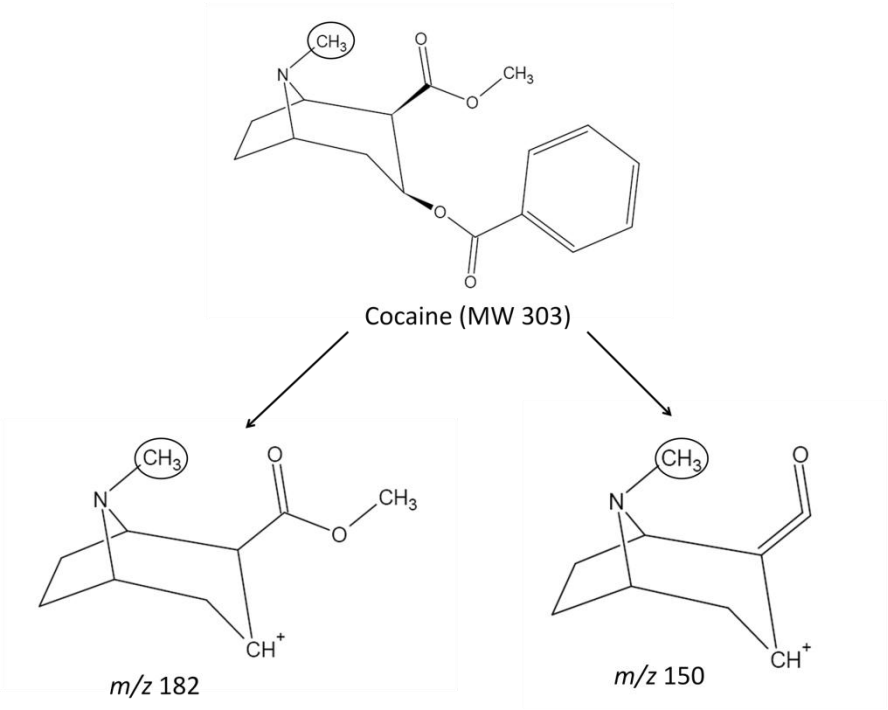

Figure 2-1. Structure of cocaine and the two main product ions observed in the MS/MS spectrum. The site of the deuterium label is circled and is preserved after fragmentation allowing for discrimination of the labeled versus unlabeled standard.

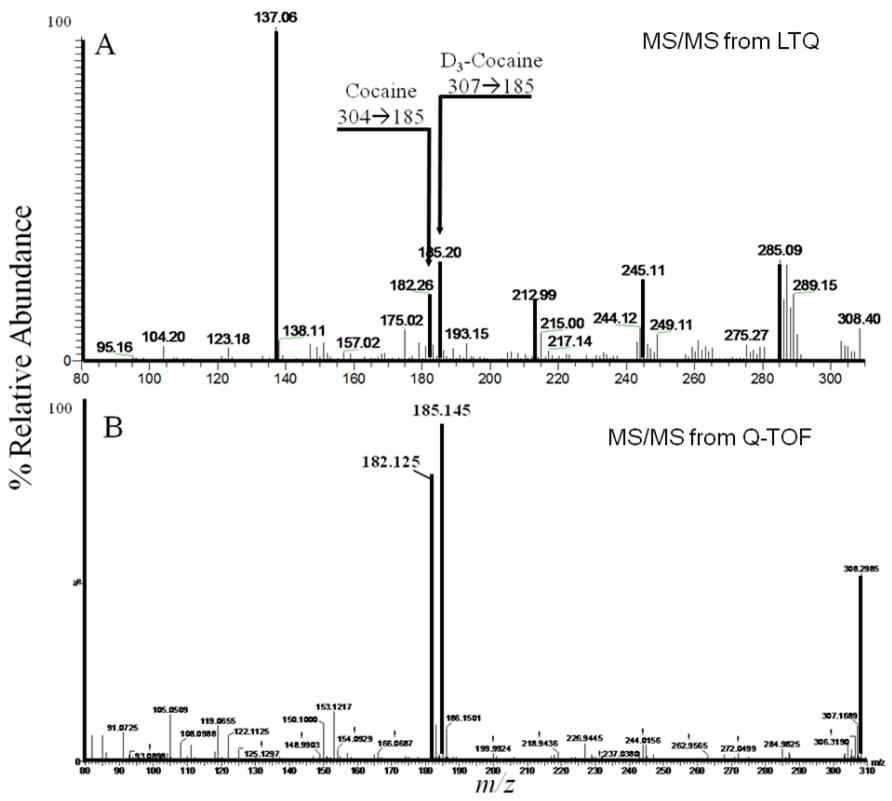

Figure 2-2. Wide-isolation MS/MS spectra of COC and d_3COC analyzed by the LTQ A) and QTOF (B) instruments. The main product ions preserve the deuterated label allowing for differentiation of the COC and d_3COC in a single MS/MS spectrum. The ratio of *m/z* 182/185 was calculated at each image position and used for quantitation and MS images.

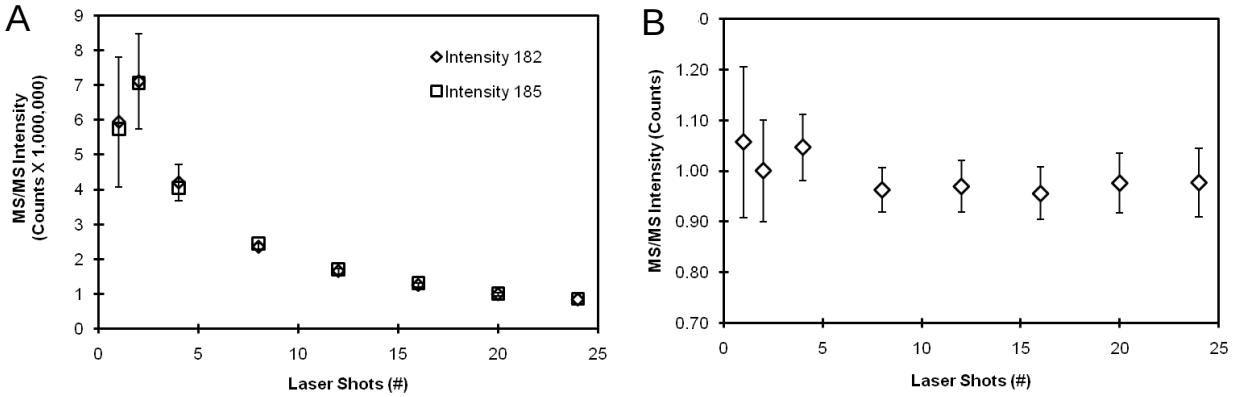

Figure 2-3. Optimization of LS with constant LE using wide-isolation MS/MS. A) Intensity of COC and d_3COC with varying laser shots. B) Ratio of COC/d_3COC (*m/z* 182/185) with varying LS. With significantly changing signal, the detected A/I ratio is preserved.

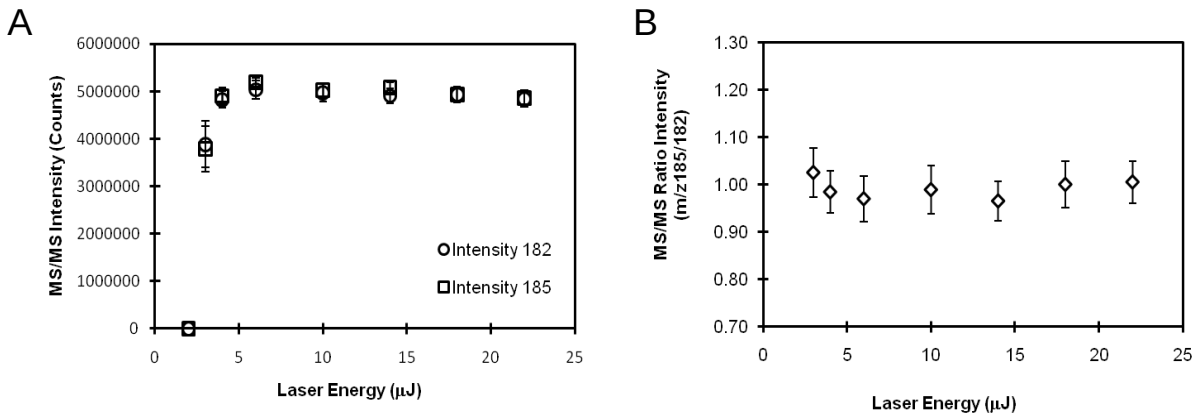

Figure 2-4. Optimization of LE with 4 LS using wide-isolation MS/MS. (A) Intensity of COC and d_3COC with varying LE. (B) Ratio of COC/d_3COC (*m/z* 182/185) with varying LE. With significantly changing signal, the detected A/I ratio is preserved.

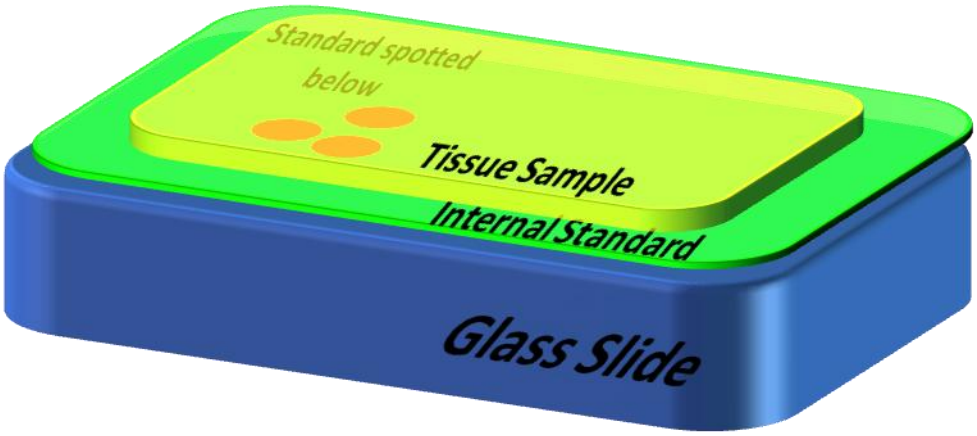

Figure 2-5. Experimental setup for quantitative imaging. Standards are pipette first and allowed to dry, followed by the uniform application of the internal standard via inkjet printing. Thin tissue sections are placed atop the standards followed by MALDI matrix.

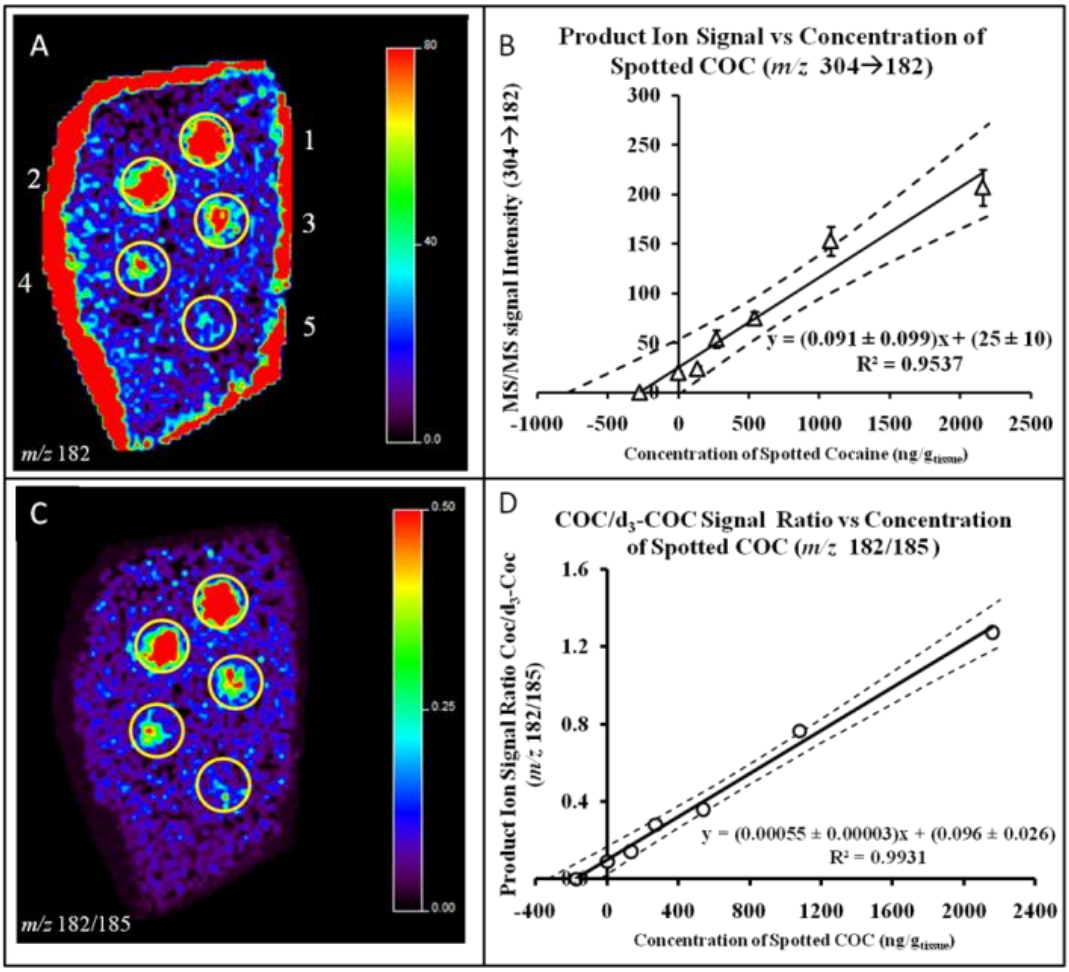

Figure 2-6. Wide-isolation MS/MS imaging experiment for the quantitative analysis of COC from nucleus accumbens. A, C) Ion intensity of *m/z* 182 and the ratio of *m/z* 182/185 (C) were used to generate MS/MS images. Calibration spots increase in concentration from 200 (spot 5) to 2200 ng/g_{tissue} (spot 1). B, D)The corresponding standard addition plots for quantitation with *m/z* 182 ion intensity and the ratio of *m/z* 182/185 are shown, respectively. Normalization to the d_3COC improved the linearity and error of the calibration plot, leading to improved quantitative estimation of COC in the tissue. Confidence bands are calculated from the 95% confidence interval and error bars represent the standard deviation of the mean.

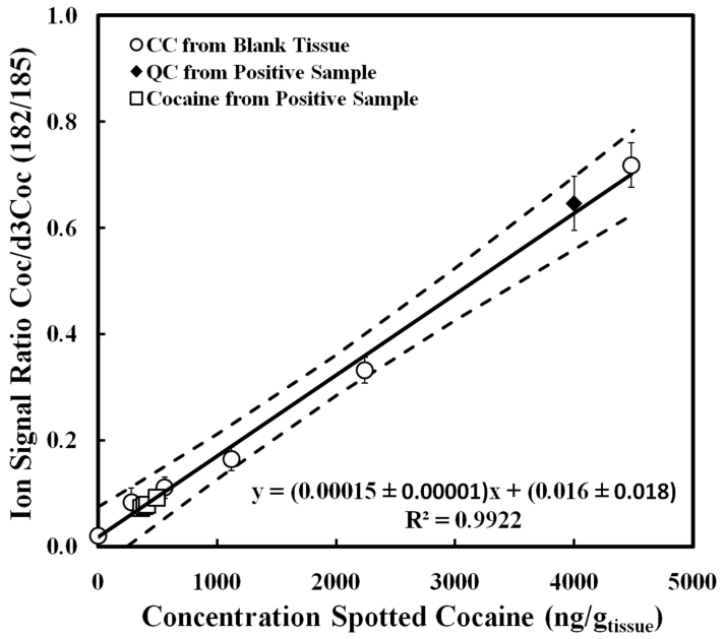

Figure 2-7. Normalized calibration plot produced from COC spotted beneath a control section of brain tissue. Product ion signal ratio (*m/z* 182/185) from the positive sample was compared to the curve to estimate the concentration of COC. The QC sample served as a means to ensure the signal between the two tissues was comparable. The calculated concentration of the QC sample from the calibration curve was within 5% of the spotted concentration. Error bars represent the standard error from the variation in the ~40 MS/MS spectra averaged for each calibration point.

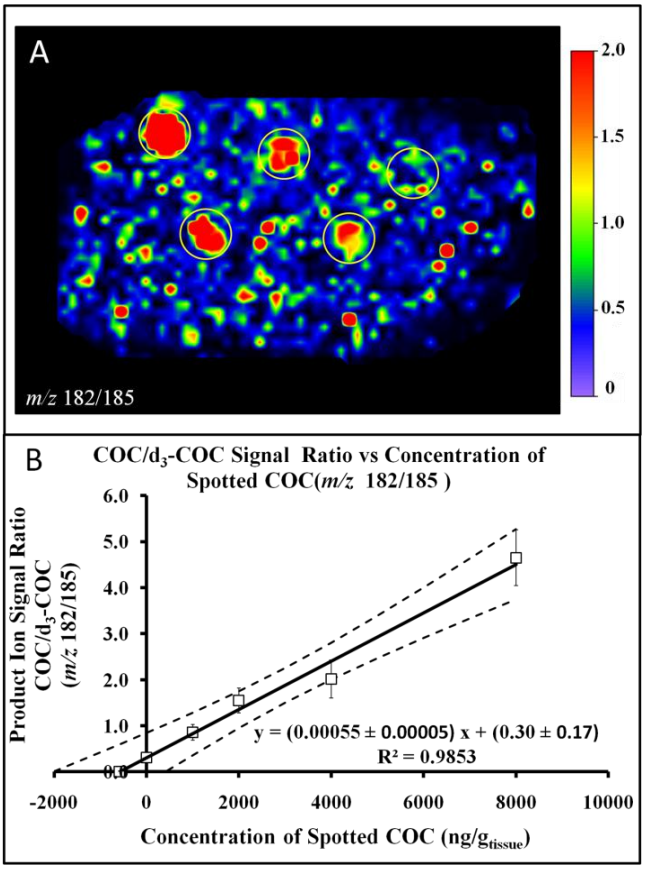

Figure 2-8. Product ion ratio image generated from wide-isolation MS/MS (A) from MSI experiment performed on the LTQ. The corresponding standard additions plot is shown in (B). From this wide-isolation MS/MS experiment, the concentration of COC was calculated to be 550 ng/g_{tissue}.

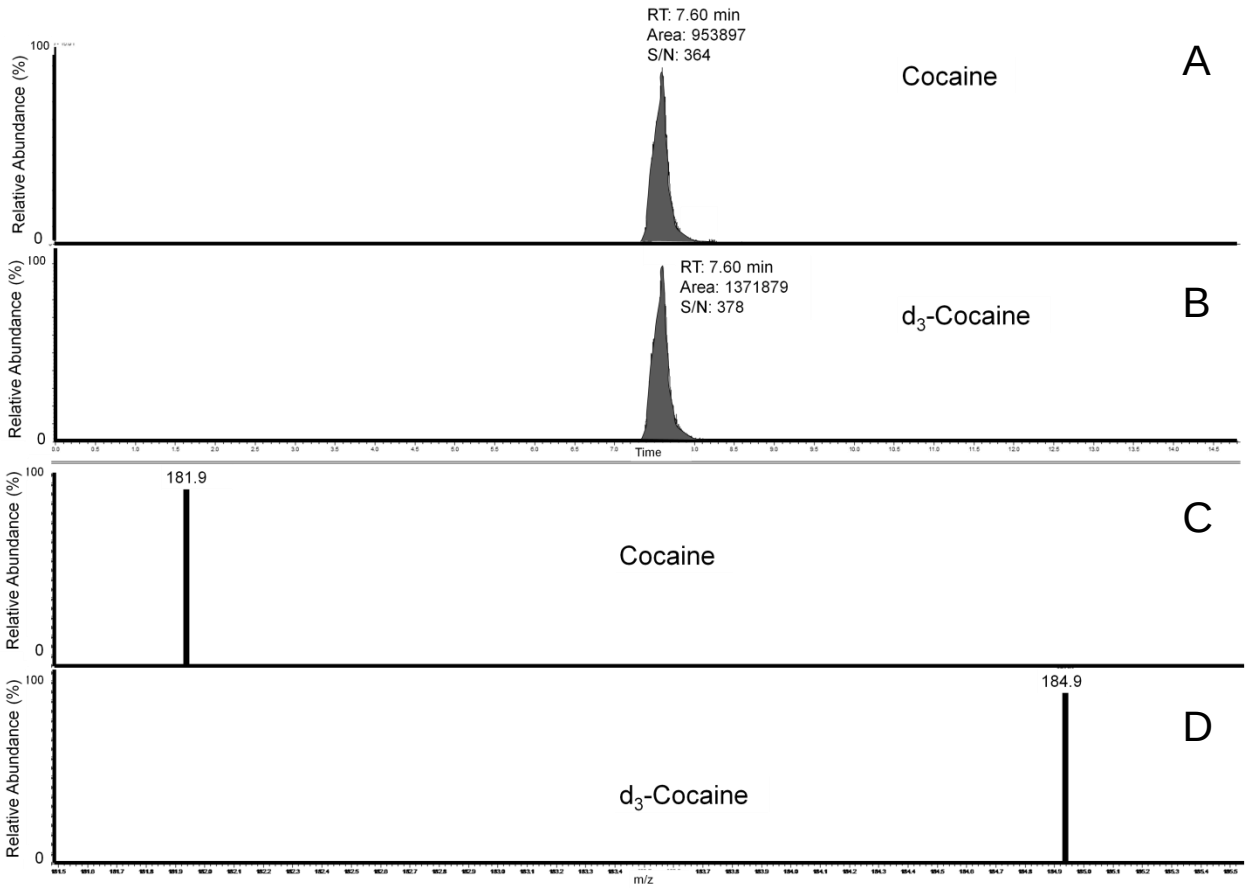

Figure 2-9. Sample LC extracted ion chromatogram of COC (A) and d_3COC (B). Chromatograms were plotted from monitoring the transition of 304→182 for COC (C) and 307→185 for d_3COC (D) by SIM.

A

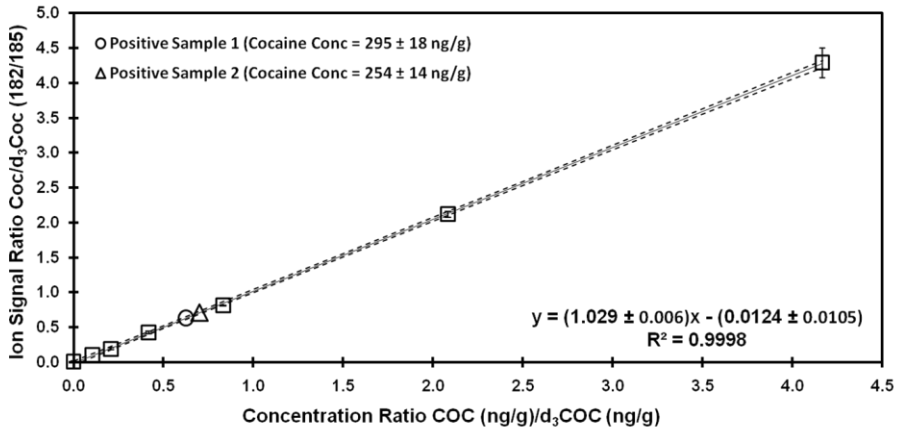

B

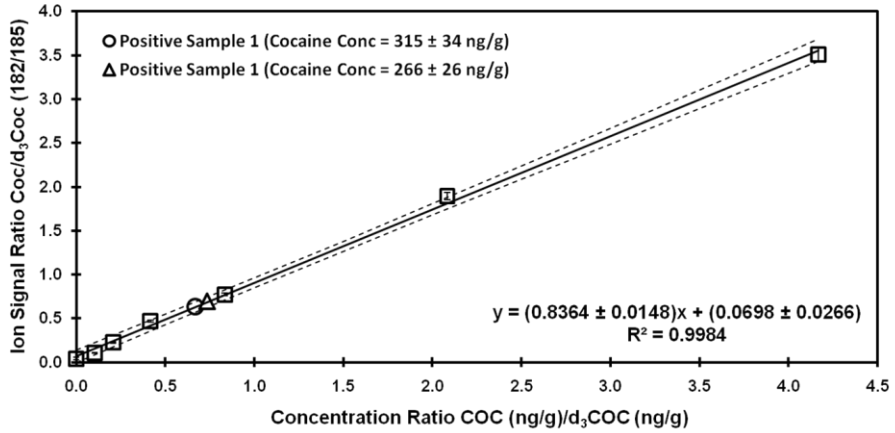

Figure 2-10. Calibration curves of the tissue extracts used to quantify COC in the nucleus accumbens determined by LC-MS/MS (A) and wide-isolation MALDI MS/MS on the LTQ (B). Analysis by MALDI MS/MS resulted in comparable COC concentrations to that of the LC-MS/MS experiment.

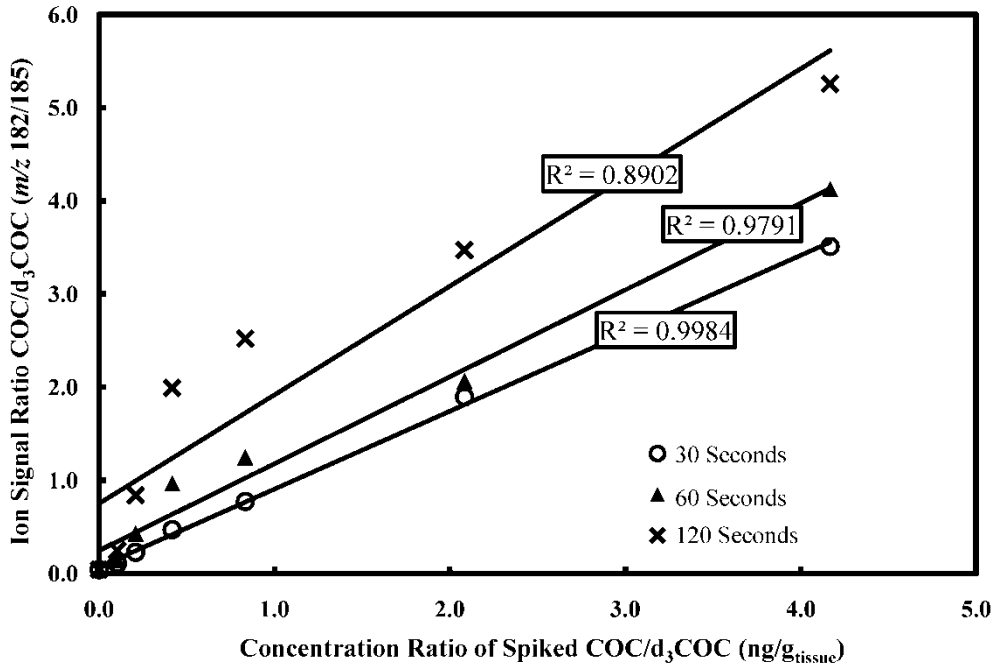

Figure 2-11. Calibration plots of the product ion signal ratio with different amounts of DHB applied to the tissue extracts analyzed by wide-isolation MS/MS on the LTQ. Since DHB was spray coated, the amount of DHB applied was varied by time sprayed atop the spotted extracts. Non-linear increases in the ratio of COC/d3COC are observed with a non-ideal M/A ratio.

Table 2-1. Summary of calibration plots and cocaine concentration determined by MALDI MSI analysis with the LTQ. Concentrations were determined by standard additions analysis.

Analysis	Line equation (y=)	R^2	Cocaine (ng/g_{tissue}) ± 95% CI
1	=(0.00027 ± 0.00002)x +(0.29 ± 0.05)	0.9853	550 ±1000
2	=(0.00055 ± 0.00002)x +(0.30 ± 0.17)	0.9979	1000 ± 700
3	=(0.00027 ± 0.00002)x +(0.16 ± 0.01)	0.9973	1100 ±400

Table 2-2. Summary of calibration plots and cocaine concentration determined by MALDI MSI analysis with the QTOF. Concentrations were determined by both standard additions and external calibration.

Analysis	Line equation (y=)	R^2	Cocaine (ng/g_{tissue}) ± 95% CI
1	= (0.00019 ± 0.00004)x + (0.071 ± 0.017)	0.9993	370 ±300
2	= (0.00055 ± 0.00003)x + (0.096 ± 0.003)	0.9931	170 ± 150
3	= (0.00104 ± 0.00003)x + (0.194 ± 0.034)	0.9973	190 ± 100
External standard	= (0.00015 ± 0.00001)x + (0.016 ± 0.018)	0.9922	400 ± 50

Table 2-3. Tissue COC concentrations determined by various analytical methods.

Method	Cocaine Concentration (ng/g_{tissue})	Std Deviation of Replicates (ng/g_{tissue})
LC-MS/MS of Extracts[1]	295	18
	254	14
MALDI MS/MS of Extracts[1]	315	34
	266	26
QTOF Standard Additions	240	110
LTQ Standard Additions	880	300
External Calibration QTOF	415	50

[1]Extracts consisted of two homogenized sections of the brain, analyzed in triplicate.

CHAPTER 3
USING AN INTERNAL STANDARD TO IDENTIFY TISSUE-SPECIFIC ION SIGNAL VARIATION IN MALDI MASS SPECTROMETRIC IMAGING

Introduction To Tissue-Specific Ion Signal Variation

The ability of mass spectrometric imaging (MSI) techniques to generate analyte-specific distribution maps is becoming a useful tool in the identification of new pharmaceutical candidates. Direct tissue analysis by matrix-assisted laser/desorption (MALDI) coupled with mass spectrometry (MS) provides molecular composition analysis directly from a tissue section. By employing multiple stages of MS, analyte specificity is further enhanced and can allow improved drug and metabolite imaging capabilities. Earlier imaging techniques such as magnetic resonance spectroscopy imaging[87] (MRI) or positron emission tomography[62] (PET) can be used to image a compound's distribution throughout a tissue or even an entire animal. These techniques, however; lack the chemical specificity to differentiate between the parent drug and its metabolites, since the labels attached to the drug may or may not be preserved through metabolism. This lack of chemical specificity necessitates the need for further characterization, usually by tissue extraction and chromatography coupled with MS^n, ultimately resulting in the nearly complete loss of spatial information. These methods can also be time consuming and cost prohibitive, especially if the use of radioactive labels is necessary. MSI however, provides a label-free, direct tissue analysis of the molecular makeup of a tissue sample which can be targeted (tandem MS imaging) or untargeted (full-scan MS imaging). Both endogenous and exogenous compounds can be analyzed and compared between tissue samples such as a comparing disease and normal states[8, 19, 72, 73, 88–92] or determining the distribution of pharmaceuticals.[71–73, 90]

MALDI-based MSI does, however, have limitations. Inherently, MALDI is a poor quantitative ionization source, although with an appropriate internal standard, adequate quantitative results can be obtained, as shown in Chapter 2.[41, 42, 47, 84] The poor quantitative ability is generally attributed to poor ion signal reproducibility resulting from heterogeneous matrix crystallization, sample variation, and laser energy fluctuation.[39] MALDI signal variability leads to a source of ion signal irreproducibility in MSI applications, thus limiting the quantitative ability of MSI. The MALDI matrix must be applied in a manner that minimizes crystal size while enhancing extraction and co-crystallization of the target analyte from the tissue and into the matrix. To minimize crystal growth, rapidly evaporating solvents may be used; however; this can limit extraction and co-crystallization. Aside from matrix crystal variability, the wide variety in the tissue types may also have major effects on the detected ion signal, especially for whole-body imaging applications. Variation between tissue types can lead to unaccountable differences in analyte extraction and ionization efficiency leading to differences in ion signal.[73] This effect was exemplified in the MSI analysis of a whole-body sample for the distribution of administered olanzapine (OLZ) and its metabolies[72]. These experiments produced remarkable images of the distribution of OLZ related compounds, but it was impossible to discern whether increases in MS signal directly corresponded to increases in concentration without further analysis, or what Stoeckli et al. has termed “tissue-specific ionization efficiency calibration” in his discussion of ion suppression effects in MSI.[73] Stoeckli, et al. address tissue-dependent ion signal variation in experiments by coating a solution containing the target compound over a whole-body section using a pneumatic sprayer until the tissue sample was completely

wetted (and the compound presumably incorporated into the tissue), followed by MSI. From the MSI data, ionization differences were determined between tissue types and these were used to normalize images from previous experiments. Areas of ion suppression were observed and accounted for by this approach; however, the application of the compound atop the tissue may not accurately reflect detecting the compound from within the tissue. These experiments did provide an excellent example of the ion suppression effect, and may lead to protocols for applications of quantitative MSI.

An alternative to identifying tissue-specific ionization variability, as described above would be to apply a uniform layer of a deuterated labeled compound, to be used as an internal standard, across the MALDI target prior to placing the tissue sample on the target for MSI analysis. Utilizing an internal standard in this manner has led to improved quantitative MALDI MSI on tissues and standards by generating and analyzing analyte-to-internal standard ratio images. Applying the internal standard with an inkjet printer resulted in improvements both ion signal reproducibility and MS/MS images, shown in Chapter 4. Two requirements for using an internal standard in MSI are that the internal standard must be applied uniformly and the analyte and internal standard are detected in a single analytical MS^n scan. This allows for scan-by-scan normalization of the resulting images and has been shown to improve quantitation and ion signal reproducibility (Chapter 2). Alternate MS/MS scan approaches have been shown to yield minimal improvements on ion signal reproducibility, and typically do not lead to improvements in quantitation.[47] In order to detect both the analyte and internal standard in a single MS/MS scan, a wide-isolation or multi-isolation approach must be

used.[47] Wide-isolation MS/MS is a simpler approach, typically requiring re-centering and expansion of the mass isolation window of the ion trap or lowering the resolution of a quadrupole (for hybrid quadruple-time of flight instruments). To utilize wide-isolation MS/MS, the deuterated label attached to the analyte must remain in the product ion. The other requirement for an internal standard is that internal standard must be as chemically similar as possible to the target analyte.

In this study, acetyl-d_3-carnitine (d_3AC) was utilized as an internal standard for the quantitative detection of acetyl-l-carnitine (AC) from piglet brain tissue and for the identification of tissue-specific ionization differences. The structure of AC is shown in Figure 3-1 with the location of the deuterated label circled. The deuterated label is preserved after fragmentation allowing for wide-isolation MS/MS. d_3AC was first evaluated as an appropriate internal standard for improving MSI results when employing wide-isolation MS/MS. Optimal cutting temperature compound (OTC), a well-known ion suppressant,[93] was utilized to generate a controlled area of ion suppression. Multiple tissue types were also analyzed for the detection of spiked AC to determine if analyzing the ratio of d_3AC and AC could account for instances ion suppression.

Materials and Methods

Chemicals

AC and d_3AC were purchased from Sigma Aldrich (St. Louis, MO). Superfrost glass plus microscope slides and LC–grade methanol, ethanol, water, and chloroform were purchased from Fisher Scientific (Pittsburgh, PA). Stainless steel microscope slides were purchased from Thermo Scientific (San Jose, CA). Optimal cutting temperature compound was provided by the EM Laboratory at the University of Florida. Working calibration standards of AC were diluted in 50/50 v/v methanol/water (v/v) at

concentrations of 0.10, 0.20, 0.040, 0.60, 0.80 and 1.0 ng/μL. d_3AC was diluted in 50/50 methanol/water (v/v) at a concentration of 10 ng/μL. An Epson Stylus R280 (Long Beach, CA) inkjet printer[86] was used to apply d_3AC and AC to microscope slides. 2,5-dihydroxybenzoic acid (DHB) was purchased from Acros Organics (Geel, Belgium) and prepared at a concentration of 20 mg/mL in 90/10 chloroform/ethanol (v/v).

Tissue Preparation

For analysis of AC, piglet brain tissue was provided by Dr. Peggy Borum's lab from the Food Science and Human Nutrition Department at the University of Florida (Gainesville, FL) and stored at −80 °C. During excision, the brain was dissected into hemispheres along the center sagittal plane and then along the coronal plane resulting in half of a hemisphere dissected into the frontal lobe and parietal/occipital lobe. The second cut was performed to reduce tissue sample size, allowing for simpler sectioning; the frontal lobe was used for analysis. Piglet brain tissue was utilized for the quantitative analysis of endogenous AC using a standard additions method. The internal standard, d_3AC, was utilized to identify tissue-specific ionization differences. Brain, liver, testes, kidney, and heart from Sprague-Dawley rats were provided by Dr. Dieter Drexler at Bristol Meyer Squibb (Wallingford, CT, USA)) and stored at −80 °C. Transverse sections of each tissue were applied to microscope slides spotted with AC and d_3AC. These tissues were used to mimic a whole-body imaging experiment. One section of each tissue was placed on one pre-coated microscope slide and the detected AC and d_3AC signals were compared.

Sectioning of the brain tissue was performed on a Microm HM 505E cryostat (Waldorf, Germany). Tissue was sliced at −25 °C to a thickness of 20 μm and thaw

mounted onto the previously coated microscope slide with d_3AC and stored at −80 °C. To minimize condensation, the tissue and slide were first warmed to room temperature in a vacuum dessicator for ~30 minutes, then DHB was applied with a Meinhard nebulizer (Golden, CO) at a flow rate of 2.4 mL/min.

Ion Suppression Studies with Standards and Tissue

Prior to performing ion suppression studies, the method of applying the internal standard was evaluated. Internal standards can be mixed with the MALDI matrix prior the matrix application step or they can be applied separately, either beneath (shown in Chapter 2) or atop a tissue sample. To evaluate this, 1 ng/μL of AC was applied to a microscope slide using an inkjet printer. One mL of 10 ng/μL d_3AC was added to 10 mL of 20 mg/mL DHB. The mixture was then spray-coated atop the applied AC. This was compared to a glass microscope slide on which both AC and d_3AC were first applied separately with an inkjet printer, followed by the application of DHB. Wide-isolation MS/MS imaging centered at *m/z* 205.5 ± 3 AMU was performed on 2 mm squares of the applied standards. Images were then generated using the product ion intensity of *m/z* 145 and *m/z* 148. Previous MS/MS studies using a 1 AMU isolation window across the *m/z* range 202–209 have shown that the product ions *m/z* 145 and *m/z* 148 almost exclusively arise from the precursor ions *m/z* 204 and *m/z* 207, corresponding to AC and d_3AC, respectively.

To determine if an internal standard could identify and account for areas of ion suppression, controlled experiments mimicking areas of ion suppression were created with a well-known ion suppresser, OCT.[93] First, 1 μL of a 1% solution of OCT was spotted onto a microscope slide followed by the addition of a 1:2 mixture of AC: d_3AC

(v/v) by the inkjet printer. DHB was then applied via pneumatic spray-coating, and both MS and wide-isolation MS/MS analyses were performed covering the entire OCT spot.

For multiple tissue analysis, 1 μL spots of a 1:2 mixture of AC: d_3AC (v/v) was applied atop a microscope slide. Brain, liver, testes, kidney, and heart sections were each placed over one of the spots. One spot was left uncovered and analyzed as a standard to determine the detected *m/z* 145/148 ratio. DHB was spray coated over the entire slide and each tissue was analyzed via wide-isolation MS/MS.

Finally, the distribution of AC was determined in a coronal section of piglet brain tissue. Calibration standards of AC were first applied to a glass slide (1 μL) with a micropipette and allowed to dry. d_3AC was then applied covering the entire slide via an inkjet printer. Coronal sections of piglet brain tissue were then sectioned to 20 μm and thaw-mounted atop the calibration standards.

Instrumentation

For the MSI experiments of AC in piglet brain tissue, all mass spectra were acquired with a Synapt MALDI-Q-Ion Mobility (T-wave cell) Time of Flight (QTOF) equipped with a 200 Hz, 335 nm, Nd:YAG laser at a frequency of 200 Hz and spot diameter of 150 μm (Waters Corporation). The QTOF instrument was operated in MS mode. All experiments evaluating ion suppression were performed on a MALDI LTQ XL equipped with a 20 Hz, 337 nm, N_2 laser with a spot size of 100 μm (Thermo Corp. San Jose, CA). For MS/MS imaging experiments on the LTQ, a 6 AMU wide-isolation window centered at *m/z* 205.5 The compounds were fragmented in both instruments using collision induced dissociation and the fragments of each compounds were monitored; AC *m/z* 204→145 and d_3AC *m/z* 207→148. Sample slides were inserted

into the vacuum chamber and rastered beneath the laser at a step size of 100 μm. Resulting data from the QTOF were processed using BioMap (Novartis, Basel, Switzerland) and images from the LTQ were processed with QualBrowser (Thermo Scientific, San Jose, CA, USA) and Surfer 8 (Golden, CO, USA). BioMap was utilized to generate internal standard normalized images with the 'divide' function built into the software. Normalized images from the LTQ were generated in Surfer 8 from extracted data. For quantitative determinations of endogenous AC, a standard additions method analysis was performed utilizing the signal from the spotted calibration standards and the uniformly applied internal standard. For ion suppression determinations, the product ion intensities of *m/z* 145, *m/z* 148, and the ratio of *m/z* 145/148 were analyzed.

Discussion

Internal Standard Application

Prior to evaluated tissue-dependent ion signal variation, methods for the application of the internal standard d_3AC were evaluated. It has previously been shown that scan-by-scan normalization with wide-isolation MS/MS spectra of AC by d_3AC resulted in significant improvements in ion signal reproducibility, calibration curve linearity and image quality (Chapter 2 and 4). To evaluate the methods of applying d_3AC for imaging studies, the d_3AC was applied separately and combined with the MALDI matrix. Wide-isolation MS/MS was performed over a 10 X 10 raster step square (100 scans with a 200 μm step size) on the applied standards. For normalized images, each MS/MS scan, the intensity of *m/z* 145 was divided by the intensity of *m/z* 148 for each MS/MS scan. The mean-centered results are plotted in Figure 3-2. Figures 3-2 A−C plot the ion intensity image generated from *m/z* 145, *m/z* 148, and *m/z* 145/148

when applying the d_3AC mixed with the matrix. The average variation in product ion intensity (defined as the % relative standard deviation of the detected ion signal) was 57% for *m/z* 145, 54% for *m/z* 148, and 60% for *m/z* 145/148. The lack of improvement in image quality and signal variation indicates that applying the internal standard with the matrix does not lead to improved analytical performance. This may be due to differences in co-crystallization between the AC and d_3AC with the DHB. Figures 3-2D−F plot the ion intensity image generated from *m/z* 145, *m/z* 148, and *m/z* 145/148 when applying the d_3AC separate from the matrix and AC. This signal intensity patterns in Figures 3-2D and 3-2E are very similar to each to other, and the normalized image in Figure 3-2F resulted in a relatively smooth ion product images. The % relative signal deviation (%RSD) in product ion intensity was 42% for *m/z* 145, 41% for *m/z* 148 and 8% for *m/z* 145/148, indicating the application of the internal standard separate from the matrix solution is superior. Both the AC and d_3AC appear to co-crystallize with the MALDI matrix in a similar manner, indicated by the similar pattern observed in Figure 3-2D and 3-2E. It is unlikely the exact pattern was replicated by the inkjet printer multiple times and is due more likely to differences in crystallization of the DHB. From these results, it was concluded that the internal standard be added separately from the MALDI matrix for all further experiments.

Ion Suppression with Standards

To determine if an internal standard could help identify and account for areas of ion suppression, analysis of AC and d_3AC was performed using OCT as an ion suppressant. MSI was performed over spots of applied OCT (1 mm across), AC and d_3AC (3 mm across) in MS and wide-isolation MS/MS mode. Images from the MSI experiments utilizing MS are shown in Figure 3-3. Three methods of image

normalization reported in the literature were compared, including normalizing the analyte signal to the matrix signal, the analyte signal to the total ion current (TIC), and the analyte signal to an externally applied internal standard.[77] These results, compare images produced using the ion intensity of the compound of interest (Figure 3- 3 A−C) to different methods of normalization (Figure 3-3 D−F). The area of the spotted OCT is clearly visible from plotting *m/z* 332, which corresponds to the additive benzyl alkonium chloride (Figure 3-3A). Areas of ion suppression resulting from OCT are shown in the MS images of AC and d_3AC. Both AC and d_3AC (Figure 3-3B and 3-3C, respectively) were applied atop the slide homogeneously with an inkjet printer, which should lead to uniform signal distribution throughout the area analyzed; however, the presence of OCT results in drastic signal reduction. Without prior knowledge of ion suppression, one may conclude an uneven distribution of AC using the ion intensity alone. These areas of ion suppression are not fully identified when normalizing AC signal to the TIC (Figure 3-3D) or to the matrix (Figure 3-3E). These normalization methods still produce images showing uneven AC signal distribution, although normalization by the TIC is more successful than normalization by the matrix. Normalizing to the d_3AC, however, does result in an image showing nearly uniform distribution of AC; the demonstrates that normalizing to the internal standard (which has nearly identical chemical properties as the target analyte) can successfully correct for ion suppression.

Tissue-Specific Ion Signal Variability

To test whether normalizing images by an internal standard can be used with tissue analysis to identify tissue−specific ion suppression, multiple tissue types were sectioned and applied atop a pipetted spot of a 1:2 mixture of AC and d_3AC. Shown in Fig 3-4A is a photograph of the slide with tissues outlined and identified. A black spot

was applied to the backside of the slide to mark where the spots of AC/d_3AC were applied. For analysis by wide-isolation MSI, a rectangle was drawn surround the applied AC/d_3AC and analyzed using a 100−μm step size. The resulting data were extracted into Excel for ratio determination and Surfer was used to produce the MS/MS images. MS/MS images of AC from the spots applied beneath the brain and liver sections are shown in Figure 3-4B and 3-4D, respectively. The ion intensity of *m/z* 145 shows a 90% reduction in the liver section compared to the brain section. This signal reduction could result from either poor extraction or ion suppression from an endogenous compound in the liver tissue; however, we were unable to make a definite conclusion on which effect was dominant.

A summary of the analysis of all the tissues is shown in Figure 3-5, which plots the summed intensity covering the entire AC/d_3AC spot. The histogram has been scaled to the maximum signal or ratio detected across the tissue types for basis of comparison. Tissue-specific signal attenuation is observed significantly in both the liver and kidney and as well as slightly in the testes. As stated previously, the cause of the signal decrease cannot be determined, but analyzing the data using only the ion intensity would lead to an incorrect conclusion that there is a lower concentration of AC in these tissues. After scan-by-scan normalization with the d_3AC internal standard, the detected AC/d_3AC ratios from tissue-to-tissue varied ±13% RSD. Clearly, using an isotopically labeled internal standard is critical for a comparison of the endogenous concentration of AC between the tissue types.

Apart from creating known instances of ion suppression or tissue−specific signal variation, this phenomenon was also observed in experiments designed to quantify AC

in a coronal section of piglet brain tissue. These data were taken using a QTOF instrument. Figure 3-6 A plots the MS intensity of *m/z* 204 corresponding to the molecular ion of AC. A clear difference between the signal in white and grey matter is observed (lower signal was observed in the white matter). Calibration spots were applied beneath the tissue section and are also visible in the MS image. Figure 3-6B is the MS image of the d_3AC internal standard, which was uniformly applied beneath the tissue by an inkjet printer. A distinct reduction in signal is also observed in white compared to grey matter, even though the d_3AC was applied uniformly observed in Figure 3-6B. This suggests the difference in the AC signal may not reflect differences in the AC concentration, but rather variations in either extraction or ionization efficiency. Analyzing the ratio of AC/d_3AC (Figure 3-6C) gives a better indication of the distribution of AC, between grey and white matter in this sample by accounting for spot-to-spot signal variation, ionization variability and extraction differences, shown in Figure 3-6C. Furthermore, comparison of the calibration curves generated from the MSI experiment show a dramatic improvement in linearity when performing scan-by-scan normalization to the deuterated internal standard, Figure 3-7 (intensity of *m/z* 204) and Figure 3-8 (ratio of *m/z* 204/207). A dramatic improvement in calibration curve linearity and precision is observed from the *m/z* 204/207 ratio plot compared to the plot generated from the intensity of *m/z* 204 alone.

Although it is not possible to determine which factor, extraction or ionization, is the dominant source of signal variation, it could well be a combination of the two. For protein analysis, multiple washing steps are routinely performed to remove the majority of the lipids prior to MSI, because they tend to suppress protein ion signals Such

washes are not typically performed for small molecule MSI due to the solubility of small molecules in washing solutions, which may result in analyte migration or loss. Differences in the amount of lipids and salts in various tissue types as well as within a single tissue may also create significant differences in the extractability of a particular compound. The extraction can be optimizing for each tissue type; however, within certain tissues such as brain, there may be regional variations, as between grey and white matter. A single tissue type may vary significantly on the millimeter scale and applying this across multiple tissue types, these effects can be exacerbated. Applying an internal standard, preferably a deuterated analog, may help control for these extraction and ionization issues, which limit otherwise limit the potential for quantitative MSI.

Conclusions To Ion-Specific Ion Suppression

These results demonstrate that performing an MSI experiment without an internal standard may lead to inaccurate conclusions about a particular compound's distribution within a tissue and more so across multiple tissue types, i.e., in a whole-body MSI experiment. Applying an internal standard corrected for tissue-specific signal variability resulting from either ion suppression or analyte extraction. The methods developed overcome these tissue-specific variations leading to more conclusive results about concentration differences in a given sample. The ability to quantitatively map a drugs time resolved distribution throughout an organ[65] or entire animal could provide invaluable information about a drug's efficacy. Unique determinations could also be made about metabolites distribution and possibly changes these compounds are inducing on the endogenous compounds present in the sample, i.e. metabolites, lipids, and proteins.

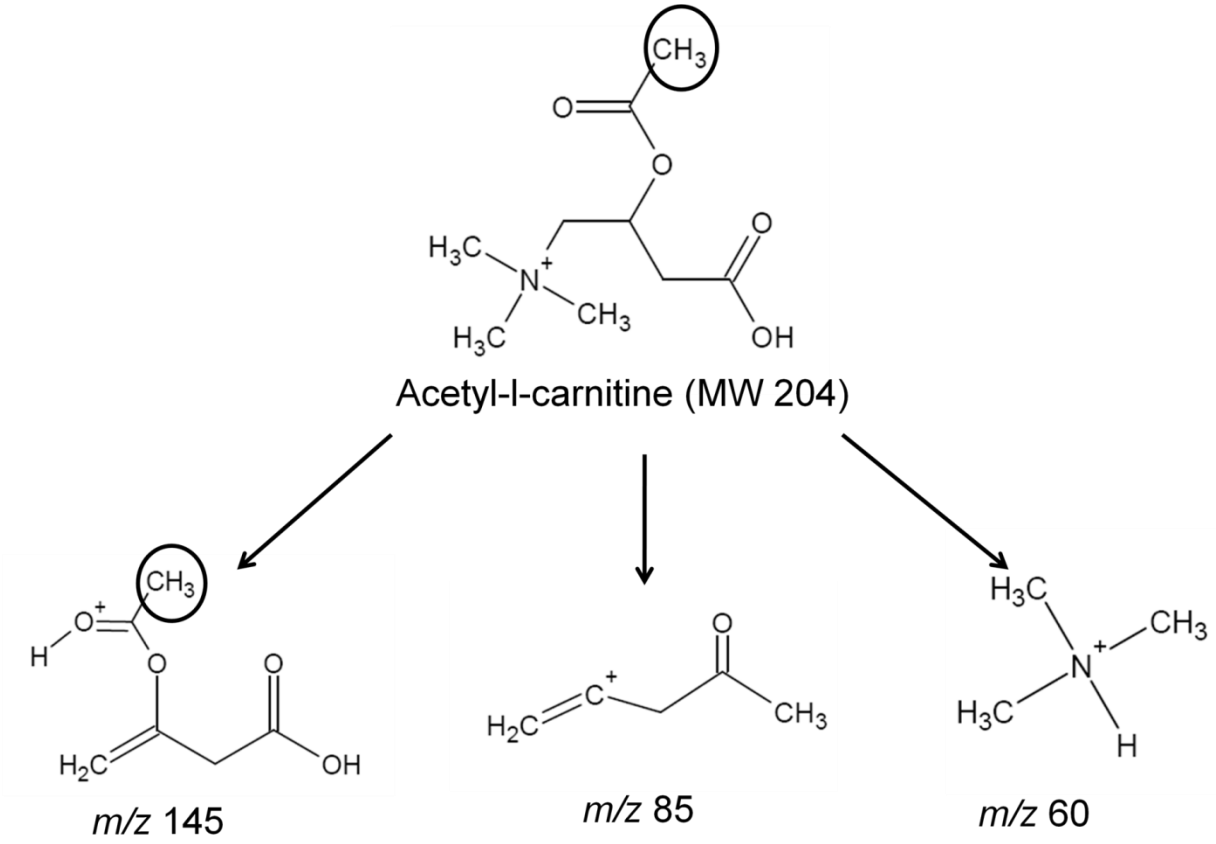

Figure 3-1. Structure of AC and the three main product ions observed in the MS/MS spectrum. The site of the deuterium label is circled and is preserved on the 145 product ion after fragmentation allowing for discrimination of the labeled versus unlabeled standard.

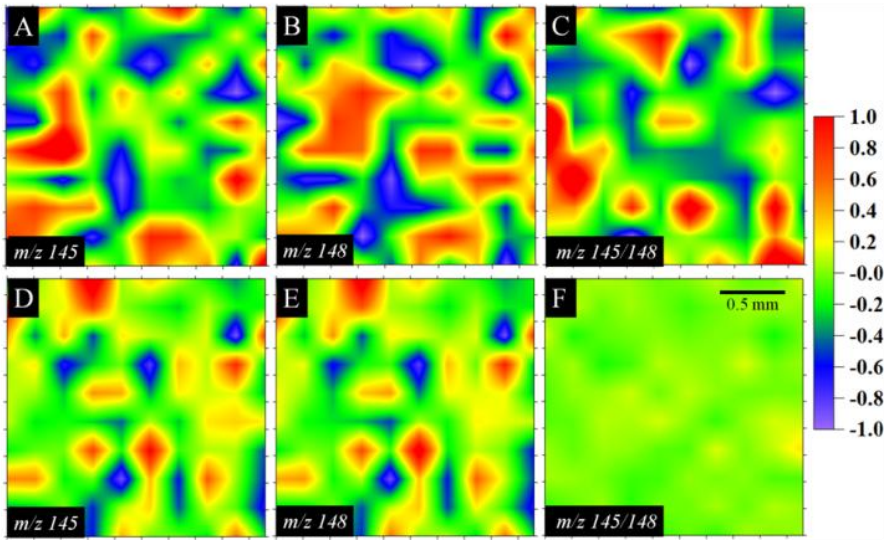

Figure 3-2. MS/MS images comparing the application of the internal standard d_3AC. d_3AC was mixed with the MALDI matrix solution and spray coated atop AC, which was applied with an inkjet printer (A–C). This was compared to applying AC and d_3AC separately (D–F) with the inkjet printer, then spray-coating the MALDI matrix solution atop. Images were generated from the intensity of the product ions *m/z* 145 and *m/z* 148 (A, B, D, E) compared to normalizing the intensity of AC by d_3AC at each raster step. The intensities are mean-centered. Thus, the average intensity is 0, and the intensities vary from −1 (zero absolute intensity) to +1 (2 times the average intensity).

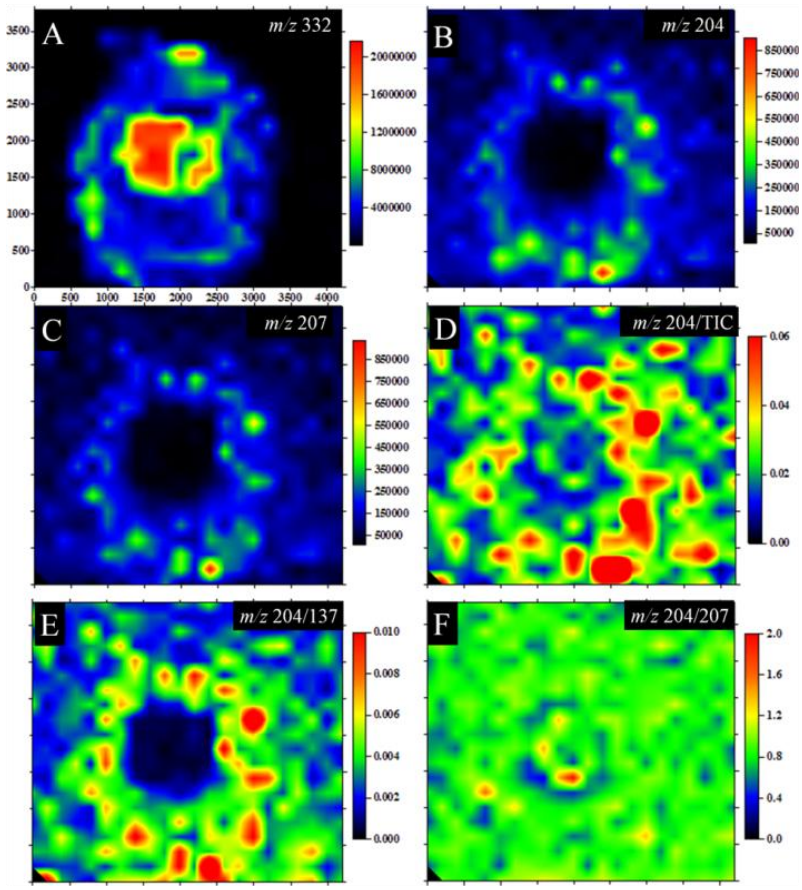

Figure 3-3. MS images of AC mixed with d_3AC (each ~3 mm across) applied atop a spot of OCT (~1 mm across) (A). Ion suppression is visible in MS images for AC and d_3AC (B,C). Multiple methods of normalization are compared in D–F. The MS image for AC should appear uniform resulting for the uniform application. This is produced only by normalizing to the internal standard. The color scales for A-C are determined from the plotted ion intensity values. The color scales for D-F are determined from the ratio of the *m/z* 204 to the respective value.

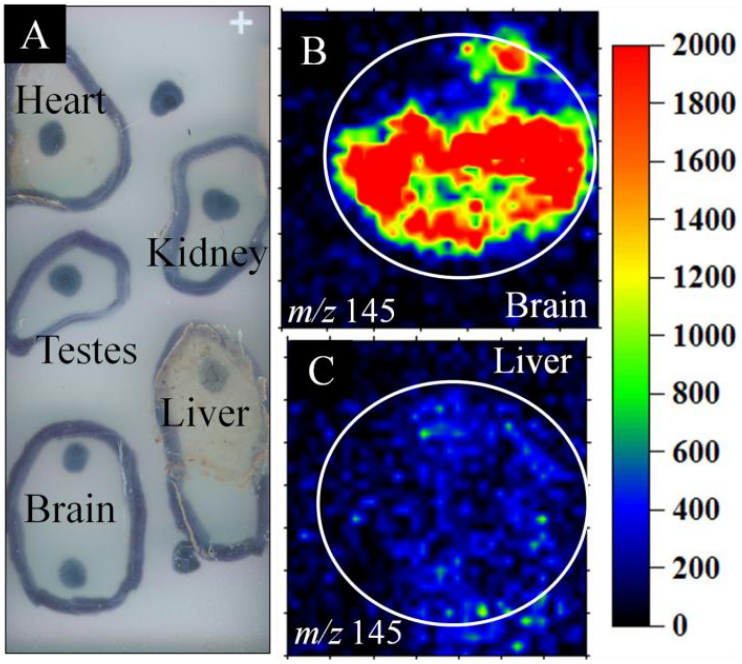

Figure 3-4. Multiple tissue analysis of AC ion signal variability using wide-isolation MS/MS. (A) Optical image of the glass slide with multiple tissue sections applied over spots of 1:2 mixture of AC:d_3AC (marked with black spots). (B) MS/MS image of product ion for AC applied under the brain section compared to MS/MS image from the liver tissue. The detected signal for AC was decreased by 90% from brain to liver tissue. The intensity scale reflects absolute counts of *m/z* 145.

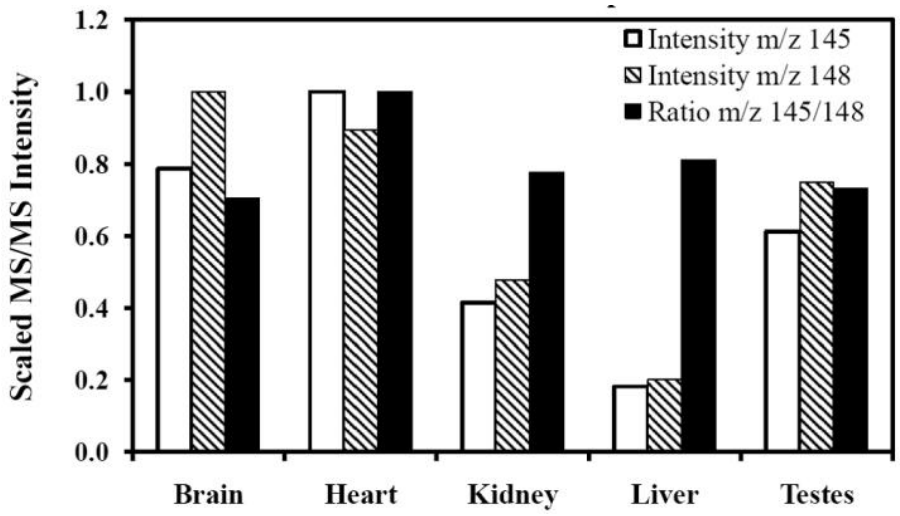

Figure 3-5. Scaled MS/MS intensities of *m/z* 145 and *m/z* 148 summed over the raster area. Data were scaled as a percentage of the maximum detected for basis of comparison. A significant decrease in ion signal is observed for both the AC and d_3AC in the kidney and liver sections compared to the brain, heart, and testes. However, the ratio of AC to d_3AC remains constant, varying only 13% RSD between the 5 tissue types, whereas the variation of AC and d_3AC 70% RSD between tissue types.

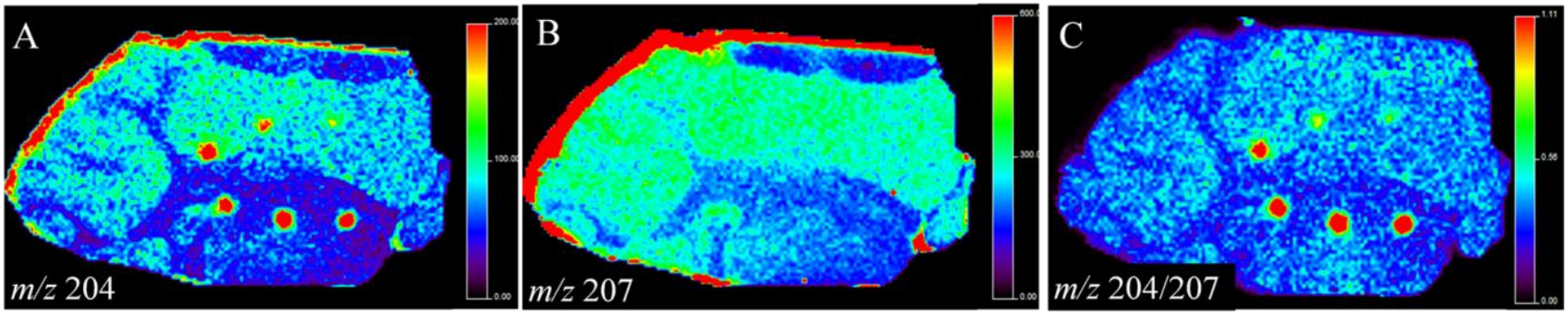

Figure 3-6. MS image of piglet brain tissue for the detection of endogenous AC. A) Image of the $[M+H]^+$ ion corresponding to AC (*m/z* 204) shows a clear differentiation between white and grey matter of the brain. B) The applied d_3AC shows a similar pattern implying there is either decreased extraction or ionization from the two tissue types. C) The ratio image of AC/d_3AC results in a better representation of the distribution of AC within the brain sample as well as improves the linearity of calibration curve, Figure 3-7 and 3-8.

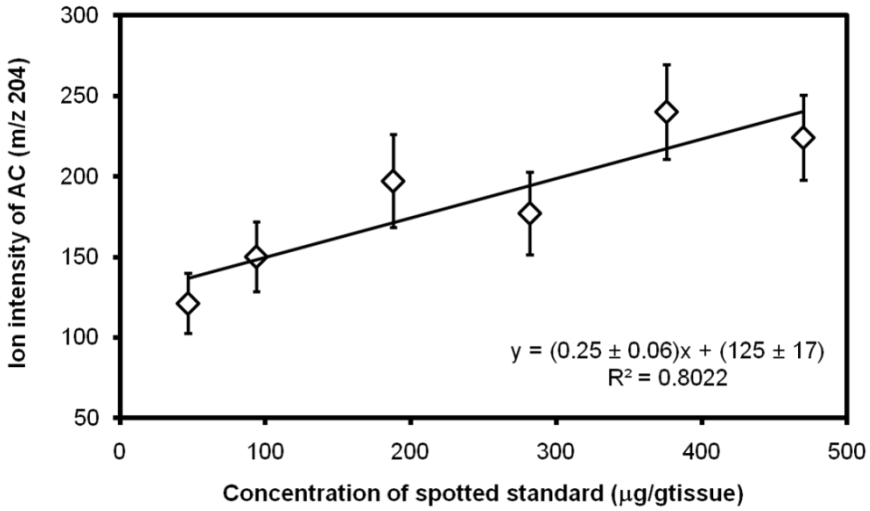

Figure 3-7. Calibration curve of spotted AC standard plotted from the intensity of *m/z* 204 corresponding to the MS image in Figure 3-6 (A).

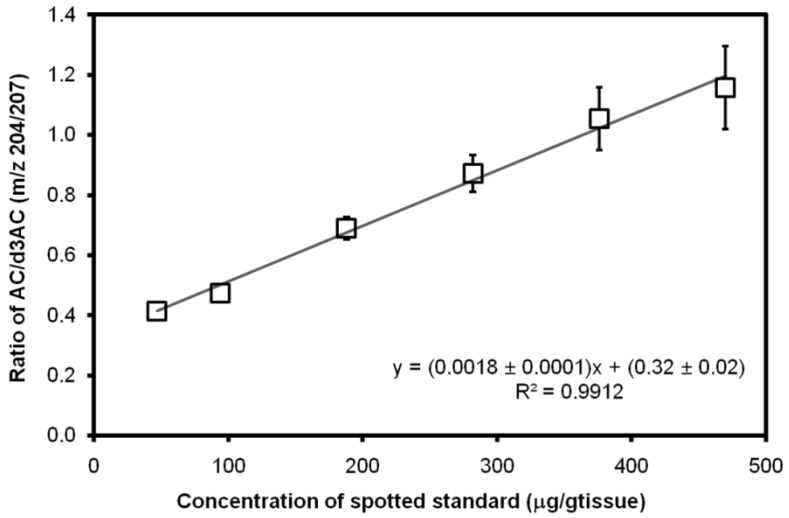

Figure 3-8. Calibration curve of spotted AC standard plotted from the ratio of *m/z* 204/207 corresponding to the MS image shown in Figure 3-6B.

CHAPTER 4
QUANTITATIVE TANDEM-MASS SPECTROMETRIC IMAGING OF ENDOGENOUS ACETYL-L-CARNITINE FROM PIGLET BRAIN TISSUE USING AN INTERNAL STANDARD

Introduction to Quantitative MSI for Tissue-To-Tissue Comparison

Matrix-assisted laser desorption/ionization mass spectrometric imaging (MALDIMSI) has become an invaluable tool for evaluating molecular changes of tissue samples, especially for differentiation between tissue states. Ever since MALDI MSI was first used to map pharmaceutical compounds in intact tissues[13] and to generate MS images of proteins,[8] MSI has rapidly expanded to include small molecules, lipids,[20] pharmaceuticals,[94] and, recently, endogenous metabolites.[68, 95] Although instrumental advancements allow for increased selectivity of a target analyte by implementing MS^n,[20, 68, 96, 97] ion signal irreproducibility limits MALDI MSI to qualitative applications. Currently, MALDI MSI has been used for relative quantitative applications[66, 73, 75]; however, these results typically must be verified by another method such as high pressure liquid chromatography (LC)-MS^n of tissue extracts.[26] Ion signal irreproducibility results from numerous factors: inhomogeneous matrix crystallization and tissue sample heterogeneity leading to inefficient analyte extraction, ionization, and matrix application.[25, 28, 76]

Applying the MALDI matrix to a tissue sample is an important step in producing quality images. Significant care must be taken to apply the matrix in an even layer of minute crystals. Currently, matrix is applied using numerous methods including: robotic micro-spotting,[22] sublimation,[25] inkjet printing,[76] and pneumatic spray coating.[8, 19, 98] Spray coating, used in this study, generally produces a more homogenous matrix layer in a shorter amount of time compared to robotic spotting; however, this method may

result in widely varying matrix crystal sizes as well as the possibility of over-wetting the tissue, thus resulting in analyte migration.[98, 99] Crystal sizes of the matrix layer can also significantly vary based on their rate of formation. Spray coating was used with different solvents to create matrix crystals varying in size to determine their effects on signal reproducibility. Improving the quality of the matrix coating has recently been shown to minimize signal variation, which could lead to improved quantitative MSI.[27]

Other quantitative methodologies such as LC–MS^n employ an internal standard (IS) to correct for signal variability arising from sample extraction, separation, and detection. Implementing an IS in MSI presents the unique challenge of applying the internal standard. A previous study utilized a pneumatic nebulizer to apply the IS by completely wetting the tissue sample then allowing it to dry prior to MSI.[73] Applying an internal standard in this manner may result in undesirable analyte migration as well as possible partitioning of the IS into different tissue types. An alternative to applying an IS atop the tissue sample is to apply a uniform layer of the IS beneath the sample (to the sample plate) and extract the IS into the tissue during matrix application.

We utilize an inkjet printer to apply an isotopically–labeled IS to a glass slide prior to mounting a tissue section to account for the significant signal variability with MALDI. Utilizing an inkjet printer has been successfully used to apply an internal lipid standard to estimate the lipid concentration in rat spinal cord with full-scan MSI.[66, 76] In this study, quantitative data were determined by averaging the signal from a large area within the tissue. By averaging ion intensities from large sections of tissue, the resolution of the MS image is lost. To generate quantitative images at a resolution near the laser spot

size, improvements in the signal reproducibility from spot-to-spot must be achieved in order to produce quantitative MS images.

In the present study, two methods were employed to improve signal reproducibility: 1) optimizing matrix application via spray coating with different matrix solvents and 2) utilizing an IS placed beneath the sample to account for spot-to-spot signal variation. An intermediate pressure MALDI linear ion trap utilizing wide-isolation MS/MS was employed for the detection of acetyl-l-carnitine (AC) from piglet brain tissue using acetyl-d_3-carntine (d_3AC) as the IS. Wide-isolation MS/MS allows for simultaneous detection of both the analyte and IS in a single MS^n scan, and it has been previously shown to be superior to using alternate scans or multiple imaging experiments.[47] The ability to detect both the analyte and IS in a single MS/MS scan allows for the ratio of the two analytes to be analyzed and not the signal intensities of the target analyte.

Upon generating a successful method of quantitation, the endogenous levels of AC were compared between two piglet brain samples. One piglet was fed a ketogenic diet during the first week after birth compared to a piglet fed a normal, carbohydrate rich diet during the same time. Changes in carnitine concentrations were hypothesized to occur as a result of the diet. By identifying endogenous metabolite concentration differences, further analysis were to be performed by our collaborator Dr. Peggy Borum of the Food and Nutritional Sciences Department at the University of Florida, to determine if these compounds were responsible for the therapeutic mechanism of the ketogenic diet for the treatment of epilepsy.

Materials and Methods

Chemicals

AC and d_3AC were purchased from Sigma Aldrich (St. Louis, MO). Superfrost glass plus microscope slides and LC–grade methanol, ethanol, water, and chloroform were purchased from Fisher Scientific (Pittsburgh, PA). Working standards of AC were diluted in 50/50 v/v methanol/water (v/v) at concentrations of 10, 8.0, 4.0, 2.0, 1.0, 0.80, 0.40, 0.20 and 0.10 ng/μL. d_3AC was diluted in 90/10 methanol/water (v/v) at a concentration of 10 ng/μL. 2,5-dihydroxybenzoic acid (DHB) was purchased from Acros Organics (Geel, Belgium) and prepared at a concentration of 40 mg/mL in either 90/10 chloroform/ethanol (v/v) or 70/30 methanol/water (v/v).

Analysis of AC Standards

Prior to tissue MSI analysis, the viability of using d_3AC as an internal standard for quantitative MSI analysis was performed. To determine if using the AC/d_3AC ion ratio to account for signal variation, AC and d_3AC were applied separately to a glass slide using the inkjet printer. DHB was then spray-coated with a Meinhard nebulizer, model number TR-30 A3, (Golden, CO) dissolved in 90/10 chloroform/ethanol (v/v) or 70/30 methanol/water (v/v) to produce matrix crystals of varying sizes from the differing evaporation rates of the solvents. Wide-isolation MS/MS was performed over the areas of the applied AC and d_3AC and the resulting images were evaluated in terms of ion signal variation. Crystal sizes were analyzed using a Leica DFC 295 (camera) coupled with a Leica DMLP microscope (Wetzlar, Germany). Matrix homogeneity was measured using percent relative standard deviation (RSD) of the detected matrix ion signal from an MS imaging experiment on a glass slide. A selected area of 50 MS/MS scans was analyzed 8 times monitoring the signal variation over multiple analysis.

For quantitative analysis, calibration standards of AC were spotted onto a glass slide at concentrations of: 0.1, 0.2, 0.4, 0.8, 1, 4, 8 ng/μL followed by the application of d_3AC via the inkjet printer. DHB diluted in 90/10 chloroform/ethanol (v/v) was applied by spray-coating with a Meinhard nebulizer. Wide-isolation MS/MS was performed covering the entire calibration curve area. MS/MS intensity from *m/z* 145 and the ratio of *m/z* 145/148 were used to produce calibration plots.

Tissue Preparation

Piglet brain tissue was provided by Dr. Peggy Borum's lab from the Food Science and Human Nutrition Department at the University of Florida (Gainesville, FL, USA) and stored at −80 °C. During excision, the brain was dissected into hemispheres along the center sagittal plane and then along the coronal plane resulting in half of a hemisphere dissected into the frontal lobe and parietal/occipital lobe. The second cut was performed to reduce tissue size for simpler sectioning; the frontal lobe was used for method development.

Prior to tissue sectioning, d_3AC was applied to a standard glass microscope slide with an Epson Stylus Photo R220 (Long Beach, CA) inkjet printer and a modified compact disc tray as a glass slide holder. d_3AC diluted in 50/50 methanol/water (v/v) to a concentration of 10 ng/μL was used to fill a cleaned, unused ink cartridge. Adobe Illustrator (San Jose, CA) was used to created the IS patterns to be applied to the glass slide. The glass slides where then inserted into the printer and the d_3AC was deposited covering the entire glass slide. This procedure was repeated 3 times to ensure adequate and uniform coverage. For quantitative MSI, calibration standards (1 μL) of AC were micropipetted onto the glass slide at concentrations of 0.10, 0.20, 0.40, 0.80,

1.0, 2.0, 4.0 ng/μL. Each spot was measured to be 2.5 mm in diameter, which was verified using the detected ion signal and raster step size of the MSI experiments. For tissue-to-tissue comparison experiments, calibration standards were spotted at concentrations of: 0.1, 0.2, 0.4, 0.6, 0.8, 1 ng/μL beneath each tissue, followed by the application of d_3AC with the inkjet printer. These calibration standards were used to produce standard additions plots to estimate the endogenous concentration of AC.

Sectioning of the brain tissue was performed on a Microm HM 505E cryostat (Waldorf, Germany). Tissue was sliced at −25 °C to a thickness of 20 μm and thaw mounted onto the glass microscope slide previously coated with d_3AC and/or AC standards and stored at −80 °C. To minimize condensation, the tissue was first warmed to room temperature in a vacuum dessicator for ~30 minutes, then DHB diluted to 40 mg/mL in 90/10 ethanol/chloroform (v/v) was applied with a Meinhard nebulizer, model number TR-30-A3, at a flow rate of 2.4 mL/min.

Mass Spectrometry

All MS images, and spectra except for the tissue-to-tissue comparison, were acquired with a MALDI LTQ–XL (ThermoFinnigan, San Jose, CA) equipped with a 337-nm nitrogen laser at a frequency of 60 Hz and spot diameter of 100 μm. For full-scan MS imaging experiments, spectra were collected using four laser shots at a laser energy of 2 μJ. All MS/MS experiments utilized a 6-amu wide-isolation window centered at *m/z* 205.5 unless otherwise noted. MS/MS imaging experiments were acquired with four laser shots with a laser energy of 16 μJ to achieve optimal ion signal. At this laser energy and number of laser shots, space charging was evident in the full MS spectrum; however, space charging was not observed using wide-isolation MS/MS

and, thus, not a concern. Furthermore, we were unable to observe space charging effects at higher laser energies (40 μJ) combined with a higher number of laser shots (50) during wide-isolation MS/MS mode.

Sample slides were inserted into the intermediate vacuum chamber (0.07 Torr) and rastered with respect to the laser at varying step sizes depending on the experiment (100–300 μm). Total and extracted ion signal were analyzed with Qualitative Browser from Thermo Fisher Scientific. A MALDI data extraction program from Thermo Fisher Scientific was used to extract the ion intensity at each corresponding MS/MS scan. Extracted data was imported into Microsoft Excel to produce analyte to internal standard ion intensity ratios at each position. All images were created using Surfer 8 (Golden, CO) by gridding the extracted data using triangulation with linear interpolation.

From the improved quantitative results shown in Chapter 3, the tissue-to-tissue comparison studies were analyzed with a Synapt MALDI-Q-Ion Mobility (T-wave cell) Time of Flight (QTOF) equipped with a 200 Hz, 355 nm, Nd:YAG laser at a frequency of 200 Hz and spot diameter of 150 μm (Waters Corporation; Milford, MA, USA. The QTOF instrument was operated in MS mode Sample slides were inserted into the vacuum chamber and rastered beneath the laser at a step size of 250 μm and MS spectra were summed from 200 laser shots at each raster step. Resulting MS data from the QTOF were processed using BioMap (Novartis, Basel, Switzerland). Normalized images were generated using the divide function in BioMap to generate AC/d_3AC (*m/z* 204/207) images. For quantitative determinations of AC in treated and

untreated tissue, a standard additions analysis was performed utilizing the product ion ratio of AC/d_3AC from the spotted AC calibration standards beneath the tissues.

Results and Discussion

MS/MS Characterization

Prior to imaging experiments, the $[M+H]^+$ of AC (*m/z* 204) and d_3AC (*m/z* 207) standards were characterized by MS/MS. Collision induced dissociation of the $[M+H]^+$ ion of AC produced three main product ions at *m/z* 145, 85, 60 and d_3AC produced product ions at *m/z* 148, 85, 60 as shown previously in Chapter 3, Figure 3-1. Product ions *m/z* 145 and 148 from AC and d_3AC, respectively, resulted from the loss of the trimethyl-amine group and were monitored for quantitative analysis. Narrow isolation experiments were performed to ensure neither the AC nor d_3AC produced product ions at *m/z* 148 and *m/z* 145, respectively. It is important to note that for wide-isolation MS/MS spectra, the observed product ions *m/z* 145 and 148 are generated from the range of *m/z* 202.5 – 208.5. Preliminary studies performed on tissue utilizing a 1-amu narrow isolation MS/MS experiment at each nominal mass from *m/z* 202–209 showed no significant contribution of *m/z* 145 and 148 signal from endogenous compounds within the isolation range.

The isotopic purity of the d_3AC was stated to be > 98% from the manufacturer, which was verified by comparing the signal intensity of the product ions at *m/z* 145 to that at *m/z* 148 when analyzing d_3AC applied to a glass slide with wide-isolation MS/MS. Three layers of 10 ng/μL d_3AC were applied using the inkjet printer and then coated with DHB diluted to 40 mg/mL in 90/10 chloroform/ethanol (v/v). Analyzing 50 MS/MS scans of the d_3AC, the contribution from the impure isotope to the product ion signal at *m/z* 145 was determined to be < 1.2% ± 0.6%.

Matrix Application for Solvent Comparisons

To determine matrix application effects, standards of AC and d_3AC were applied to a glass slide with an inkjet printer and analyzed using wide-isolation MS/MS. One-inch squares AC of were applied atop two previously d_3AC-coated glass microscope slides. DHB crystals that were formed from the two solvent mixtures, 90/10 chloroform/ethanol (v/v) and 70/30 methanol/water (v/v) are compared in Figure 4-1. The chloroform/ethanol solvent mixture resulted in a more uniform matrix coating with significantly smaller crystal sizes. In Figure 4-1A, the water/methanol solvent produced crystals of varying sizes that approached upwards of 250 μm in length, whereas the chloroform/ethanol solvent mixture resulted in crystal sizes consistently smaller than 60 μm. The smaller crystal sizes in the chloroform/ethanol solvent can be attributed to the rapid evaporation of the matrix solvent, Figure 4-1B.

MSI was used to analyze matrix uniformity between the solvent systems by selecting an area of each DHB coated glass slide and comparing the percent RSD of 500 MS scans of signal intensity of *m/z* 137, $[DHB-H_2O]^+$. As reported in Table 4-1, the reproducibility of the matrix ion signal was improved from 66% (methanol/water) to 31% (chloroform/ethanol) utilizing a more volatile solvent that enhances rapid crystal formation. The improved signal reproducibility of the matrix ion signal reflects a more uniform coating of smaller matrix crystals resulting from rapid evaporation of the solvent. Conversely, the observed increase percent RSD of the signal from methanol/water is attributed to larger crystal formation resulting in significant sample differences when probed on a 100-μm scale.

To determine if improved matrix signal reproducibility correlates to improved analyte signal reproducibility, wide-isolation MS/MS experiments were performed over areas of the slides where AC and d_3AC were applied. Within each 1-inch square, 50 MS/MS scans were acquired and the percent RSD of the product ion signal of *m/z* 145, 148 and the ratio of *m/z* 145/148 were calculated and reported in Table 4-1. The improved matrix coverage from chloroform/ethanol mixture resulted in better ion signal reproducibility for the product ions of both AC and d_3AC. The improved matrix coverage produced a more homogenous sample when analyzed on a 100-μm scale. Matrix crystals that were significantly larger than the laser-spot diameter resulted in irreproducible signal resulting from the large variation in crystallization at each raster step. This larger variation of the ion signal intensity across a sample may only be due to the differences in matrix crystallization. Laser energy fluctuation may also cause signal variation; however, the manufacturer's stated laser energy variance (4%) is too low to account for the observed signal variability. Furthermore, the percent RSD for both AC and d_3AC are comparable, which indicates that d_3AC is acting as an adequate IS. To further account for signal variability, normalizing the AC by the d_3AC intensity on a scan-by-scan basis resulted in a four- to five-fold improvement in percent RSD.

To further determine if d_3AC is behaving as an adequate IS, wide-isolation MSI experiments of the AC standard were performed on the chloroform/ethanol coated slide. Within the 1-inch square of AC, an 11 × 11 step raster pattern was created using a 100-μm step-size. After wide-isolation MSI, separate MS images were generated using the normalized intensities of the product ions *m/z* 145 (AC), 148 (d_3AC), and 145/148 versus scan position, shown in Figure 4- 2. To produce the normalized images on the

same color scale, the mean ion intensity or ratio was calculated for each image. At each raster step, the percent difference from the average intensity was calculated for the detected ion signal, which produced images showing the relative variation in signal. The images produced from the ion intensity of AC and d_3AC (Figures 4-2A and 4-2B) show similar ion intensity distributions indicating that d_3AC is co-crystallizing and ionizing mutually with AC. This effect is further exhibited in Figure 4-2C, where the ratio of the two ions exhibits a uniform distribution across the image, suggesting the signal variability observed in Figures 4-2A and 4-2B is attributed to differences in matrix crystallization and not the application of the standards by the inkjet printer. The viability of the IS is further exemplified in Figure 4-3, showing normalized intensities of a line scan of 11 spectra across the image indicated in Figure 4-2A. For each scan, the intensities of both the AC and d_3AC vary similarly; however, the ratio of the two ions is conserved resulting in improved signal reproducibility.

The statistical range of ion intensities may also be important for determining concentration differences on an area scale approaching that of the laser diameter. The range of absolute signal intensities for the product ions of AC and d_3AC (AC = 5200–170000; d_3AC = 6200–260000) were separated by a factor of 34 and 43, respectively; however the range of the ratio (0.57–0.97) was reduced to a factor of 1.7. Clearly, utilizing an internal standard to control for ion signal variability may be necessary for quantitative MALDI-MSI application. As the data in Figures 4-2 and 4-3 show, quantitative MSI from tissue, where matrix crystallization differences are compounded by sample heterogeneity, spot-to-spot comparisons of intensities alone may be

statistically irrelevant; in contrast, the use of an internal standard to correct for sample heterogeneity and matrix crystallization variability can result in informative images.

The signal variability over multiple analyses was also determined by reanalyzing a given raster area eight times. The variation in AC and d_3AC signal is plotted in Figure 4-4. As the matrix is ablated away, thus varying the M/A ratio, the detected ion signal varies non-linearly as the matrix is ablated away. Although the absolute ion signal varies dramatically, the detected AC/d_3AC ratio does not vary significantly as illustrated by the relatively flat plot. This suggests the internal standard may also account for differing M/A ratios in a given imaging experiment and can be especially important for imaging a particular compound that may vary significantly in concentration in a given sample.

Calibration Curve Experiments

For calibration linearity comparisons; 1 μL of AC at concentrations of 0.1–8 ng/μL were spotted using a micropipette onto a glass microscope slide previously coated with d_3AC (3 layers, 10 ng/μL) as shown in Figure 4-5. DHB diluted in chloroform/ethanol was then applied and each spot was analyzed using wide-isolation MS/MS. Wide-isolation MS/MS signal intensity for *m/z* 145 (AC) and the *m/z* 145/148 (AC/d_3AC) ratio from 35 scans within each calibration spot were averaged and used to calculate two calibration curves. Signal variability of the ion signal for *m/z* 145, 148 and 145/148 within each calibration spot is listed in Table 4-2. Shown in Figure 4-6A, the signal intensity of *m/z* 145 versus concentration resulted in line of best fit of y ($counts_{145}$) = (12700 ± 2500) × (μg/mL) + (12800 ± 8600) with an R^2 = 0.8332. The curve plotted using the ratio of *m/z* 145/148, Figure 4-6B, resulted in a line of best fit of y ($ratio_{145/148}$)

= 0.470(±0.018) × (μg/mL) – 0.065(±0.061) with an R^2 = 0.9929. Linearity and scan-to-scan reproducibility were significantly improved when normalizing by the internal standard. The average percent RSD from the calibration standards using the *m/z* 145 ion intensity was 84% with a range of 56–122 compared to averaging the percent RSD of the ratio of *m/z* 145/148, which had a percent RSD of 22% with a range of 9.2–45.1%. No correlation was observed between the percent RSD and an increase in concentration monitoring the intensity of *m/z* 145; whereas the percent RSD of the averaged ratio improved with an increase in concentration of AC. Utilizing a uniformly applied IS coupled with wide-isolation MS/MS showed considerable improvement in precision using a scan−by−scan analysis.

Imaging of Piglet Brain Tissue with Spotted Standards

Three layers of 10 ng/μL d_3AC followed by spotting 1 μL of calibration standards (0.1-8 ng/μL) of AC in 50% methanol were applied to a glass slide. A 20-μm thick tissue section was placed over the calibration standards and the entire slide was coated with DHB diluted in chloroform/ethanol. The entire tissue was analyzed using a 6-amu wide-isolation window centered at *m/z* 205.5. The imaging experiment was performed using four laser shots with a raster step-size of 200 μm, and the laser energy was set at 14 μJ to ensure optimum MS/MS signal without space charging the ion trap.

The estimated concentration (moles/kg_{tissue}) of the spotted standards in estimated weight of the wet tissue was calculated using the area of the spotted standards incorporated into a 20-μm thick tissue section. For the experiments discussed in this paper, significant care was taken in the spotting of the AC standards to ensure reproducible droplets measuring ~2.5 mm in diameter. Upon extraction through a 20-

μm section of tissue, a 1-μL spot of 1 ng/μL results in a tissue concentration 0.02 $\mu mol/kg_{tissue}$ assuming the density of brain tissue is nearly that of water, 1.05 g/mL.[100]

In Figure 4-7A-C, Surfer 8 was used to produce images of the AC (Figure 4-7A) and d_3AC (Figure 4-7B) using the intensity of *m/z* 145 and 148, respectively, as well as an image of the ratio of the two ions, *m/z* 145/148 (Figure 4-7C) in each scan. Areas where standards were applied are circled and increase in concentration from 0.1 to 4 ng/μL starting with the lower left spot moving clockwise around the tissue. Signal intensity is observed in three main locations from the image of *m/z* 145: 1) the area where no tissue is present; 2) the area of spiked AC standards and 3) the area on tissue where no AC had been added. The detected *m/z* 145 signal on the glass slide is due to the isotopic impurity of AC in the d_3AC (> 98% isotopic purity) standard used to coat the entire slide. The signal ratio of AC to the d_3AC in this area was calculated to be ~1.2% ± 0.2%. Assuming the same contribution for the tissue area, the signal contribution would be insignificant as the average signal intensity from d_3AC is ~500 counts. Averaged signal from ~20 scans within the area of the spiked AC standards was used to produce two calibration curves from 40-200 $nmol/kg_{tissue}$ using the intensity of *m/z* 145 and resulted in a curve with the equation: $y\ (counts_{145}) = 7.70\ (\pm 0.74) \times (\mu g/mL) - 113.0\ (\pm 85.9)$; $R^2 = 0.982$, and from the ratio of *m/z* 145/148: $y\ (ratio_{145/148}) = 0.00972\ (\pm 0.00029) \times (\mu g/mL) - 0.116\ (\pm 0.033)$; $R^2 = 0.998$. The improved R^2 value for the calibration curve using the ratio of 145/148 may be attributed to the d_3AC extraction and co-crystallization in a similar manner to AC as well as improved matrix coating crystallization producing a more reproducible signal from each of the spotted standards.

The detected *m/z* 145 signal from areas within the tissue where AC was not spiked is thought to arise from endogenous AC with minimal or no contribution from the impure d_3AC. This is further supported by the image in Figure 4-7C, which shows the *m/z* 145 signal on the glass slide to be reduced to nearly zero due to the comparatively low ratio of AC to d_3AC present. Thus, ratio increases greater than the contribution from the impure standard may be from the endogenous metabolite. Using the calibration equation from the ratio of *m/z* 145/148, the concentration of AC detected at each raster step can be estimated and a quantitative image generated, shown in Figure 4-8. From this image, the concentration of AC is estimated to be in the range of 20–100 $nmol/kg_{tissue}$ and falls within the concentration expected. A limitation of this type of quantitative estimation assumes that the standards spotted beneath the sample will extract, co-crystallize, and ionize in the same manner as the endogenous compound, which is difficult to determine via MALDI MSI. However, analyte concentration differences may be observed within a tissue sample or from tissue-to-tissue. These concentration differences may be determined with improved confidence due to the control for numerous factors including matrix application heterogeneity, tissue-specific ion suppression,[73] or any other cause of signal variation.

Quantitative Comparison Between Treated and Untreated Tissue

For the quantitative comparison of the endogenous AC content between treated (ketogenic diet) piglets and untreated piglets (normal diet), MSI was performed using MS imaging on the QTOF instrument. The resulting AC/d_3AC images from the MSI experiments are shown in Figure 4-9. Figure 4-9A is the MS images of the ketogenic treated sample and Figure 4-9B is the MS image of the untreated sample. Concentrations of endogenous AC were estimated using a standard additions analysis

shown in Figure 4-10. Estimations of the endogenous AC concentrations were determined to be 170 ± 50 $ng_{AC}/\mu g_{tissue}$ for the treated (ketogenic) sample and 100 ± 70 $ng_{AC}/\mu g_{tissue}$ for the untreated sample. These values corresponded to an estimated upper limit of concentration of 600 μmolar for the untreated sample and 500 μmolar for the untreated sample. These values represent the upper limit as the integrated areas to generate the y-intercept on the standard additions plots were taken from areas of higher signal intensity. From the generated MS images, most of the endogenous signal was between 50-100% of the maximum ratio of *m/z* 204/207 indicating a range of endogenous concentration of AC between 300–600 μmolar for the treated sample and 250–500 μmolar for the untreated sample. However, the error in these measurements is large preventing the accurate differentiation of endogenous AC concentration between the two samples. Although we detected no significant difference in AC concentration, the ability to perform quantitative tissue-to-tissue comparison is considered an advancement of MALDI MSI.

Quantitative MSI Of Endogenous AC Conclusions

Developing quantitative MALDI MSI methods is critical for its expansion into new applications. Two approaches were successfully utilized that leads to better signal reproducibility for MSI: 1) optimizing the matrix application method 2) implementing an isotopically labeled internal standard to improve signal reproducibility. A source of signal variation was shown to be caused by the matrix crystallization layer applied during MSI. Improving this matrix layer leads to better quantitative mass spectral images as well as better signal reproducibility. Utilizing an isotopically labeled internal standard resulted in a significant reduction of signal variability leading to quantitative

tissue imaging. The quantitative information generated from an imaging experiment may reveal regional distribution of an analyte or may be used to determine overall tissue concentrations. This may be significant for whole-body tissue imaging experiments, as outlined in Chapter 1, to determine concentration differences of a drug between different tissue types.

Although, we did not detect a significant change in AC concentration between the treated and untreated piglet brain samples, the differences we did detect may be proven with a much larger sample size. Our preliminary experiments consisted of one brain sample from each piglet type; however, with numerous biological errors combined with the large error in our measurement, an estimation of ~20 samples would need to be analyzed of each piglet type.

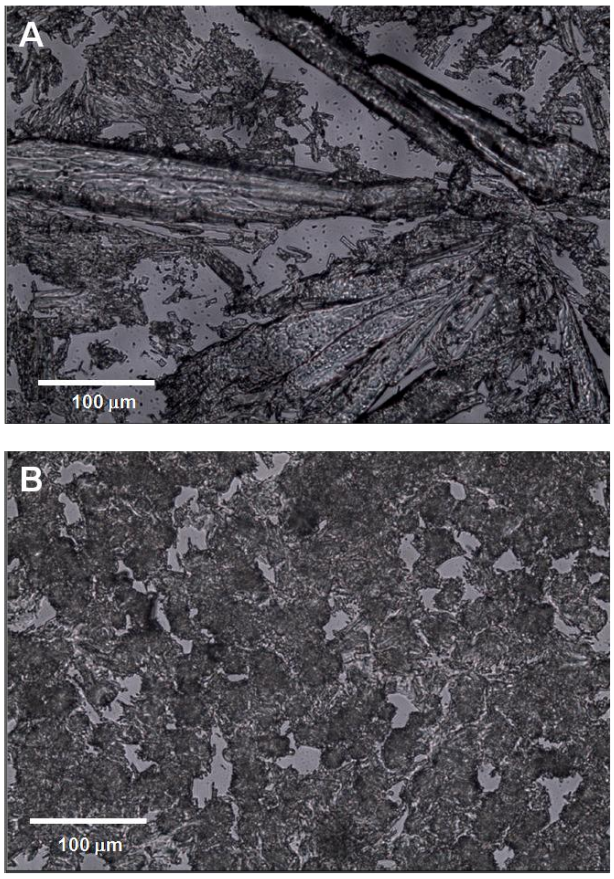

Figure 4-1. Microscope images (20×) of formed DHB crystals applied with a Meinhard nebulizer onto a glass slide using two different solvents: (A) diluted to 40 mg/mL in 70/30 methanol/water (v/v) and (B) diluted to 40 mg/mL in 90/10 chloroform/ethanol (v/v). The largest crystals observed in A were measured to be <250 μm compared to the largest crystals in B, measured at <60 μm.

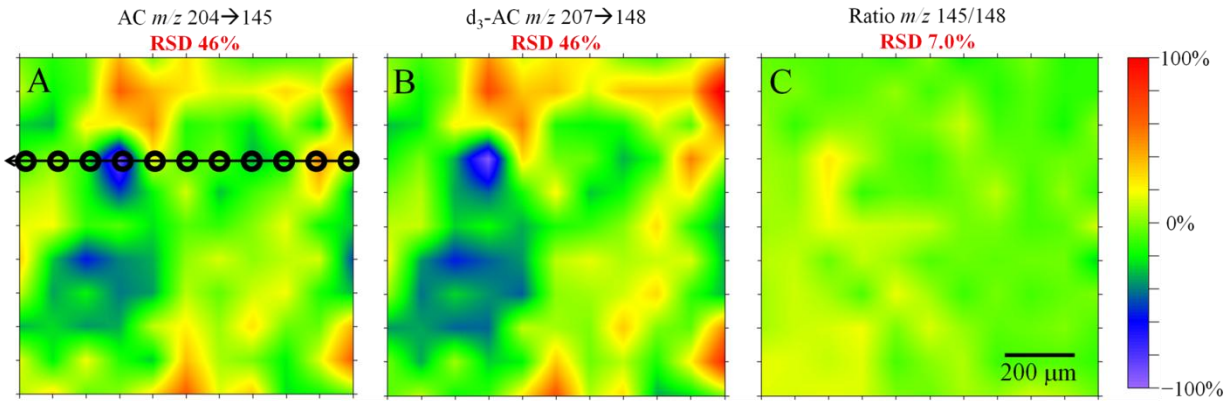

Figure 4-2. Extracted wide-isolation MS/MS images of the normalized product ions of: AC, *m/z* 145 (A), d_3AC *m/z* 148 (B), and the ratio of *m/z* 145/148 (C) at each position. The color-scale is determined from calculating the percent difference from the mean. AC and d_3AC exhibit significant signal variation within the area imaged; however, this variation is significantly reduced by plotting the ratio of *m/z* 145/148 (C) for each analytical scan.

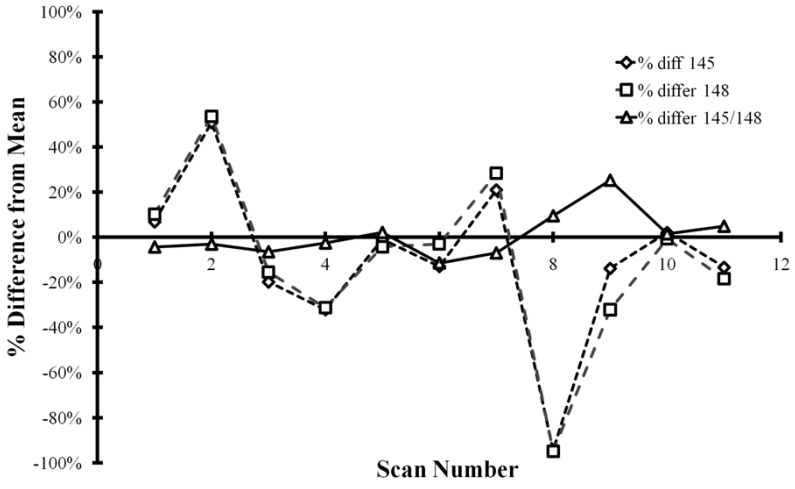

Figure 4-3. Line scan intensities normalized to the mean for each ion and ratio. Intensities of *m/z* 145, 148 and 145/148 of a line scan right (scan #1) to left (scan #11) from area indicated in Figure 4-2A.

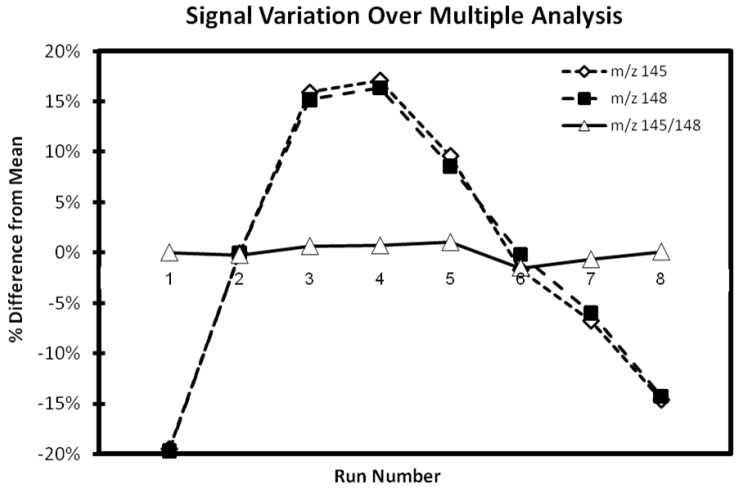

Figure 4-4. Signal variation over subsequent MALDI MSI analysis.

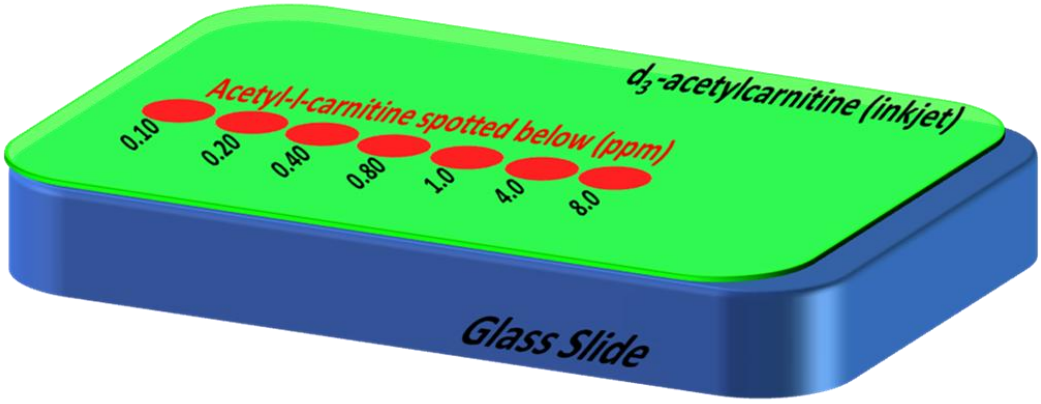

Figure 4-5. Experimental setup for quantitative analysis of AC standards spotted onto a glass slide. AC was applied with a pipette and d_3AC was applied uniformly with an inkjet printer.

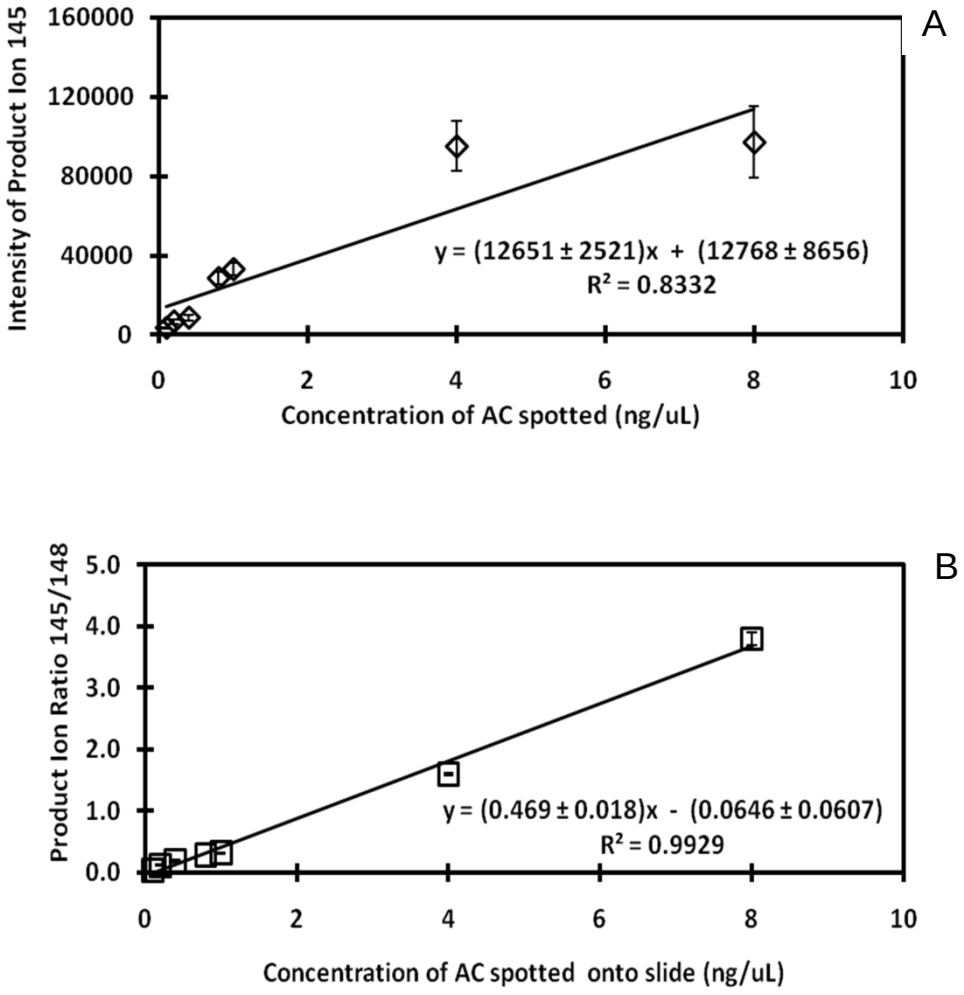

Figure 4-6. Calibration plots from standard of AC spotted onto a glass microscope slide. (A) Calibration plot from the intensity of *m/z* 145 (AC) versus concentration. (B) Calibration plot of the ratio of *m/z* 145/148 (AC/d_3AC) showing improved linearity and signal reproducibility. Error bars represent the standard error of the average MS/MS intensities.

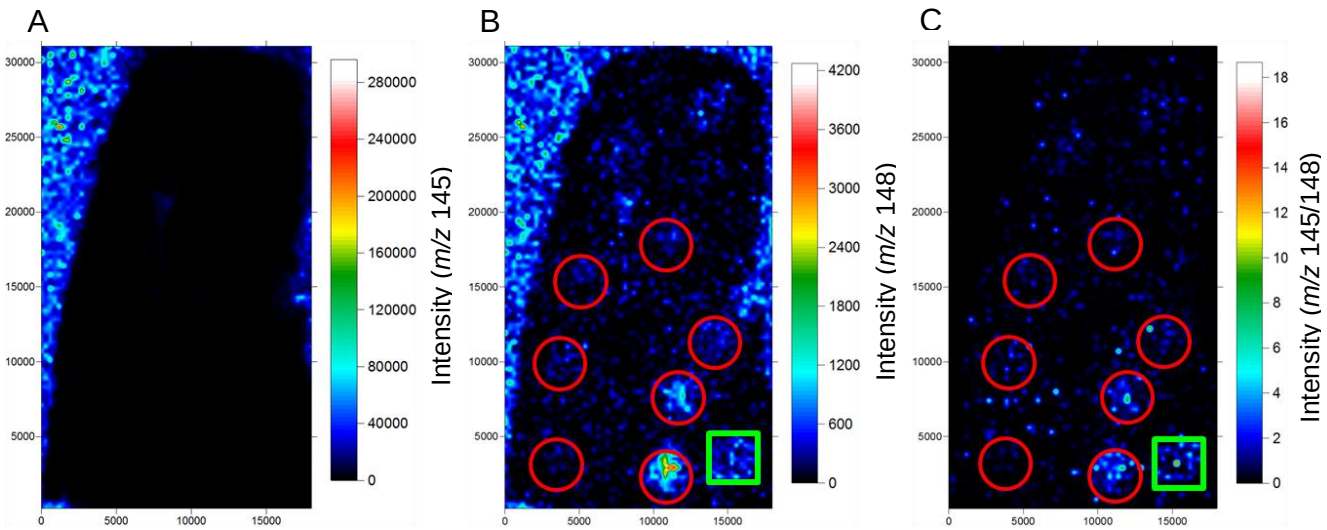

Figure 4-7. Wide-isolation MS/MS images quantifying AC in piglet brain tissue. A) d_3AC, absolute intensity of *m/z* 148. B) AC absolute intensity of *m/z* 145. C) The ratio of AC/d_3AC (C) at each position. The internal standard image A exhibits intense signal outlining the tissue sample. In images B and C, red circles indicate the location of the spotted AC standards, starting with the lower left as 0.1 ng/μL and moving clockwise ending with 4 ng/μL. The green square indicates a 4 ng/μL standard spotted atop the tissue sample for comparison with the standards spotted beneath. The color-scale for A and B is determined from the absolute intensities of the ions *m/z* 145 and 148, respectively. The color-scale for C is determined from the ion intensity ratio of *m/z* 145/148.

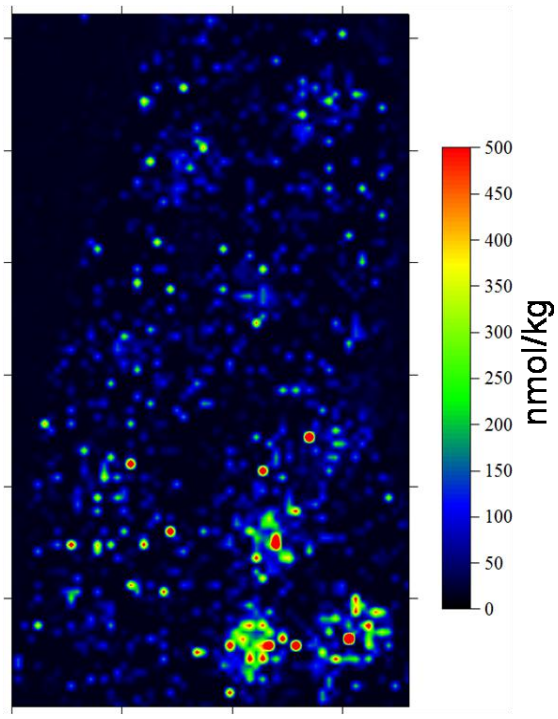

Figure 4-8. Quantitative image of AC in the frontal lobe of a piglet brain slice. Concentration of AC was calculated from standards placed beneath the tissue using a calibration curve normalized by an internal standard. The color-scale is determined from the calculated concentration of endogenous AC from the calibration curve of the spotted standards of AC and is plotted in $nmol_{AC}/kg_{tissue}$.

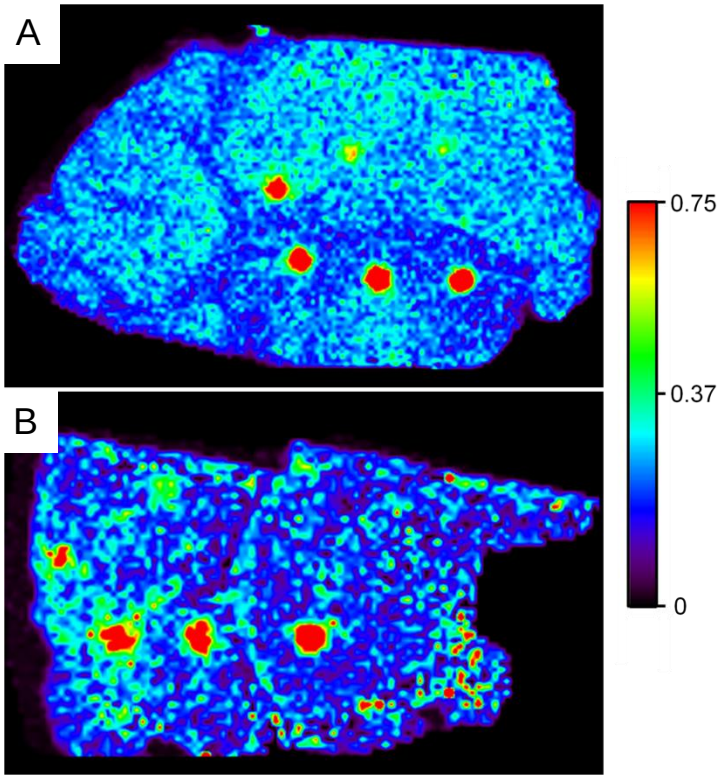

Figure 4-9. Full MS images of AC distribution in piglet brain tissue obtained from the QTOF. Images were normalized by the d_3AC signal by determining the *m/z* 204/207 ratio at each raster position (scale bar indicates ratio of *m/z* 204/207). The endogenous AC was quantitatively compared between piglets fed a ketogenic diet (A) to piglets fed a normal diet (B).

Treated

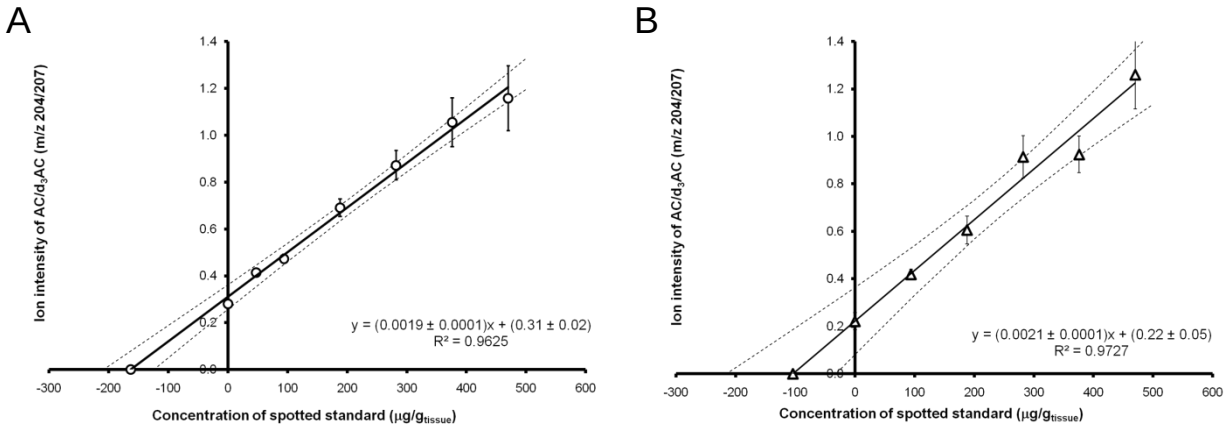

Figure 4-10. Standards addition plots for the quantitative determination of AC in piglet brain thin tissue sections. A) AC concentration is compared between a piglet fed a ketogenic diet and (B) a piglet fed a normal diet. From these experiments, the differences in endogenous AC concentration were unable to be detected using quantitative MSI.

Table 4-1. Matrix dependence on signal MALDI ion signal variation.

	Ion Intensity Signal (%RSD)			
DHB Solvent	AC *m/z* 204→145	d_3AC *m/z* 207→148	AC/d_3AC *m/z* 145/148	DHB-H_2O *m/z* 137
70/30 MeOH/H_2O	63	72	16	66
90/10 $CHCl_3$/EtOH	46	46	7.0	31

Table 4-2. Signal variation of MS/MS ion signal within calibration spots. Variation is reported in %RSD.

	%RSD of MS/MS Scans Within Each Spot		
Concentration (ng/μL)	AC *m/z* 204→145	d_3AC *m/z* 207→148	AC/d_3AC *m/z* 145/148
0.1	55	62	59
0.2	49	52	10
0.4	38	39	10
0.8	51	47	8
1	49	42	7
4	42	40	7
8	25	29	8

CHAPTER 5
CONCLUSIONS AND FUTURE WORK

Conclusions

The goal of this research was to develop quantitative MALDI MSI methods and to evaluate these methods for the analysis of acetyl-l-carnitine (AC) in piglet brain tissue. Initial method development of a quantitative MALDI MSI method was performed on the analysis of cocaine (COC) from a human brain sample. Quantitative determinations made from the analysis by MALDI MSI were compared to quantitative results from the well-established analytical technique LC-MS/MS. The need for a deuterated internal standard was identified during this method development phase. Further analysis employing a deuterated internal standard for MALDI MSI was performed with AC and d_3AC. It was shown that the internal standard not only improves the quantitative ability of MALDI, but also can control for other limitations of MSI, such as tissue-specific ion signal variation. Finally, quantitative estimates of the AC content in piglet brain samples were made, using the methods developed and analyzed in Chapters 2 and 3. The methods and analysis presented in this research are not limited to COC and AC, but can be generally employed for any small-molecule target analyte, provided an isotopically-labeled internal standard is available.

Initial experiments with cocaine showed that quantitative analysis could be performed with MALDI with the uniform application of an internal standard. The internal standard is used to normalize the target analytes ion signal at each MS scan, thus accounting for the significant ion signal variation associated with MALDI. Quantitative results from MALDI MSI experiments by standard additions analysis compared very well to LC-MS/MS results from tissue extracts. COC brain concentrations from the MSI

analysis were within 20% of the concentration determined by LC-MS/MS; however, the MSI results were significantly less precise, primarily due to the lack of sample cleanup steps such as tissue extraction and chromatography. MALDI MSI allows for directs sampling of the tissue performed in a two-dimensional manner which preserves the physical integrity of the sample.

Quantitative MALDI MSI was also compared to LC-MS/MS for the analysis of tissue extracts. With an appropriate internal standard, wide-isolation MS/MS was used in place of chromatography to separate interfering ions. Analysis of the tissue extracts resulted in quantitative COC values within 5% of each other when analyzed by MALDI and LC-MS/MS. The LC analysis was performed with a triple quadrupole mass spectrometer employing selected reaction monitoring, which is generally considered the best MS/MS approach for quantitative analysis. However, employing chromatography significantly increases analysis time and the consumption of resources. A typical LC analysis can last between 5 and 20 minutes for each sample analyzed. Including analysis of solvent blanks a calibration experiment can take many hours to complete. For the triplicate LC-MS/MSanalysis presented here, the total analysis time was approximately 15 hours. Analysis by MALDI shortens the analysis time significantly. For the experiments performed, 50 MS/MS scans were recorded in quadruplicate, resulting in analysis time of only 30 minutes for the entire quantitative experiment. A disadvantage of the MALDI approach, however, is the potential for non-linear response, thus limiting the linear dynamic range. These non-linear effects result from differences in the matrix to analyte ratio across the calibration curve. Either too little or too much matrix may result in attenuation of ion signal. Automated matrix application methods

such as the Bruker ImagePrep may be used to apply a constant amount of matrix from analysis to analysis.

Using an internal standard for MALDI MSI also allowed for the identification of tissue-specific ion signal variation. This is a well known limitation in MALDI MSI applications, preventing the technique from being used as a standalone technique to draw biological conclusions. Differences in ion signal were monitored: by spotting a constant concentration of AC beneath multiple tissue types. These differences in ion signal are a result of numerous factors, including differences in matrix crystallization atop the tissues, variations in analyte extraction from the tissue, and ionization variability resulting from the presence of potential ion suppressing compounds. However, when monitoring the analyte to internal standard ratio these differences in ion signal were accounted for. Ion signal of AC varied by a factor of 10 from tissue to tissue for the same concentration of AC applied beneath the sample. This variation in ion signal could lead to false conclusions about the concentration of AC in the tissue without normalization by an internal standard. The AC/d_3AC ratio, however, varied only by a factor of 1.3, producing a far more accurate representation of the spotted AC concentration. Using an internal standard in this manner should also lead to better confidence in resulting MS images, and provide a better quantitative representation of analyte concentrations between tissues.

Lastly, MSI was used to make a quantitative comparison of the endogenous levels of AC between two samples. Since quantitative MALDI is challenging on any given sample, quantitative comparison between two samples is difficult. Ion signal can vary based on differences in tissue makeup, matrix application, and tissue thickness.

Analysis with an internal standard was shown to account for many of these differences, thus allowing for tissue-to-tissue comparisons. The method does contain a significant amount of error in the measurements due to the lack of sample cleanup such as extraction and chromatography. This error associated with quantitative measurements means that small changes in concentration will be difficult to determine. For this application, the concentration of AC was expected to change very little due to homeostasis, and indeed, the differences in AC concentration between these two samples was too small to determine with reasonable confidense. However, developing methods to make tissue-to-tissue comparisons has the potential to be used in numerous other applications.

Future Work

With the development of a quantitative MALDI MSI method, the reproducibility of the experimental setup should also be improved. Currently, calibration standard are manually spotted onto the MALDI target. This produces error from spot-to-spot based on pipette delivery differences and uneven deposition as the spot dries. Developing and employing a more uniform spot delivery system would produce calibration standards applied in a uniform manner with a defined spot area. Keeping the spot area consistent between samples is crucial for quantitative analysis, as the area is used in calculating tissue concentrations. Other deposition techniques may be employed to produce a uniform layer of the internal standard onto the MALDI target. The modified inkjet printer produces picoliter droplets; however, these may merge to produce larger droplets formed on the target. This effect is solvent-dependent and the inkjet printer is only compatible with methanol and water. Employing other spotting techniques such as

the LabCyte Portrait spotter may result in more reproducible internal and calibration standard applications.

Sensitivity is also a potential limitation of the technique. This work shows quantitative estimations in the micromolar range; however, many applications require detection limits at least an order of magnitude less. MSI quantitation was improved with the QTOF instrument. Complete ablation of the tissue sample from spot-to-spot resulted in a more reproducible sample size analyzed at each raster position. Taking advantage of the complete ablation of the sample, thicker tissue sections may be used to increase the amount of the target analyte for detection.

Employing MS^n in the ion trap may also improve sensitivity through the reduction of background interferences; however, CID efficiency and ion loss from increased storage time can limit this approach. Space-charging in the ion trap also limits the dynamic range of quantitation. This effect is not observed in the QTOF instrument; however, the large noise levels in the low mass range require a large number of spectra to be summed. This requires a large number of laser shots (>100) at each raster position. Comparing each instrument, the LTQ was more sensitive on a laser shot to ion signal basis; however, space charging and differences in samples size at each raster step result in variable ion signal. The QTOF results in better quantitative MSI data, but is limited in sensitivity on a laser shot to ion signal basis. Developing MSI instrumentation that could offer the sensitivity of the LTQ without the space-charging issues may result in significant improvements in the overall sensitivity of MALDI MSI.

In summary, generating more reproducible sample preparation methods and improving sensitivity are the main areas of quantitative MALDI MSI to be improved

upon. This would advance the methodology and allow it to be used in a wide array of applications.

LIST OF REFERENCES

(1) Rontgen, W. K. *Science.* **1896**, *3*, 726-729.

(2) Damadian, R. *Science.* **1971**, *171*, 1151-1153.

(3) Raylman, R. R.; Majewski, S.; Lemieux, S. K.; Velan, S. S.; Kross, B.; Popov, V.; Smith, M. F.; Weisenberger, A. G.; Zorn, C.; Marano, G. D. *Phys.Med.Biol.* **2006**, *51*, 6371-6379.

(4) Yuan, C.; Kerwin, W. S.; Ferguson, M. S.; Polissar, N.; Zhang, S.; Cai, J.; Hatsukami, T. S. *J.Magn.Reson.Imaging.* **2002**, *15*, 62-67.

(5) Chalfie, M.; Tu, Y.; Euskirchen, G.; Ward, W. W.; Prasher, D. C. *Science.* **1994**, *263*, 802-805.

(6) Helveg, S.; Lopez-Cartes, C.; Sehested, J.; Hansen, P. L.; Clausen, B. S.; Rostrup-Nielsen, J. R.; Abild-Pedersen, F.; Norskov, J. K. *Nature.* **2004**, *427*, 426-429.

(7) Svatos, A. *Trends Biotechnol.* **2010**, *28*, 425-434.

(8) Caprioli, R. M.; Farmer, T. B.; Gile, J. *Anal.Chem.* **1997**, *69*, 4751-4760.

(9) Castaing, R.; Slodzian, J. *J. Microsc.* **1962**, *1*, 395.

(10) Kaufmann, R.; Hillenkamp, F.; Wechsung, R. *Med.Prog.Technol.* **1979**, *6*, 109-121.

(11) Kaufmann, R.; Hillenkamp, F.; Wechsung, R.; Heinen, H. J.; Schurmann, M. *Scan.Electron Microsc.* **1979**, *2*, 279-290.

(12) Perchalski, R. J. Characteristics and Application of a Laser Ionization/Evaporation Source for Tandem Mass Spectrometry. Ph.D. Dissertation, University of Florida, Gainesville, FL, **1985**,

(13) Troendle, F. J.; Reddick, C. D.; Yost, R. A. *J.Am.Soc.Mass Spectrom.* **1999**, *10*, 1315-1321.

(14) Reddick, C. D. The Detection of Pharmaceutical Drug Compounds from Intact Biological Tissue by Matrix-Assisted Laser Desorption Ionization (MALDI) Quadrupole Ion Trap Mass Spectrometry. Ph.D. Dissertation, University of Florida, Gainesville, FL, 1997.

(15) Cheng, J.; Winograd, N. *Anal.Chem.* **2005**, *77*, 3651-3659.

(16) Luxembourg, S. L.; McDonnell, L. A.; Duursma, M. C.; Guo, X.; Heeren, R. M. *Anal.Chem.* **2003**, *75*, 2333-2341.

(17) Wiseman, J. M.; Ifa, D. R.; Zhu, Y.; Kissinger, C. B.; Manicke, N. E.; Kissinger, P. T.; Cooks, R. G. *Proc.Natl.Acad.Sci.U.S.A.* **2008**, *105*, 18120-18125.

(18) Wiseman, J. M.; Ifa, D. R.; Song, Q.; Cooks, R. G. *Angew.Chem.Int.Ed Engl.* **2006**, *45*, 7188-7192.

(19) Garrett, T. J.; Prieto-Conaway, M. C.; Kovtoun, V.; Bui, H.; Izgarian, N.; Stafford, G.; Yost, R. A. *Int. J. Mass spectrom.,.* **2007**, *260*, 166-176.

(20) Garrett, T. J. Imaging Small Molecules in Tissue by Matrix-Assisted Laser desorption/ionization Tandem Mass Spectrometry. Ph.D. Dissertation [Online], University of Florida, Gainesville, FL, 2006. http://etd.fcla.edu/UF/UFE0013807/garrett_t.pdf (Accessed Jan 2011)

(21) Chaurand, P.; Schwartz, S. A.; Reyzer, M. L.; Caprioli, R. M. *Toxicol.Pathol.* **2005**, *33*, 92-101.

(22) Aerni, H. R.; Cornett, D. S.; Caprioli, R. M. *Anal.Chem.* **2006**, *78*, 827-834.

(23) Klerk, L. A.; Altelaar, A. F. M.; Froesch, M.; McDonnell, L. A.; Heeren, R. M. A. *Int. J. Mass spectrom..* **2009**, *285*, 19-25.

(24) Chaurand, P.; Norris, J. L.; Cornett, D. S.; Mobley, J. A.; Caprioli, R. M. *J.Proteome Res.* **2006**, *5*, 2889-2900.

(25) Hankin, J. A.; Barkley, R. M.; Murphy, R. C. *J.Am.Soc.Mass Spectrom.* **2007**, *18*, 1646-1652.

(26) Goodwin, R. J.; Scullion, P.; Macintyre, L.; Watson, D. G.; Pitt, A. R. *Anal.Chem.* **2010**, *24*, 1682-1686

(27) Trimpin, S.; Herath, T. N.; Inutan, E. D.; Wager-Miller, J.; Kowalski, P.; Claude, E.; Walker, J. M.; Mackie, K. *Anal.Chem.* **2010**, *82*, 359-367.

(28) Puolitaival, S. M.; Burnum, K. E.; Cornett, D. S.; Caprioli, R. M. *J.Am.Soc.Mass Spectrom.* **2008**, *19*, 882-886.

(29) Wei, H.; Nolkrantz, K.; Powell, D. H.; Woods, J. H.; Ko, M. C.; Kennedy, R. T. *Rapid Commun.Mass Spectrom.* **2004**, *18*, 1193-1200.

(30) Karas, M.; Bachmann, D.; Bahr, U.; Hillenkamp, F. *Int. J. Mass spectrom. and Ion Processes,.* **1987**, *78*, 53-68.

(31) Karas, M.; Bachmann, D.; Hillenkamp, F. *Anal.Chem.* **1985**, *57*, 2935-2939.

(32) Tanaka, K.; Waki, H.; Ido, Y.; Akita, S.; Yoshida, Y.; Yoshida, T. *Rapid Commun.Mass Spectrom.* **1988**, *2*, 151.

(33) Karas, M.; Hillenkamp, F. *Anal.Chem.* **1988**, *60*, 2299-2301.

(34) Knochenmuss, R.; Karbach, V.; Wiesli, U.; Breuker, K.; Zenobi, R. *Rapid Commun.Mass Spectrom.* **1998**, *12*, 529.

(35) Zenobi, R.; Knochenmuss, R. *Mass Spectrom.Rev.* **1998**, *17*, 337-366.

(36) Puretzky, A. A.; Geohegan, D. B. *Chem. Phys. Lett.* **1998**, *286*, 425-432.

(37) Hillenkamp, F. and Peter-Katalinic, J. *MALDI MS: A Practical Guide to Instrumentation, Methods and Applications,* ed.; Wiley-VCH:2007.

(38) Karas, M.; Gluckmann, M.; Schafer, J. *J.Mass Spectrom.* **2000**, *35*, 1-12.

(39) Gusev, A. I.; Wilkinson, W. R.; Proctor, A.; Hercules, D. M. *Anal. Chem.* **1995**, *67*, 1034.

(40) Yu, H.; Lopez, E.; Young, S. W.; Luo, J.; Tian, H.; Cao, P. *Anal.Biochem.* **2006**, *354*, 182-191.

(41) Hatsis, P.; Brombacher, S.; Corr, J.; Kovarik, P.; Volmer, D. A. *Rapid Commun.Mass Spectrom.* **2003**, *17*, 2303-2309.

(42) Bucknall, M.; Fung, K. Y.; Duncan, M. W. *J.Am.Soc.Mass Spectrom.* **2002**, *13*, 1015-1027.

(43) Knochenmuss, R. *J.Mass Spectrom.* **2002**, *37*, 867-877.

(44) Schwartz, J. C.; Senko, M. W.; Syka, J. E. P. *J. Am. Soc. Mass. Spectrom.* **2002**, *13*, 659-669.

(45) Paul, W.; Steinwedel, H. **June 7, 1960**, U.S. Patent# *2,939,952*

(46) Reich, R. Quantitative Imaging of Cocaine and its Metabolites in Brain Tissue by Matrix-Assisted Laser desorption/ionization Linear Ion Trap Tandem Mass Spectrometry. Ph.D. Dissertation [Online], University of Florida, Gainesville, FL, 2010. http://purl.fcla.edu/fcla/etd/UFE0041855 (Accessed Jan 2011)

(47) Reich, R. F.; Cudzilo, K.; Levisky, J. A.; Yost, R. A. *J.Am.Soc.Mass Spectrom.* **2010**, *21*, 564-571.

(48) Setou, M. *Imaging Mass Spectrometry: Protocols for Mass Microscopy,* 1st ed.; Springer:Tokyo, Japan; 2010.

(49) Pringle, S. D.; Giles, K.; Wildgoose, J. L.; Williams, J. P.; Slade, S. E.; Thalassinos, K.; Bateman, R. H.; Bowers, M. T.; Scrivens, J. H. *Int. J. Mass spectrom..* **2007**, *261*, 1-12.

(50) Yost, R. A.; Enke, C. G. *Anal.Chem.* **1979**, *51*, 1251-1264.

(51) Paul, W.; Helmut, S. **1960**, U.S. Patent # *2,939,952*

(52) Freeman, J. M., Freeman, J. B., Freeman,John Mark Epilepsy diet treatment and Kelly, M. T. *The Ketogenic Diet : A Treatment for Epilepsy,* 3rd ed.; Demos:New York; 2000.

(53) Hartman, A. L.; Gasior, M.; Vining, E. P.; Rogawski, M. A. *Pediatr.Neurol.* **2007**, *36*, 281-292.

(54) Kalapos, M. P. *Med.Hypotheses.* **2007**, *68*, 1382-1388.

(55) Ma, W.; Berg, J.; Yellen, G. *J.Neurosci.* **2007**, *27*, 3618-3625.

(56) Borum, P. R. *Annu.Rev.Nutr.* **1983**, *3*, 233-259.

(57) Nalecz, K. A.; Miecz, D.; Berezowski, V.; Cecchelli, R. *Mol.Aspects Med.* **2004**, *25*, 551-567.

(58) Fariello, R. G.; Zeeman, E.; Golden, G. T.; Reyes, P. T.; Ramacci, T. *Neuropharmacology.* **1984**, *23*, 585-587.

(59) Hack, A.; Busch, V.; Pascher, B.; Busch, R.; Bieger, I.; Gempel, K.; Baumeister, F. A. *Pediatr.Res.* **2006**, *60*, 93-96.

(60) Aureli, T.; Di Cocco, M. E.; Puccetti, C.; Ricciolini, R.; Scalibastri, M.; Miccheli, A.; Manetti, C.; Conti, F. *Brain Reas.* **1998**, *796*, 75-81.

(61) Brass, E. P.; Hoppel, C. L. *J. Biol. Chem.* **1978**, *253*, 2688.

(62) Kuratsune, H.; Watanabe, Y.; Yamaguti, K.; Jacobsson, G.; Takahashi, M.; Machii, T.; Onoe, H.; Onoe, K.; Matsumura, K.; Valind, S.; Kitani, T.; Langstrom, B. *Biochem.Biophys.Res.Commun.* **1997**, *231*, 488-493.

(63) Minkler, P. E.; Stoll, M. S.; Ingalls, S. T.; Yang, S.; Kerner, J.; Hoppel, C. L. *Clin.Chem.* **2008**, *54*, 1451-1462.

(64) Hsieh, Y.; Li, F.; Korfmacher, W. A. *Methods Mol.Biol.* **2010**, *656*, 147-158.

(65) Nilsson, A.; Fehniger, T. E.; Gustavsson, L.; Andersson, M.; Kenne, K.; Marko-Varga, G.; Andren, P. E. *PLoS One.* **2010**, *5*, e11411.

(66) Landgraf, R. R. Analysis of Lipids In Nerve Tissue by MALDI Tandem Mass Spectrometric Imaging. Ph.D. Dissertation [Online], University of Florida, Gainesville, FL, 2009. http://purl.fcla.edu/fcla/etd/UFE0024156 (Accessed Jan 2011)

(67) Quia, H.; Piyadasa, G.; Spicer, V.; Ens, W. *Int. J. Mass Spectrom.* **2009**, *281*, 41.

(68) Zaima, N.; Hayasaka, T.; Goto-Inoue, N.; Setou, M. *J.Oleo Sci.* **2009**, *58*, 415-419.

(69) Willmann, J. K.; van Bruggen, N.; Dinkelborg, L. M.; Gambhir, S. S. *Nat.Rev.Drug Discov.* **2008**, *7*, 591-607.

(70) Wiseman, J. M.; Ifa, D. R.; Zhu, Y.; Kissinger, C. B.; Manicke, N. E.; Kissinger, P. T.; Cooks, R. G. *Proc.Natl.Acad.Sci.U.S.A.* **2008**, *105*, 18120-18125.

(71) Signor, L.; Varesio, E.; Staack, R. F.; Starke, V.; Richter, W. F.; Hopfgartner, G. *J.Mass Spectrom.* **2007**, *42*, 900-909.

(72) Khatib-Shahidi, S.; Andersson, M.; Herman, J. L.; Gillespie, T. A.; Caprioli, R. M. *Anal.Chem.* **2006**, *78*, 6448-6456.

(73) Stoeckli, M.; Staab, D.; Schweitzer, A. *Int. J. Mass Spectrom.* **2007**, *260*, 195-202.

(74) Hankin, J. A.; Murphy, R. C. *Anal.Chem.* **2010**,

(75) Koeniger, S. L.; Talaty, N.; Luo, Y.; Ready, D.; Voorbach, M.; Seifert, T.; Cepa, S.; Fagerland, J. A.; Bouska, J.; Buck, W.; Johnson, R. W.; Spanton, S. *Rapid Commun. Mass Spectrom.* **2011**, *25*, 503-510.

(76) Baluya, D. L.; Garrett, T. J.; Yost, R. A. *Anal.Chem.* **2007**, *79*, 6862-6867.

(77) Naofumi, H.; Yuki, S.; Mitsutoshi, S. *J. Mass Spectrom. Soc. Jpn.* **2008**, *56*, 77.

(78) Gobey, J.; Cole, M.; Janiszewski, J.; Covey, T.; Chau, T.; Kovarik, P.; Corr, J. *Anal.Chem.* **2005**, *77*, 5643-5654.

(79) Lowe, R. H.; Barnes, A. J.; Lehrmann, E.; Freed, W. J.; Kleinman, J. E.; Hyde, T. M.; Herman, M. M.; Huestis, M. A. *J.Mass Spectrom.* **2006**, *41*, 175-184.

(80) Chen, R.; Hui, L.; Sturm, R. M.; Li, L. *J.Am.Soc.Mass Spectrom.* **2009**, *20*, 1068-1077.

(81) Andersson, M.; Groseclose, M. R.; Deutch, A. Y.; Caprioli, R. M. *Nat.Methods.* **2008**, *5*, 101-108.

(82) Solon, E. G.; Schweitzer, A.; Stoeckli, M.; Prideaux, B. *AAPS J.* **2010**, *12*, 11-26.

(83) Heeren, R. M. A.; Smith, D. F.; Stauber, J.; Kükrer-Kaletas, B.; MacAleese, L. *J.Am.Soc.Mass Spectrom.* **2009**, *20*, 1006-1014.

(84) Sleno, L.; Volmer, D. A. *Rapid Commun.Mass Spectrom.* **2005**, *19*, 1928-1936.

(85) Rohner, T. C.; Staab, D.; Stoeckli, M. *Mech.Ageing Dev.* **2005**, *126*, 177-185.

(86) Gobey, J.; Cole, M.; Janiszewski, J.; Covey, T.; Chau, T.; Kovarik, P.; Corr, J. *Anal.Chem.* **2005**, *77*, 5643-5654.

(87) Beckmann, N.; Laurent, D.; Tigani, B.; Panizzutti, R.; Rudin, M. *Drug Discov.Today.* **2004**, *9*, 35-42.

(88) Shimma, S.; Sugiura, Y.; Hayasaka, T.; Hoshikawa, Y.; Noda, T.; Setou, M. *J.Chromatogr.B.Analyt Technol.Biomed.Life.Sci.* **2007**, *855*, 98-103.

(89) Cornett, D. S.; Frappier, S. L.; Caprioli, R. M. *Anal.Chem.* **2008**,

(90) Hsieh, Y.; Chen, J.; Korfmacher, W. A. *J.Pharmacol.Toxicol.Methods.* **2007**, *55*, 193-200.

(91) Reyzer, M. L.; Caprioli, R. M. *Curr.Opin.Chem.Biol.* **2007**, *11*, 29-35.

(92) Landgraf, R. R.; Garrett, T. J.; Calcutt, N. A.; Stacpoole, P. W.; Yost, R. A. *Anal.Chem.* **2007**, *79*, 8170-8175.

(93) Schwartz, S. A.; Reyzer, M. L.; Caprioli, R. M. *J.Mass Spectrom.* **2003**, *38*, 699-708.

(94) Reyzer, M. L.; Hsieh, Y.; Ng, K.; Korfmacher, W. A.; Caprioli, R. M. *J.Mass Spectrom.* **2003**, *38*, 1081-1092.

(95) Nemes, P.; Woods, A. S.; Vertes, A. *Anal.Chem.* **2010**,

(96) Garrett, T. J.; Yost, R. A. *Anal.Chem.* **2006**, *78*, 2465-2469.

(97) Drexler, D. M.; Garrett, T. J.; Cantone, J. L.; Diters, R. W.; Mitroka, J. G.; Prieto Conaway, M. C.; Adams, S. P.; Yost, R. A.; Sanders, M. *J.Pharmacol.Toxicol.Methods.* **2007**, *55*, 279-288.

(98) Chen, Y.; Allegood, J.; Liu, Y.; Wang, E.; Cachon-Gonzalez, B.; Cox, T.; Merrill, A.; Sullards, M. *Anal. Chem.* **2008**, *80*, 2780.

(99) Puolitaival, S. M.; Burnum, K. E.; Cornett, D. S.; Caprioli, R. M. *J.Am.Soc.Mass Spectrom.* **2008**, *19*, 882-886.

(100) Adelina Pellicer; Francisco Gayá; Rosario Madero; José Quero, M.; Fernando Cabañas. *Pediatrics.* **2002**, *109*, 434.

BIOGRAPHICAL SKETCH

David Andrew Pirman, Jr. was the first of two children to parents Brenda Carsey Henderson and David Andrew Pirman, Sr. From the his first introduction to chemistry freshman year while attending Gulf High School in New Port Richey, FL, David has been continuously intrigued with the subject. Ms. Margaret Peek was his first chemistry instructor and challenged him from the first day of class. She still serves a source of motivation and inspiration, not only in his ongoing chemistry education but his life as well. Something is to be said about a teacher who set in motion the ultimate path in one's life, and David uses this opportunity to recognize and thank one of the most influential teachers in his life.

After his initial interest in chemistry developed in high school, David enrolled at the University of Florida and immediately selected his major as chemistry. During his junior year, David began doing undergraduate research under the late Dr. Merle Battiste in synthetic organic research. David also spent many hours volunteering in the Gainesville community with local and campus organizations. Upon graduation, David worked at the University of Florida Racing Laboratory doing method development for instrumental screening techniques for the analysis of drugs of abuse in the horse and dog racing industries. This position initiated his genuine interested in field of analytical chemistry.

David then began his graduate career at the University of Florida in August of 2006, pursuing a Ph.D. in chemistry under the advisement of Dr. Richard A. Yost. His graduate research focused on method development for quantitative MALDI and its application to tissue imaging. David thoroughly enjoys the work he does and hopes to

continue a similar scientific research in the field of analytical research in the biomedical field.